DEVELOPMENT OF XYLOGLUCAN-CHITOSAN COMPLEX INCORPORATING BETALAIN FROM DRAGON FRUIT PEEL FOR INTELLIGENT PACKAGING FILM AND ITS APPLICATION

LASUARDI PERMANA

A THESIS SUBMITTED IN PARTIAL FULFILLMENT
OF THE REQUIREMENT FOR DOCTOR OF PHILOSOPHY
OF FOOD SCIENCE AND TECHNOLOGY
(INTERNATIONAL PROGRAM)
SCHOOL OF FOOD INDUSTRY
KING MONGKUT'S INSTITUTE OF TECHNOLOGY LADKRABANG
2025

KMITL-2025-FI-D-0851-494

Dissertation Title	Development of Xyloglucan-Chitosan Complex Incorporating Betalain from Dragon Fruit Peel for Intelligent Packaging Film and Its Application
Student Name	Lasuardi Permana
Student ID	64608031
Degree	Doctor of Philosophy
Program	Food Science and Technology
Academic year	2025
Advisor	Asst. Prof. Dr. Pongsert Sriprom
Co-advisor	Assoc. Prof. Dr. Pornsawan Assawasaengrat

Abstract

Dragon fruit peels, often considered waste in the food industry, are rich in phytochemicals, particularly betalains. This research aimed to optimize the extraction of betalains from dragon fruit peels using water as an eco-friendly solvent, employing a Box-Behnken design to examine the effects of pH (2.0–6.0), temperature (30–60 °C), time (10–60 min), and solid-to-liquid ratios (1:15–1:40 by weight) on the extraction process. The study identified that the solid-to-liquid ratio significantly influenced the extraction of betacyanin, the primary component of betalains in dragon fruit peels. Optimal extraction conditions were determined to be a pH of 3.6, a temperature of 30 °C, an extraction time of 10 minutes, and a solid-to-liquid ratio of 1:15, yielding an expected betacyanin content of 72.37 mg/L. The extracted betalain exhibited notable changes in color parameters (CIELAB) with increasing pH, likely due to betacyanin degradation into betalamic acid, highlighting the potential application of betalains in pH-dependent products.

Building on these findings, the research further explored the application of dragon fruit peel betalain extract (EB) in developing intelligent packaging films. By incorporating EB in-situ into a tamarind seed kernel xyloglucan and chitosan blend, the films' chemical, physical, mechanical, antimicrobial, and functional properties were characterized. Analyses confirmed electrostatic interactions and hydrogen bonding between the components, with the addition of EB enhancing film thickness and color intensity. Mechanical testing revealed an optimal 1:5 (w/v) EB ratio, achieving a tensile strength of 22.35 ± 2.25 MPa and an elongation-at-break of 185.07 ± 4.42%. The films demonstrated suitable barrier properties and exhibited antibacterial activity against *Escherichia coli* and *Staphylococcus aureus*. Notably, the films could detect ammonia levels indicative of spoilage within 6 days of shrimp storage at 4 °C, correlating with total volatile base nitrogen (TVB-N) levels. This study underscores the potential of utilizing

dragon fruit peel betalains not only as natural pigments but also as components of intelligent packaging hydrogels that visually indicate food freshness and spoilage.

Acknowledgment

I would like to express my deepest gratitude to Asst. Prof. Dr. Pongsert Sriprom, my principal advisor, whose invaluable guidance and unwavering support have been instrumental throughout my research journey. Their insightful feedback, constructive criticism, and constant encouragement have helped me navigate the complexities of this work and motivated me to push beyond my limits.

I am also grateful to Assoc. Prof. Dr. Pornsawan Assawasaengrat for their generous support and expert guidance. Their profound knowledge and thoughtful advice have significantly enhanced the quality of my research and provided me with valuable perspectives throughout this academic pursuit.

Special appreciation is extended to my internal examiners, Asst. Prof. Dr. Soraya Kerdpiboon and Asst. Prof. Dr. Songsak Wattanachaesareekul, for their critical feedback and constructive suggestions. Their meticulous review and valuable input have greatly improved the quality of this work. I would also like to express my deepest gratitude to Assoc. Prof. Dr. Woatthichai Narkrugsa and Assoc. Prof. Dr. Wanna Tungchareonchai, who served as my external examiners. Their expertise and comprehensive feedback have been invaluable in refining this research.

I am thankful to all my fellow researchers and friends at KMITL, whose friendship and support have made this journey more meaningful. The collaborative spirit and mutual encouragement we shared created an enriching academic environment.

I extend my heartfelt appreciation to the KMITL Doctoral Scholarship for providing financial support through the grant that made this research possible.

My deepest gratitude goes to my beloved family—my parents, my wife, and my children—for their unconditional love, patience, and understanding throughout this challenging journey. Their unwavering support and encouragement have been my greatest source of strength.

Finally, I would like to thank the faculty and campus staff for providing the necessary facilities and support that enabled this research.

.

TABLE OF CONTENT

Page

LIST OF FIGURE

Page

LIST OF TABLE

Page

CHAPTER 1
INTRODUCTION

1.1 Introduction

The food industry is an essential sector in sustaining human life. Within this industry, various food supply chains and production processes operate, each with the potential to generate significant amounts of waste. Waste in the agroindustry can arise from diverse sources, including crop residues, process residues, fruit and vegetable waste, vegetable oil waste, poultry, and slaughterhouse waste. This waste accumulation contributes to environmental challenges and leads to substantial economic losses due to discarded products and ineffective waste management practices. However, this challenge presents an opportunity to harness the untapped potential of these waste materials, which often contain valuable compounds. Innovative solutions are required to convert food waste into valuable products within the food industry to address these issues and promote a more sustainable and circular economy.

One of the potential wastes from the food industry is dragon fruit peels. Dragon fruit, also known as pitaya, is a member of the Cactaceae family and Hylocerous genus and is well-known for its pleasant taste and abundance of phytochemicals with health-promoting properties (Elmarzugi et al., 2016; Jiang et al., 2021a). The increasing demand for new and exotic fruits rich in phytochemicals has led to the significant commercial potential of dragon fruit in various countries (Ortiz-Hernández & Carrillo-Salazar, 2012). With its highly soluble fiber and bioactive compounds, Betalain is a type of pigment that contains nitrogen and is only found in a few plant families, such as Cactaceae, Amaranthaceae, Basellaceae, Portulacaceae, and Nyctaginaceae. Contribute to its popularity (Cheok et al., 2020). Apart from their aesthetic appeal, Betalain has been shown to have several health-promoting properties, such as antioxidant, anticancer, anti-inflammatory, and antibacterial effects (Gengatharan et al., 2015; Moreno-Ley et al., 2021; Thippeswamy et al., 2022; Yong et al., 2018). However, the dragon fruit peel, which contains approximately 22% of the whole fruit, is often discarded as waste, leading to environmental issues (Bakar et al., 2011). Due to the abundant vital nutritional ingredients found in these peels, they have the potential for applications in the food and pharmaceutical industries (Jalgaonkar et al., 2022), as well as being utilized as food and packaging colorants.

Another waste that can be utilized is waste from tamarind seed kernels, that typically around 34% of whole fruit (Mansingh et al., 2021). This waste was produced from tamarind, widely grown in Asia, including India and Thailand. This waste is abundant and cheaply produced by industries that utilize tamarind in foods or medicinal products. Tamarind is mainly produced especially in the northern and northeastern of Thailand, such as Phetchabun, Uttaradit, Phitsanulok Nan, and Lamphun for north region, and Loei, Khonkaen, Udonthani, Nongbualamphu, and Kalasin for the northeastern region of Thailand (Wattanadumrong & Liampreecha, 2023). This high tamarind production and utilization results in a high amount of tamarind seed kernel as waste. Valorization of tamarind seed kernels has been researched, including the utilization of this kernel into adhesive for particleboards (Islam et al., 2020), food formulation (Bagul et al., 2018; Narkrugsa et al., 2019), biodiesel fuel (Kumbhar et al., 2022), and pharmaceuticals (Amnuaikit et al., 2019; G. Kumar et al., 2011). Tamarind seed kernel is mainly extracted to obtain xyloglucan, which is abundant in the seed kernel. Xyloglucan is a nonionic polysaccharide that can be extracted from tamarind seed kernel. This xyloglucan is a main constituent of hemicellulose in the middle of the plan with a structure like cellulose. Its favorable physicochemical properties, low processing cost, and widespread regulatory acceptance have led to its widespread application. Much research on xyloglucan has been conducted to explore the potential uses of xyloglucan in the food and pharmaceutical industries. These were also supported by The Food and Drug Administration, which approved the uses of xyloglucan as a food additive, such as stabilizing agent, thickening agent, or gelling agent when combined with other additives (Dutta et al., 2020; Mishra & Malhotra, 2009).

Although xyloglucan has potential uses beyond food and pharmaceuticals, there have been limited studies on its exploration in packaging. Adair et al. (2023)) successfully developed the use of xyloglucan and chitosan in film packaging and characterized its properties. Leray et al. (2022) have conducted an efficient strategy to establish a hydrogel layer film consisting of two layers of xyloglucan and cellulose nanocrystals, exhibiting high strength, improved transparency, and swelling capacities. However, the utilization of xyloglucan in packaging applications remains relatively unexplored.

Therefore, this study aims to explore the potential of Betalain extracted from dragon fruit peel waste using water extraction method as an indicator of raw food material freshness and xyloglucan derived from tamarind seed kernel waste as a biopolymer material for film packaging. By combining the possibilities of Betalain and xyloglucan, we can create intelligent packaging solutions. The goal is to positively impact the food industry by discovering new applications for dragon fruit peels and tamarind seeds, ultimately reducing waste and creating

valuable products that benefit both the environment and consumers. This research strives to foster a greener and healthier future by promoting a more sustainable and efficient food system.

1.2 Objectives of the research

a) To study the optimization of betalain extraction from dragon fruit peels and gain insights into the stability of betalain across varying pH conditions.
b) To study the properties of hydrogel films made from betalain, xyloglucan, and chitosan, and the in situ incorporation mechanism.
c) To study the practical application and efficacy of intelligent packaging, employing betalain as an indicator, in the quality maintenance of food products.

1.3 Scope of the research

a) Optimization of extraction: Evaluate the effects of pH, temperature, extraction time, and solvent ratio on betalain yield from dragon fruit peels using Response Surface Methodology and assess the stability and color change of the extracted betalain under different pH values.
b) Intelligent-film packaging formation: Understanding the mechanism of interaction between xyloglucan-chitosan-betalain hydrogel.
c) Intelligent-film packaging application: Develop and evaluate the application of intelligent packaging, using betalain as an indicator in food products.

1.4 Keywords

Betalains, Dragon fruit peels, Box-Behnken design, pH change, Intelligent packaging, Xyloglucan-chitosan film, Freshness indicator

1.5 Expected outcome

a) This study is expected to demonstrate that optimizing the extraction conditions of betalain from dragon fruit peels enhances yield. By evaluating the effects of pH, temperature, extraction time, and solvent ratio using Response Surface Methodology, this research will provide a systematic approach to improving betalain extraction efficiency and stability across different pH conditions.
b) The second part of this study will establish that incorporating betalain into xyloglucan-chitosan hydrogel films leads to improved physicochemical properties. This includes interaction mechanisms, which are crucial for the development of

intelligent packaging materials with effective responsiveness to environmental changes.

c) The third part of this study is particularly significant as it develops and evaluates an intelligent packaging system utilizing betalain as a food freshness indicator. The packaging will be tested for its ability to monitor and indicate food quality changes in real time, providing a sustainable and natural alternative for food preservation. This innovation has the potential to enhance food safety and reduce waste by offering a visual and responsive packaging solution.

CHAPTER 2
LITERATURE REVIEW

2.1 Dragon Fruit

Dragon fruit (*Hylocereus spp*) is a fresh fruit derived from plants classified in the Cactaceae family (climbing cacti), originating from the American continent and widely distributed in tropical and subtropical regions (Central and South America). There are several cultivated varieties of dragon fruit, such as *Hylocereus undatus* (red skin with white flesh), *Hylocereus monacanthus* (red skin with red flesh), *Hylocereus costariscensis* (red flesh and skin), and *Selenicereus megaliths* (white flesh with yellow skin) (Ortiz Hernández & Carrillo Salazar, 2012). The super red dragon fruit (*Hylocereus costaricensis*) is a popular choice because of its vibrant color and the widespread belief that it is more potent than other types. Dragon fruit skin can benefit food production and natural food and beverage coloring industries. Additionally, dragon fruit skin can be a raw material for cosmetic manufacturing in the cosmetic industry. In pharmacology, dragon fruit skin can be a natural herbal remedy with antioxidant properties.

Dragon fruit skin contains vitamin C, vitamin E, vitamin A, alkaloids, terpenoids, flavonoids, thiamine, niacin, pyridoxine, cobalamin, phenolics, carotenoids, and phytoalbumin (Jaafar et al., 2009). According to the research conducted by Wu et al. (2006), the advantages of dragon fruit skin lie in its rich polyphenol content, making it a source of antioxidants. Dragon fruit skin is rich in organic acids, proteins, minerals such as potassium and magnesium, and vitamin C (Rebecca et al., 2010). Dragon fruit contains nitrogenous betalain pigments. Betalain consist of betacyanins, red-violet pigments with a maximum absorption at 535 nm, and betaxanthins, yellow pigments with a maximum absorption at 480 nm. Red dragon fruit contains the betacyanin pigment, giving it a dark purple.

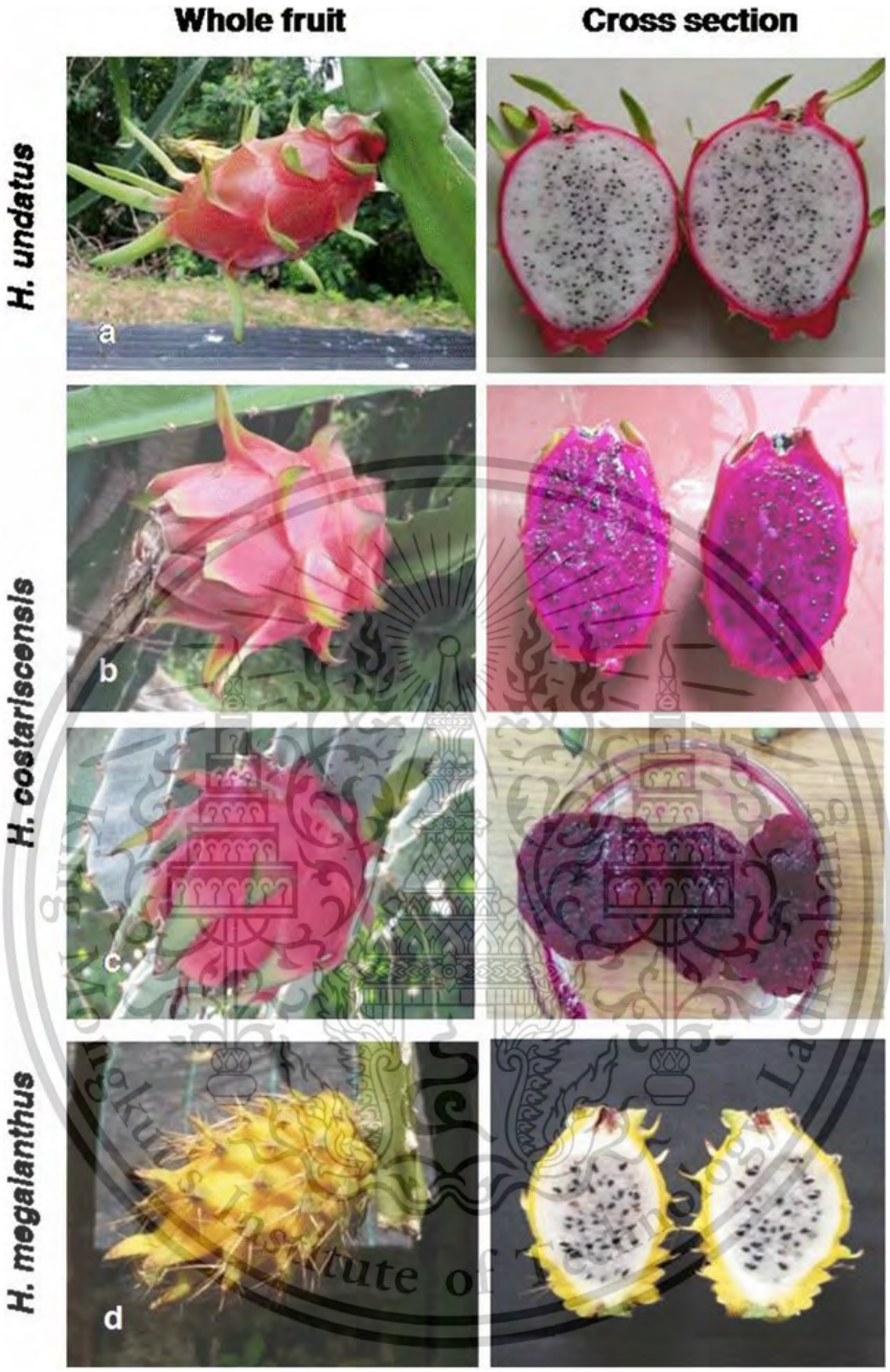

Figure 1 Various type of dragon fruit (a) H. undatus (b,c); H. costariscensis—and H. megalanthus (d). (Abirami et al., 2021).

2.2 Betalain

Betalain is a group of water-soluble pigment compounds with a nitrogenous group. This pigment is a product of tyrosine amino acid synthesis, divided into two groups based on residue attached in betalamic acid, betacyanin that have reddish-purple color, and betaxanthin, that have yellowish color (H. M. C. Azeredo, 2009). Betalamic acid is the chromophore common to all betalain pigments. Betacyanin is a derivative of betalamic acid condensated with cyclo-DOPA (cyclo-dihydroxyphenylalanine), betaxanthin, on the other hand, contains amine side chain or different amino acids (Strack et al., 2003). Betalain has maximum absorbance at around 480-540 nm, whereas betacyanin has maximum absorbance at 540 nm (violet) and Betaxanthin at 480 nm (Herbach et al., 2006c). This shift absorption was due to the closed structure of cyclo-Dopa condensed in betalamic acid. Therefore, the electronic resonance expanded to the phenolic aromatic ring (Strack et al., 2003).

Betalain sources include red, amaranth, swiss chard, yellow beetroot, and cactus pea(Stintzing & Carle, 2007). While red beetroot is the primary commercial source of betalain pigments, its utilization as a natural food dye is restricted due to the presence of geosmin and pyrazine, imparting an earth-like taste sensation (Moßhammer et al., 2005). Yellow beetroot, known for betaxanthin content, remains unsuitable for commercial betaxanthin pigment sourcing due to its susceptibility to oxidation (Stintzing et al., 2005).

In contrast, dragon fruit emerges as an alternative commercial source of betalain, both from its flesh and skin, as it exhibits a range of vibrant colors. (Wybraniec et al., 2001) Conducted pigment compound identification in red dragon fruit using an extraction method involving 80% ethanol (1:2 w/v) at room temperature, followed by concentration at 25°C. Subsequently, HPLC (High Performance Liquid Chromatography) was employed for pigment characterization, revealing six betalain components: betanin, isobetanin, phyllocactin, isophyllocactin, hylocerenin, and isohylocerenin.

Betalain have a more consistent color across a broad pH range than anthocyanins (between 3 and 7). Their betacyanins are degraded at higher pH levels so that Betalain will turn orange at pH 8–9 and yellow at pH 10–12. Because of their ability to change color based on pH, betalain have found use as a promising indicator in innovative halochromic packaging. Due to their antioxidant properties, these all-natural, eco-friendly dyes are also helpful for preserving fatty foods like meat in packaging (Priyadarshi et al., 2021).

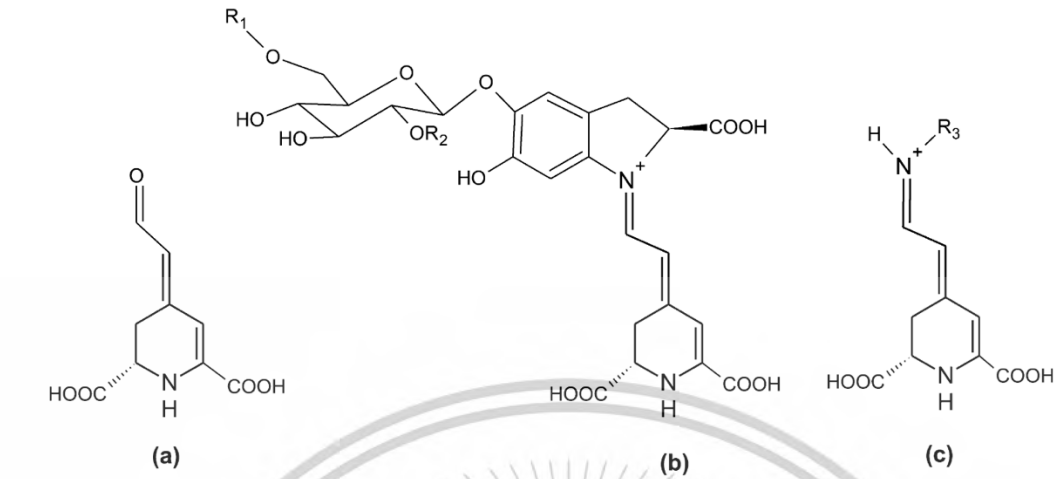

Figure 2 General structure of betalain (a) betalamic acid, (b) betacyanin, (c) betaxanthin. Betanin: R1 = R2 = H R3 = amine or amino acid group (Strack et al. (2003) as cited in (Azeredo, 2009)

However, betalain are highly sensitive, as their properties and coloring power are affected by various variables. Temperature is one of the most influential factors on betalain because of how readily it alters their structure (Prieto-Santiago et al., 2020). The introduction of oxygen, light, metal cations, oxidizing agents, and degrading enzymes hastens the degradation of the pigment. In contrast, betalain that have undergone extensive glycosylation and acetylation, are exposed to nitrogen-rich environments, have low water activities, and are surrounded by metal chelators and antioxidant compounds are more likely to be stable (Calva-Estrada et al., 2022; Kanatt, 2020)

Betalain have been utilized as natural food colorants. Betalain extract from beetroot has been acknowledged as a natural colorant and designated as GRAS, with code E162. This means that the European Union permitted Betalain from beetroot, which is considered safe as a natural colorant (Basavaraja et al., 2022). Therefore, the utilization of Betalain in several application forms, especially in food, is not limited. Hence, Betalain has excellent potential to become the source of a freshness indicator since the specific conditions can alter the properties of Betalain related to the deterioration of food products.

The chromatic behavior of betalains is governed by structural modifications in their conjugated electron systems. These pigments consist of betalamic acid linked to cyclo-DOPA (betacyanins) or amino acids/amines (betaxanthins), where protonation/deprotonation of carboxyl and amine groups under varying pH alters resonance structures, shifting absorption

spectra (Nowacka et al., 2021). In acidic environments, protonation strengthens the electron-sharing structure within betalamic acid, the core component of betalains. This stabilizes the molecule's light-absorbing properties, enhancing red-violet colors in betacyanins by maintaining their resonance system—a network of alternating single and double bonds critical for color intensity (Gandía-Herrero & García-Carmona, 2013). Betalamic acid's structure (4-(2-oxoethylidene)-1,2,3,4-tetrahydropyridine-2,6-dicarboxylic acid) relies on this resonance to produce color, with protonation preserving its conjugated electron system. At higher pH levels, deprotonation (loss of H^+ ions) disrupts the resonance system, altering the molecule's ability to absorb light. This shifts the color toward yellow-orange due to structural rearrangements in betalamic acid. The key transition occurs near pH 6.8, where deprotonation reduces the pigment's free radical-scavenging ability and changes its spectroscopic properties (Khan, 2016). For example, the absorption peak of betacyanins shifts from 530 nm (red) to longer wavelengths, causing visible color fading (H. M. C. Azeredo, 2009). However, environmental factors such as light exposure and thermal processing can induce degradation through oxidation pathways, particularly in betacyanin-rich tissues.

Even stable betalains degrade under light or heat. Light exposure generates reactive oxygen species that break down betalamic acid's structure, while thermal processing accelerates hydrolysis of the bond between betalamic acid and cyclo-DOPA. Betacyanins, despite their initial stability, are particularly vulnerable in high-light or high-temperature conditions (Nowacka et al., 2021).

2.3 Extraction of Betalain

Betalain can be extracted from various sources using different processes. Since Betalain is a water-soluble pigment, it can be extracted using water, ethanol, methanol, or another polar solvent for maceration or ground. However, an acidic extraction solvent results in better Betalain pigment stability than other solvents. Since more than twenty years ago, various studies have been conducted regarding the extraction of betalain pigments using various methods. (Wiley & Lee, 1978) used the diffusion extraction method, while their other work used the solid-liquid extraction method (Lee & Wiley, 1981). On the other hand, the ultrafiltration method has been introduced by (Bayindirli et al., 1988). Delgado-Vargas et al., 2000) found that rapid and brief heating increased the yield of pigment extraction and prevented enzymatic degradation of Betalain. Heating can damage the cell wall and increase

the permeability of cell membranes, thus allowing maximum pigment extraction (Rastogi et al., 1999, quoted in Azeredo, 2009).

Research by Harivaindaran, Rebecca, and Chandran (2008) showed that the optimal condition for extracting Betalain from red dragon fruit peel using water as a solvent is heating at 100°C for 5 minutes at a pH of 5. This extraction produces isobutane (an isomer of betaine) with a pigment content of 25. 74 mg/L. Research conducted by Liaotrakoon et al. (2013) supported this finding, in which heating increased the color, antioxidant, and physicochemical properties in red and white dragon fruit flesh pulp. Heating helps the dragon fruit cell walls melt, allowing its bioactive components to be extracted optimally.

Some other studies have been conducted to extract Betalain using advanced methods. However, due to the nature of Betalain, several factors, such as temperature, pH, and extraction time, should be considered. The use of a solvent, enzyme, and the application of non-conventional methods such as ultrasonic-assisted (Ahmad et al., 2015), microwave-assisted (Cardoso-Ugarte et al., 2014), or pulse-electric fields (López et al., 2009) may be considered. However, their method required advanced instruments and a high price, although the extraction yield might be higher than the conventional method.

2.4 Tamarind Seed kernel

Tamarind seed kernel is a product from the tamarind industry that took the fruit pulp in various processing for foods, cosmetics, textiles, pharmaceuticals, and confectionaries. These seeds have flat, glossy, and have an orbicular to rhomboid shape, measuring about 3-10 cm x 1.3 cm. They are dicotyledonous seeds. The seeds are complex and have a reddish-to-brownish-purple color. The seed cavity is lined with a parchment-like membrane. The cotyledons are thick. The size of tamarind seeds varies between 320-700 g per kg of fruit. Tamarind seeds consist of the seed coat or testa (20-30%) and the kernel or endosperm (70-75%) (Mercy et al., 2019).

India is the leading country producing tamarind, followed by Thailand, Bangladesh, Sri Lanka, and Indonesia. However, India's primary producer, tamarind, is cultivated in more than 54 countries worldwide. From the whole tamarind fruit, around 34% of the total weight of the fruit is tamarind seed and can be considered as a by-product of commercial industries for various purposes (Mansingh et al., 2021).

Figure 3 Tamarind and tamarind seed kernel

2.5 Xyloglucan

Xyloglucan, present in the primary cell walls of numerous higher plants, is a polysaccharide consisting of beta-1→4 linked D-glucan units with xylose substituted for one of the glucan units. The use of xyloglucan as a food additive and as an excipient for drug delivery has been approved by the FDA and is generally considered safe (GRAS) (Dutta et al., 2020; Mishra & Malhotra, 2009). Depending on the source of xyloglucan, the xylose units are further substituted with galactose, and it was discovered that the sol–gel transition temperature of xyloglucan formulations decreased as the galactose removal ratio increased (Brun-Graeppi et al., 2010). Almost 75% of the glucose residues in tamarind seed xyloglucan are substituted with α (1→6) linked xylose side residues with an additional β (1→2) linked galactose residue in some of these xyloses (FRY, 1989; Gidley et al., 1991; Urakawa et al., 2002). The molecular weight (Mw) of xyloglucan in tamarin seed kernel was reported to be around 650.000 to 2.500.000 (Lang & Kajiwara, 1993; Muller et al., 2011; Picout et al., 2003), which is much larger compared to the other wood-derived hemicelluloses that have low molecular weights in around 10,000 – 50,000 Da (Hansen & Plackett, 2008).

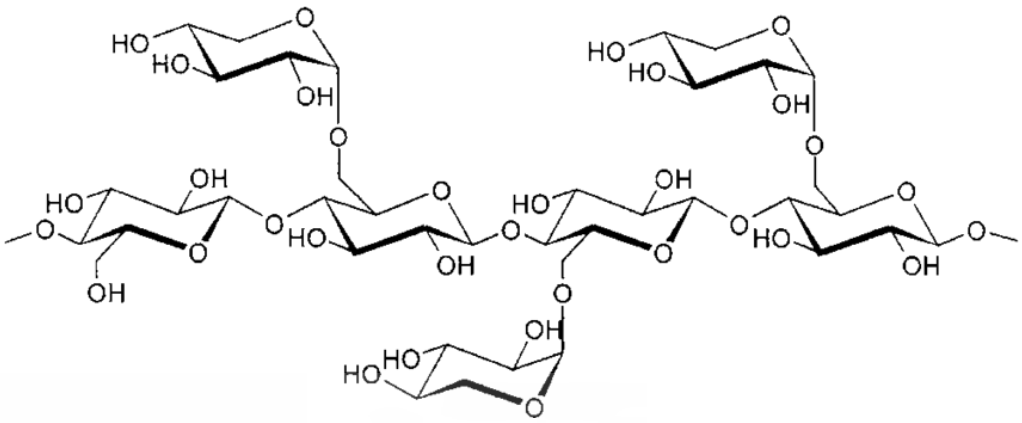

Figure 4 Structure of xyloglucan (Ebringerova (2005) in (Di Donato et al., 2014))

Four oligosaccharides, with varying numbers and distribution of galactose residues, serve as the fundamental repeating units of tamarind seed xyloglucan. These units are conveniently denoted as XXXG, XLXG, XXLG, and XLLG, where X represent aα-1,6 xylosyl, X represent a glucosyl residue, and L represent a β -1,2 galactosyl residue (L). The relationship between b(1→4) and Glcp residues occurs implicitly, where when written sequentially, the reducing end is placed on the right, similar to a cellulose chain (Ravachol et al., 2016).

2.6 Intelligent Packaging

Several types of foods have limited shelf life. However, until today, there are several methods to increase its shelf life. One of them is food packaging with different types of materials sources. Food packaging has different functions and can be divided into four different functions; there are containment, protection, communication, and convenience for the products (Robertson, 2013). In the last decade, studies about improving food packaging have been conducted. There are new technologies and innovations in food packaging, such as active packaging, intelligent packaging, nanotechnologies, biopolymers, and biosensors. Packaging designed to intentionally release or absorb substances into, or from, the food or its surroundings to increase its shelf life or maintain or improve its condition is considered "active packaging" (Day & Potter, 2011). These active packaging can be divided into several types based on the specific substance that is released or absorbed; there is, oxygen scavenger, carbon dioxide scavenger, moisture absorber, ethylene absorber, flavor absorber, odor absorber, stain remover, carbon dioxide emitter, ethanol absorber, antioxidants, as well as maintain temperature control and be responsible for temperature changes (Day & Potter, 2011).

Oppositely, intelligent packaging has a different definition than active packaging. Robertson, (2013) has defined intelligent packaging as the packaging with an indicator on it, whether inside the packaging or externally put outside the packaging, that is intended to show specific information about the condition of the packaging and/or the quality of food stored inside the packaging. Intelligent packaging is a sensor that can monitor food quality and safety and also to predict the shelf life of food (Yam et al., 2005). The model of packaging function related to active and intelligent have been described by Yam et al., (2005), as shown in figure 5.

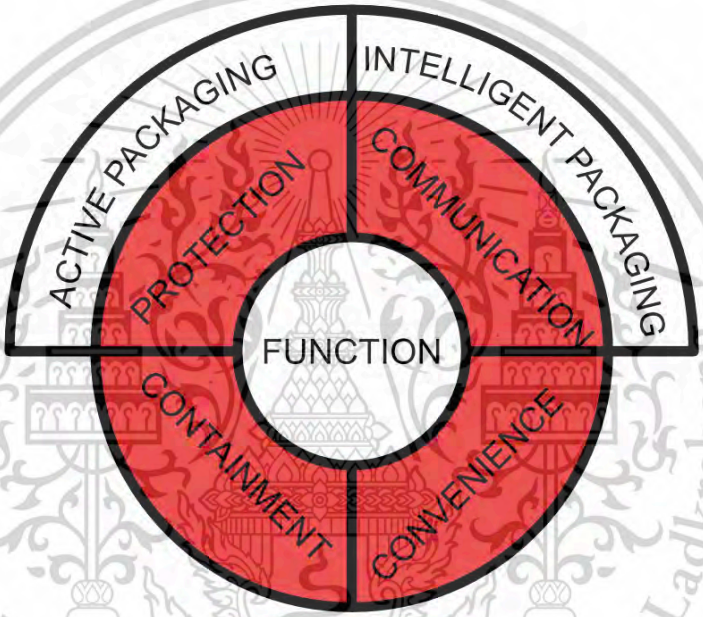

Figure 5 Packaging function model (Yam et al., 2005).

In application, intelligent packaging used indicator or sensor that stored internally inside the packaging near the head-space or attached in the closure. For example gas indicator (Mohammadian et al., 2020), humidity indicator (Pereira et al., 2020), microbial growth indicator (Heredia et al., 2016), and time and temperature indicator (J. Yang & Xu, 2021).

Humidity sensors play a crucial role in smart packaging, serving as monitoring devices for relative humidity conditions to assess food quality by detecting changes in water content (Pereira et al., 2020). These sensors are widely used due to their ease of application and compatibility with conventional food packaging systems. For instance, a humidity sensor based on folic acid and graphene oxide has been developed using a chitosan/polyvinyl alcohol matrix for packaging applications (Moustafa et al., 2023). Additionally, humidity sensors can be integrated with electronic systems to provide consumers with real-time information.

Notably, wireless humidity sensors incorporating planar inductors and capacitors on paper substrates have been explored (Tan et al., 2007) Furthermore, the combination of humidity sensors with radio frequency identification (RFID) technology has been investigated to enable wireless monitoring (Deng et al., 2018; Sipilä et al., 2016)

The proliferation of microorganisms in food products can impact quality in two distinct ways. First, non-pathogenic microbes naturally present in the supply chain can cause spoilage, thereby compromising product quality. Second, pathogenic microorganisms, such as Listeria and Campylobacter, which may be introduced through contamination during production or distribution, pose significant public health risks (Jay et al., 2005). As a result, microbial detection is essential in food safety monitoring systems. Traditional methods, such as culture-based assays and molecular techniques, are often costly, time-consuming, and require sophisticated laboratory equipment, limiting their field applicability (Law et al., 2015). To overcome these challenges, lateral-flow strip technology (LFTS) has been developed as a cost-effective and practical alternative (Luo et al., 2020; Ramos et al., 2017; Tominaga, 2018). This method utilizes gold or magnetic nanoparticles conjugated with specific antibodies to detect target bacteria. When a food sample is applied to the strip, a complex forms between the bacterial cells and the nanoparticles, producing a visible colored line in the detection zone. Given its rapid detection capability, ease of use, and non-destructive nature, LFTS represents a promising approach for large-scale implementation in the food industry.

Another widely applied intelligent packaging technology is time-temperature indicators (TTIs). These indicators function by displaying color changes based on storage time and temperature conditions, allowing the assessment of potential quality degradation due to improper storage. (Gurunathan, 2024). TTI systems can be categorized into three main types: critical temperature indicators, critical time-temperature indicators, and full-history indicators. Critical temperature indicators are designed to detect temperature changes exceeding a reference value within a specific time frame, which can affect the organoleptic quality of food (Pennanen et al., 2015). These indicators typically exhibit an irreversible color shift. For example, Freshtag™, developed by Vitsab™ International AB, utilizes enzymatic reactions to trigger a color change (e.g., orange) when food is exposed to temperatures above the reference limit, indicating possible spoilage (*Freshtag by Vitsab | Freshtag 4 your business*, n.d.). On the other hand, critical time-temperature indicators account for both time and temperature exposure, providing information about food quality when it has been stored above the reference temperature for a prolonged period. Meanwhile, full-history indicators continuously monitor temperature fluctuations throughout the product's lifecycle, recording irreversible changes that

consumers can interpret regarding the product's safety and quality. These indicators are particularly valuable in the food industry due to their compact size, cost-effectiveness, and simplicity compared to other monitoring devices (Pandian et al., 2021; J. Yang & Xu, 2021; L. Yang et al., 2025).

Figure 6 Example of TTIs application

Several researchers have contributed to developing intelligent packaging with different approaches and applications and can be found in Table 1.

Table 1 Example of Intelligent Packaging and Applications in Food Freshness Monitoring

Approach & Application	Key Findings & Contributions	Study
pH-sensitive indicator for food freshness monitoring	Developed pH-sensitive paper with alizarin for rainbow trout fillet freshness monitoring.	Ezati et al., (2019)
Intelligent gelatin films with anthocyanin from natural sources	Utilized butterfly pea anthocyanin as an effective pH indicator in packaging films.	Narayanan et al., (2023); Rawdkuen et al.,(2020)
Nanocomposite biopolymer film with pH-responsive indicators	Nanofiber films with anthocyanins for freshness monitoring and preservation.	Tavassoli et al., (2022).
Natural coloring extracts for freshness indicators	Explored various natural colorants like anthocyanin, alizarin, naphthoquinone, curcumin, and betalain for food packaging.	Echegaray et al., (2023)
Betalain-based freshness indicators	Incorporated Betalain into natural polymers, including polyvinyl alcohol, for effective food freshness monitoring.	Halloub et al., (2023); Qin et al., (2020a).
Electrospun nanofibers with colorimetric indicators	Developed PVA/chitosan nanofibers with curcumin for intelligent food packaging.	B. Li et al., (2025)
Smart packaging with natural extracts for meat freshness	Incorporated purple sweet potato extracts into chitosan films for pork freshness monitoring and cherry preservation.	Ke et al., (2024)
Smart packaging with QR Code on packaging	Implemented QR codes on packaging for enhanced traceability and consumer information access.	Tarjan et al., (2014)
Time-temperature indicators for cold chain monitoring	Developed irreversible time-temperature indicators based on enzymatic reactions for cold chain management.	Pandian et al., (2021)
RFID-enabled intelligent packaging for supply chain management	Utilized RFID technology for real-time monitoring and tracking of perishable goods.	Wisudawaty et al., (2024)

CHAPTER 3
MATERIAL AND METHODS

3.1 Materials

Main material used in this research was dragon fruit peels waste, tamarind seed kernel powder, and chitosan. Dragon fruit peels was collected from Ladkrabang, Bangkok (Thailand). The peels were reduced to 2 cm long and dried in a 50 × 70 cm tray drier (Model: PG-93, Progress Electronic Co., Ltd., Thailand) at 55°C until the weight is constant. The dried dragon peel fruit then was grounded into a powder using a lab-scale grinder (Model RT-04, Mill Powertech, Taiwan) and sieved to obtain a uniform particle size, which was used as a substrate for the extraction of betacyanin. Tamarind seed kernel powder was obtained from Pinphet Co., Ltd., Thailand, chitosan extracted from shrimp shell was produced by Ta Ming Enterprise Co., Ltd., Thailand.

3.2 Chemicals

The chemicals that was used in this experiment are as follows:

- Hydrochloric Acid - Fisher Scientific, Usa
- Potassium Chloride - Sigma-Aldrich, Usa
- Tri-Sodium Citrate Dihydrate - Fisher Chemical, Usa
- Citric Acid - Loba Chemie, India
- Potassium Di-hydrogen Phosphate - Kemaus, Australia
- Di-sodium Hydrogen Phosphate Anhydrous - Kemaus, Australia
- Sodium Tetraborate - Kemaus, Australia
- Hydrochloric Acid - Loba Chemie, India
- Sodium Bicarbonate - Kemaus, Australia
- Sodium Hydroxide - Kemaus, Australia
- Potassium Chloride - Merck, Germany
- Isopropyl Alcohol - World Chemical Group, Country Not Specified
- Sodium Acetate - Kemaus, Australia
- Acetic Acid - Merck™, Germany
- Sodium Carbonate Anhydrous - Q Rëc™, Australia
- Hydrochloric Acid - Fisher Scientific, USA

- Potassium Chloride - Merck™, Germany
- Filter Paper 90 Mm, No.1 - Whatman, USA
- Luria Bertani Broth - Himedia, India
- Luria Bertani Agar - TM Media, India
- Plate Count Agar - Himedia, India
- Mueller Hinton Agar - Himedia, India
- Mueller Hinton Broth - Himedia, India

3.3 Instruments and Equipments

Table 2 List of equipment used in this research

Name	Model Brand	Country of Origin
Tray drying	PROGRESS ELECTRONIC CO., LTD.	Thailand
Centrifuge	5810 Eppendorf	Hamburg, Germany
Colorimeter	ColorQuest XE HunterLab	USA
Colorimeter	Konica Minolta CR-400	Japan
Desiccator	Local Brand	Thailand
Distillation system	Vapodest 30S, Gerhardt GmbH & Co	Germany
FTIR	Nicolet 6700, Thermo Scientific	Waltham, MA, USA
Moisture analyzer	HX 204, Mettler Toledo	Switzerland
Magnetic stirrer	Fisher Scientific	USA
Micrometer	Mitutoyo No. 293–766, Tester Sangyo Co., Ltd.,	Tokyo, Japan
Rheometer	Physica MCR 301 rheometer, (Anton Paar TA Instruments Inc	New Castle, DE, USA
SEM	Apreo S, Thermo Fisher Scientific	Waltham, MA, USA
Texture Analyzer	TA.XT2i, Stable Micro Systems	Godalming, UK
UV-Vis spectrophotometer	Shimadzu UV1800	Kyoto, Japan
Zetasizer	Nano ZS, Malvern Zetasizer	Thailand
Contact angle meter	Dataphysics OCA20	Germany
Turbidity meter	TurbiCheck TB 211 IR (Lovibond)	Germany

Table 3 List of equipment used in this research (cont.)

Name	Model Brand	Country of Origin
pH meter	Mettler Toledo pH meter model AG 8603, Greifensee,	Switzerland

3.4 Methodology

This study was divided into three major sections. The first section involved optimization of betalain from dragon fruit peel waste using safe and environmentally friendly method. The second section investigating the mechanism of interaction between xyloglucan, chitosan, and betalain. The third section involved producing intelligent film from a combination of xyloglucan, chitosan, and betalain, and the application of intelligent packaging film in food products.

3.4.1 Optimization of Extraction: Evaluate The Effects of pH, Temperature, Extraction Time, and Solvent Ratio on Betalain Yield

3.4.1.1. Experimental Design and Optimization of Betalain Extraction

Betacyanin extraction was conducted according to Kushwaha et al., (2018) with modification. Powdered dried dragon fruit peels was mixed with distilled water of varying pH (2.0–6.0) at different solid-to-liquid ratios (1:15–1:40 by weight) and kept in a water bath at various temperatures (30–60°C) for different times (10–60 min). The material was then centrifuged for 15 minutes at 9,000 rpm. The supernatant was collected, sealed, refrigerated in amber-colored vials, and examined on the same day as the extraction.

Box-Behnken Design was used to optimize the extraction yield of betacyanin from dragon fruit peels with four factors at three levels (-1, 0, and +1). The extraction variables (pH, temperature, time, and solid-to-liquid ratio) are considered because it is known that they affect the extraction method. Minitab Statistical Software (version 16.0; Minitab et al., Australia) was utilized to assess the experimental design and statistical analyses.

3.4.1.2. Quantification of Betacyanin Content

Betacyanin extracted from dragon fruit peels then diluted with phosphate buffer (0.1 M) pH 6.5 and measured at 538 nm wavelength using a UV-1800 spectrophotometer (Shimadzu, Japan), and calculated using the following equation:

$$\text{Betacyanin (mg/L)} = (A \times MW \times DF \times 1000)/(\varepsilon \times L) \quad \text{(Eq 1)}$$

A is absorption, DF is the dilution factor, and L is the cuvette path length (1 cm). Molecular weight (MW) and molar extinction coefficient (ε) was applied (MW538 = 550 g mol−1; ε538 = 60,000 L mol−1 cm−1) (Kushwaha et al., 2018).

3.4.1.3. Effect of pH on Betalain Extracted From Dragon Fruit Peels

The influence of pH on betalain color changes was evaluated over a pH range of 2.0 to 13.0. The betacyanin extract was diluted with distilled water to a final volume of 5 mL and then transferred to plastic cuvettes containing buffer solutions of different pH values. After adding the betacyanin extract to the buffer solutions, the mixture was equilibrated for one h. Spectrophotometry, color, and infrared spectroscopy was performed on the stabilized solutions.

3.4.1.4. Color Change and Measurement of Betalain in Different pH

The maximum absorbance of the extract at various pH values was measured using a UV-1800 spectrophotometer (Shimadzu, Japan) at 350 – 700 nm at 2 nm intervals. The changes in the color of betalain extract at various pH values was measured using the ColorQuest XE from HunterLab (USA) (do Carmo Brito et al., 2017). The resulting data was analyzed to determine the effect of pH on the color changes of the betacyanin extract. The overall color difference (∆E) was calculated using the following equation:

$$\Delta E^* = \sqrt{(\Delta L^*)^2 + (\Delta a^*)^2 + (\Delta b^*)^2} \quad \text{(Eq. 2)}$$

Where ΔE is the overall color difference, and ΔL*/Δa* /Δb* is the difference in the L*/a*/ b* values between the compared samples.

3.4.1.5. Fourier Transform Infrared (FTIR) Spectroscopy of Betacyanin Extract

The functional group changes in the betacyanin extract at different pH values was observed using Fourier-transform infrared spectroscopy (FT-IR) (Nicolet 6700, Thermo Scientific, Germany). Attenuated total reflectance –Fourier transform infrared (ATR-FTIR) analysis was performed at 400 – 4000 cm^{-1} wavelengths.

3.4.1.6. Statistical Analysis

The experimental data was analyzed using multiple regression analysis and analysis of variance (ANOVA). The ANOVA tables generated to present the results. The adequacy of the models was tested using the coefficient of determination (R^2) and adjusted coefficient of determination (Adjusted R^2). The models was fitted, and the generated data was used to plot the response surfaces and contour plots. Minitab Statistical Software (version 16.0; Minitab Pty Ltd, Australia) was used for all statistical analyses.

3.4.2 Intelligent-Film Packaging Formation: Understanding The Mechanism of Interaction Between Xyloglucan-Chitosan-Betalain Hydrogel.

3.4.2.1. Betalain Extraction

Betalain was extracted according to Permana et al. (2024). Briefly, dried dragon peel fruit powder was mixed with distilled water at pH 3.2 with solid-to-liquid ratio of 1:15 in centrifuge tube. Then the tube was placed in a 30 °C water bath for 10 minutes. A Centrifuge (Eppendorf 5804R Centifuge, Germany) set at 9780 g for 15 min was used to separate the supernatant. The supernatant was labelled as extracted betalain and stored in closed amber-colored vials under refrigerated conditions before use.

3.4.2.2. Preparation of Xyloglucan from Tamarind Kernel Powder

In order to prepare the xyloglucan analysis, several steps are followed, according to (Adair et al., 2023). A mixture of distilled water and the defatted TKP was prepared at a ratio of 1:10. To achieve the desired pH of 4.5, and citric acid was added to the mixture, which is subsequently stirred for 45 minutes at room temperature. The resulting solution will then be centrifugated at 6000 rpm for 10 minutes. Afterward, the TKP cake obtained from the centrifugation process was mixed with distilled water at a ratio of 1:40 and stirred at a temperature range of 85-90°C for 30 minutes. Once again, the centrifugation step was carried out. A 95% alcohol at a ratio of 1:1.5 was used to precipitate the supernatant of two times centrifugations. The resultant fibrous precipitate was filtered and dried at 50°C for 24 hours in a hot-air oven. Finally, the dried xyloglucan was finely powdered and stored in a desiccator for future use.

3.4.2.3. Preparation of Betalain Xyloglucan-Chitosan Hydrogel

The xyloglucan-chitosan film-forming solution preparation was adapted from Adair et al. (2023), as illustrated in the Figure 7. The extracted betalain was used to study the interaction between xyloglucan, chitosan, and betalain. 1 g of xyloglucan powder was dissolved in 10 mL distilled water, heated to 85 °C, and stirred for 15 min. Subsequently, 25 mL of 4% (v/v) acetic acid was added, and the mixture was stirred using an overhead stirrer (RW20 Digital, IKA, Germany) at 220 rpm for 30 min. In parallel, a chitosan solution (1%, w/v) was prepared by dissolving 0.25 g of chitosan in 25 mL of 4% (v/v) acetic acid. After complete dissolution, this solution was set aside until further use. EB was added to the prepared xyloglucan solution at varying volumes to achieve different concentration ratios. Specifically, 3, 5, and 7 mL of extracted betalain were gradually added to the xyloglucan solution These formulations corresponded to weight/volume ratios of 1:3, 1:5, and 1:7, respectively, and were designated as XC-EB3, XC-EB5, and XC-EB7. The mixture was stirred at 220 rpm for 10 min at room temperature to ensure uniform dispersion.

The previously prepared chitosan solution was then added to each xyloglucan-betalain mixture and stirred at 220 rpm for 10 min. Glycerol (35% w/w of total solid content, based on the combined weight of xyloglucan, chitosan, and betalain) was then incorporated, and the solution was stirred for 5 min at room temperature to achieve a homogenous film-forming solution.

3.4.2.4. Mechanism Interaction of Xyloglucan, Chitosan, and Betalain

3.4.2.4.1. Zeta Potential

Zetasizer (Nano ZS, Malvern Zetasizer Thailand) was used to measure the zeta potential of the film hydrogel to undersand the interaction between betalain, xyloglucan, and chitosan. The samples were diluted 10-fold in deionized water and analyzed at 25 °C using a disposable folded capillary cell (DTS1070) with an applied voltage of 150 V. Two min equilibration time in 25 C room temperature was set before the measurement. The experiment was repeated three times to confirm the results and find the average zeta potential.

3.4.2.4.2. Fourier Transform Infrared (FTIR) Spectroscopy

Functional group of film hydrogel were observed using Fourier-transform infrared spectroscopy (FTIR) (Invenio S, Bruker, Massachusetts, USA). For each solution, a wavelength of a wavelength of 400 – 4000 cm−1 with 32 scans at 4 cm-1 resolution was used.

3.4.2.5. Characterization of Xyloglucan, Chitosan, and Betalain Hydrogel

3.4.2.5.1. Rheological Property

The rheological characteristics of the freshly prepared film solutions were evaluated at 30°C using a Physica MCR 301 rheometer (Anton Paar TA Instruments Inc., New Castle, DE, USA), equipped with a concentric cylinder system with a gap width set to 1 mm. Stress sweep measurements were initially conducted to ensure data reliability within the linear viscoelastic strain region. Subsequently, dynamic frequency sweep tests were performed by applying a constant strain of 1%, which fell within the linear region, across a frequency range of 0.1 to 100 rad/s.

3.4.2.5.2. Antimicrobial Properties of Film Forming Solution

The antimicrobial susceptibility of the films was evaluated against foodborne pathogenic bacteria: *E. coli* and *S. aureus*. Bacterial strains were cultured in LB broth at 37°C for 24 hours prior to use. Minimum inhibitory concentration (MIC), and minimum bactericidal concentration (MBC) analyses were performed according to the Clinical and Laboratory Standards Institute (CLSI) protocol (Romainor et al., 2022).

3.4.2.5.2.1. Minimum Inhibition Concentration (MIC)

The Minimum Inhibitory Concentration (MIC) and Minimum Bactericidal Concentration (MBC) of hydrogel samples were assessed using a broth microdilution method. Initially, samples were diluted by mixing 1 mL of the sample with 5 mL of sterile distilled water. These diluted samples were further serially diluted with sterile distilled water to achieve double the final concentration required for testing. The dilutions were prepared in a 96-well plate, with each well containing 50 µL of the sample at ten different concentrations. The bacterial strains *E. coli* ATCC 25922 and *S. aureus* ATCC 25923 were cultured on Mueller Hinton agar at 37°C for 24 hours. A bacterial suspension for each strain was prepared using the direct colony suspension method in a 0.85% NaCl (w/v) solution, adjusted to match the turbidity of McFarland Standard No. 0.5, corresponding to approximately 1×10^8 CFU/mL. From this suspension, 100 µL was further diluted in 9.9 mL of Mueller Hinton Broth (MHB) to achieve a final concentration of approximately 1×10^6 CFU/mL. Subsequently, 50 µL of the bacterial suspension was added to each well containing the hydrogel samples, resulting in a final bacterial concentration of approximately 5×10^5 CFU/mL and halving the hydrogel sample concentration. The 96-well plates were incubated at 37°C for 18 hours. The MIC was defined as the lowest concentration of the hydrogel sample where no growth was observed by

comparing the turbidity in each well with the growth control (containing bacterial suspension and media without the hydrogel sample) and sterility control (containing media and diluent without bacteria).

3.4.2.5.2.2. Minimum Bactericidal Concentration (MBC)

For the determination of the Minimum Bactericidal Concentration (MBC), the wells showing no visible bacterial growth (clear wells) after the incubation period were identified. The contents of these wells were then plated onto Mueller Hinton agar plates and incubated at 37°C for 24 hours. The MBC was defined as the lowest concentration of the hydrogel sample at which no bacterial colonies were observed on the agar plates, indicating complete bacterial killing.

3.4.2.6. Statistical Analysis

All measurements were performed in triplicate and reported as the mean ± standard deviation. One-way analysis of variance with Tukey's Multiple Comparison Test was performed to determine the effect of wall material in different formulations.

3.4.3 Intelligent-Film Packaging Formation: Develop and Characterize Intelligent-Film Packaging Based on The Xyloglucan-Chitosan-Betalain Complex and Its Application.

3.4.3.1. Preparation of Intelligent Packaging Film

The xyloglucan-chitosan film-forming solution preparation was adapted from Adair et al. (2023), as illustrated in the Figure 7. The extracted betalain was used to study the interaction between xyloglucan, chitosan, and betalain. 1 g of xyloglucan powder was dissolved in 10 mL distilled water, heated to 85 °C, and stirred for 15 min. Subsequently, 25 mL of 4% (v/v) acetic acid was added, and the mixture was stirred using an overhead stirrer (RW20 Digital, IKA, Germany) at 220 rpm for 30 min. In parallel, a chitosan solution (1%, w/v) was prepared by dissolving 0.25 g of chitosan in 25 mL of 4% (v/v) acetic acid. After complete dissolution, this solution was set aside until further use. EB was added to the prepared xyloglucan solution at varying volumes to achieve different concentration ratios. Specifically, 3, 5, and 7 mL of extracted betalain were gradually added to the xyloglucan solution These formulations corresponded to weight/volume ratios of 1:3, 1:5, and 1:7, respectively, and were designated as XC-EB3, XC-EB5, and XC-EB7. The mixture was stirred at 220 rpm for 10 min at room temperature to ensure uniform dispersion.

The previously prepared chitosan solution was then added to each xyloglucan-betalain mixture and stirred at 220 rpm for 10 min. Glycerol (35% w/w of total solid content, based on the combined weight of xyloglucan, chitosan, and betalain) was then incorporated, and the solution was stirred for 5 min at room temperature to achieve a homogenous film-forming solution. Each 50 mL of film-forming solution was poured onto a silicone sheet (17 cm × 17 cm) and dehydrated in a humidity chamber (KBF 240, Binder, Germany) at 25°C and 50% RH for 24 h. After drying, the films were carefully peeled off from the silicone sheet and stored in plastic bags with silica gel under refrigerated conditions (4°C, 0% RH) until further analysis

3.4.3.2. Chemical Properties of Intelligent Packaging Film

3.4.3.2.1. Moisture Content

The moisture content (MC) of each film sample was determined using a halogen moisture analyzer (HX 204, Mettler Toledo, Switzerland) according to Pechová et al., (2018). Samples (2.5 cm × 2 cm) were analyzed using the thermogravimetric principle. The pre-weighed specimens were heated to 130°C until they reached a constant weight after 50 seconds.

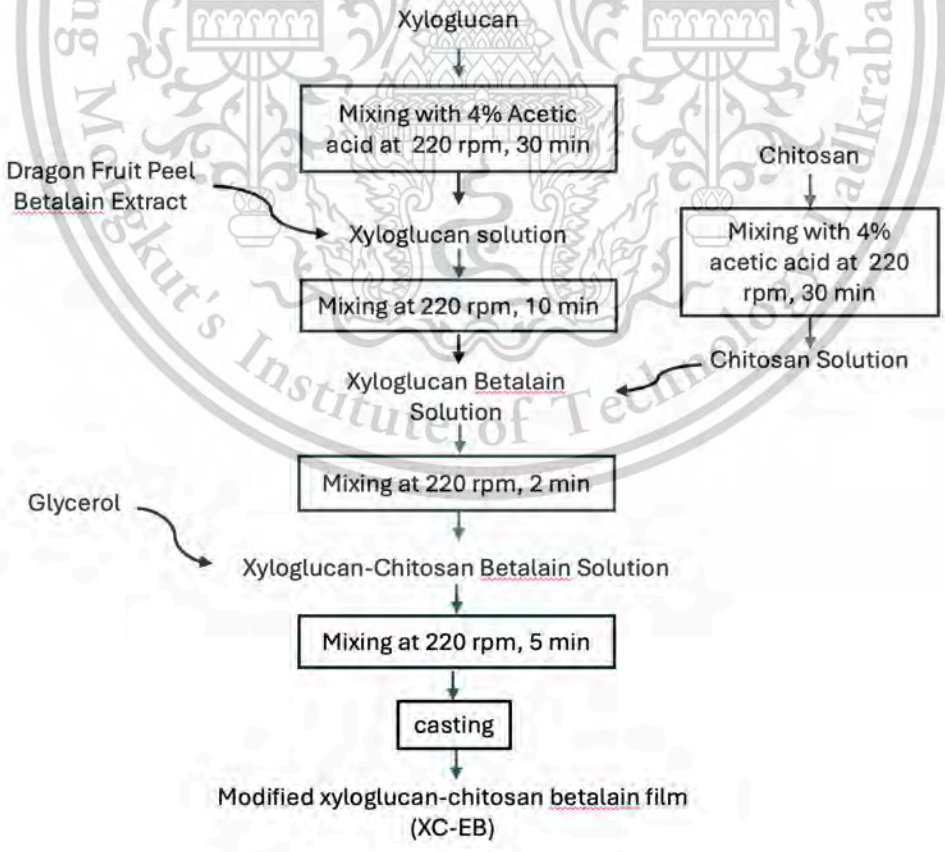

Figure 7 Flowchart of the preparation of modified xyloglucan-chitosan with betalain

3.4.3.3. Physical Properties of Intelligent Packaging Film

3.4.3.3.1. Thickness

The thickness of each film was measured using a micrometer with 0.01 mm resolution (APB-3D 422-230, Mitutoyo, Japan). Five random locations on each film (8 × 8 cm) were measured, and the average value was calculated.

3.4.3.3.2. Surface Morphology Analysis Films via Scanning Electron Microscopy (SEM)

The surface morphology of the films were examined using a field emission scanning electron microscope (Thermo Scientific Apreo S, Thermo Fisher Scientific, Waltham, MA, USA) according to Ke et al., (2024). Prior to imaging, film samples were mounted on aluminum stubs using double-sided carbon tape and sputter-coated with a thin layer of gold using a Quorum Q150T ES plus sputter coater (Quorum Technologies Ltd., Laughton, East Sussex, UK) to enhance conductivity. Micrographs were captured at 2000× magnification using an accelerating voltage of 10 kV.

3.4.3.3.3. Color Measurement of Films

Film color was evaluated under room temperature using a using a Konica Minolta CR-400 Chroma Meter (Konica Minolta Sensing Americas, Inc., Ramsey, NJ, USA). The colorimeter was calibrated with a standard white plate before each measurement. L*, a*, and b* values were recorded, representing lightness, redness/greenness, and yellowness/blueness, respectively. A white sheet of paper was utilized as base for color analysis, as the films were transparent. Total color difference (ΔE) was calculated to assess the overall color change of the films in response to ammonia exposure. The total color difference (ΔE) was calculated using Eq 3.

$$\Delta E = \sqrt{(\Delta L^*)^2 + (\Delta a^*)^2 + (\Delta b^*)^2} \quad \text{(Eq. 3)}$$

3.4.3.3.4. Swelling Index

Different film samples were prepared according to Chaari et al., (2022). Sample was prepared by cutting film into small squares (2 cm × 2 cm). Each sample was weighed before being submerged in water for two minutes (W1). After soaking, the samples were weighed again (W_2). The percentage of swelling index (% SI) was calculated using the following equation:

$$SI\ (\%) = \frac{(W_2 - W_1)}{W1} \times 100 \qquad \text{(Eq. 4)}$$

3.4.3.3.5. Water Contact Angle

The water contact angle (WCA) of the films was measured using a contact angle meter (Dataphysics OCA20, Germany) according to X. Li et al., (2020). Droplets of ultrapure water (10 μL) were placed at three random spots on each film surface. A camera attached to the instrument were used to capture the images and calculate the WCA value.

3.4.3.3.6. Water Vapor Transmission Rate

The water vapor transmission rate (WVTR) of the films was determined according to ASTM E96/E96 M standard as described by Huang et al. (B. Huang et al., 2012) with modification. The films was placed on the test cups containing anhydrous silica gel (0 % RH), sealed with the silicone grease and laboratory film (Parafilm M, Pechiney Plastic Packaging, Chicago, IL), The test cups then placed in a humidity chamber (KBF240, Binder, Germany) and set to standard temperature (25°C and 50% relative humidity). The weight gain of the cups was measured at regular intervals of 1 h for a 24 h period and the WVTR was presented in $g \cdot h^{-1} \cdot m^{-2}$, calculated from the slope of the regression curve of the transmitted moisture content from the film versus of the time. WVP was calculate according to the following equation by using WVTR results:

$$WVTR = \frac{\Delta w}{A\Delta t} \qquad \text{(Eq. 5)}$$

The WVTR value was used to calculate Water Vapor Permeability (WVP) according to the following equation

$$WVP = \frac{WVTR \times x}{\Delta P} \qquad \text{(Eq. 6)}$$

where, WVP ($g.\ m^{-1}.\ h^{-1}.\ Pa^{-1}$), x is the film thickness, and ΔP is the water vapor pressure difference between the inner and outer surface of the film.

3.4.3.4. Mechanical Properties

Mechanical properties, including tensile strength (TS) and elongation at break, were determined using a texture analyzer (TA.XT plus, Stable Micro Systems, Surrey, UK) following the ASTM D882-12 with modification for biopolymer films (Daei et al., 2022). The films were cut into strips with a size of 10 mm × 50 mm, and mechanical tests were conducted at a speed 60 mm/min (1 mm/s). The films were conditioned at standard laboratory conditions (23°C ± 2°C and 50% ± 5% relative humidity) for a minimum of 48 hours before analysis.

3.4.3.5. Ammonia-sensitivities of Film

The ammonia-sensitive properties of the films in response to volatile ammonia were evaluated following the method described by Shuhan et al. with modification (You et al., 2022). Film samples measuring 1 cm × 1.5 cm were positioned at the top of a transparent polyethylene terephthalate (PET) box (15 cm × 15 cm × 10.5 cm) at room temperature. containing 15 mL of 5 mol/L ammonia solution. Color changes in the films were recorded every 10 minutes for a total duration of 60 minutes using a Konica Minolta CR-400 Chroma Meter (Konica Minolta Sensing Americas, Inc., Ramsey, NJ, USA)

3.4.3.6. Application of Intelligent Films to Shrimp Spoilage Detection

The efficacy of films in detecting food spoilage was evaluated using fresh shrimp. A raw, unshelled shrimp was placed near a film sample in a sterile Petri dish and stored 4°C for 8 days. The color values were recorded every 2 days.

Total Volatile Base Nitrogen (TVB-N) was determined according to Standard Nasional Indonesia (SNI) 2354.8:2009 (Badan Standardisasi Nasional, 2009). Briefly, 10 g of food sample was homogenized in 90 mL of 6% perchloric acid for 2 minutes and then filtered to obtain a shrimp filtrate. A 50 mL of shrimp and then placed into distillation tube, and then 3 drops of Phenolphthalein were added into tube, followed by addition of 10 mL of 20% NaOH. The mixture was become alkaline, indicated by the formation of red color. Distillation process were performed using distillation system (Vapodest 30S, Gerhardt GmbH & Co, Germany). The system was programmed with the addition of 41 ml water, 4 mins distillation time, 100% distillation power, and 25 secs suction time after distillation, to obtain 200 ml of distillate. An erlenmeyer containing 100 ml of 3% H3BO4 and 5 drops of Tashiro indicator was used to collect the distillate. The solution was then titrated using a hydrochloric acid solution (0.02 N). The formula for calculating TVB-N (mg/100 g) is:

$$TVB - N\ \left(\frac{mg}{100}g\right) = \frac{(Vc-Vb)\times N\times 14.007\times 100}{m} \qquad \text{(Eq. 7)}$$

where Vc is the volume of hydrochloric acid solution consumed during titration of the sample (mL), Vb is that consumed during titration of the blank control (mL), N is the normality of hydrochloric acid solution, and m is the mass of food sample.

3.4.3.7. Statistical Analysis

All the analysis were performed three times, and the data are reported as mean ± standard deviation. A statistical software, SPSS Statistics 29 (Chicago, IL, USA) was used for ANOVA. Duncan's multiple range tests was used to ensure statistical significance at $p < 0.05$.

CHAPTER 4
RESULTS AND DISCUSSION

Betalains, natural pigments from agro-waste like dragon fruit peels, offer potential as sustainable colorants and pH-responsive indicators for intelligent packaging. However, optimizing their extraction and stabilizing their integration into biopolymer matrices like xyloglucan-chitosan hydrogels remain critical challenges. This study focused on systematically optimize betalain extraction using Response Surface Methodology (RSM) to evaluate pH, temperature, extraction time, and solvent ratio effects on yield, and develop and characterize intelligent films from xyloglucan (tamarind seed waste), chitosan, and betalain for food freshness monitoring.

The extraction process employed Box-Behnken Design (BBD) to identify ideal parameters, while FTIR and colorimetric analyses assessed betalain stability under varying pH. For film development, interactions between xyloglucan, chitosan, and betalain were studied via zeta potential, FTIR, and rheological tests. The resulting hydrogels were processed into films, with properties (mechanical strength, moisture content, ammonia sensitivity) and antimicrobial efficacy evaluated. Finally, the films' real-world applicability was tested in shrimp spoilage detection.

4.1 Optimization of extraction: Evaluate the Effects of pH, Temperature, Extraction Time, and Solvent Ratio On Betalain Yield from Dragon Fruit Peels

4.1.1 Optimization of Betalain Extraction

In our study, we utilized Box-Behnken to establish an optimized model for the extraction process involving four variables: pH (X_1), temperature (X_2), time (X_3), and solvent ratio (X_4). The yield of betacyanin, a betalain pigment responsible for the coloration of dragon fruit peels, was utilized as an indicator. The results in Table 3 show that different combinations of variables produced an actual response yield of 16.81-72.37 mg/L of betacyanin. The extraction yields and predictions for the various treatment combinations are presented in the same table. In Figure 8, the points clustered around the diagonal line indicate that the betacyanin extraction experiments match the model results. This suggests that the model fits the data well, with minimal deviation between the experimental and predicted values.

Table 4 Betacyanin extraction yields for various treatment combinations.

Run	X1: pH	X2: Temp. (°C)	X3: Time (minutes)	X4: Ratio (w/v)	Actual Betacyanin Response (mg/L)	Predicted Betacyanin Response (mg/L)
1	2	45	10	1:27.5	31.62	33.83
2	4	60	10	1:27.5	40.64	38.88
3	6	45	10	1:27.5	38.51	39.51
4	4	45	60	1:40	24.24	25.55
5	6	45	35	1:15	48.17	52.00
6	4	45	10	1:15	72.37	69.14
7	4	30	35	1:15	64.95	65.00
8	2	45	60	1:27.5	34.73	34.19
9	2	45	35	1:40	16.81	14.44
10	2	30	35	1:27.5	35.69	34.73
11	6	30	35	1:27.5	38.50	35.70
12	4	60	60	1:27.5	30.62	30.94
13	4	30	60	1:27.5	35.84	39.06
14	2	60	35	1:27.5	29.33	30.20
15	4	45	35	1:27.5	39.35	35.46
16	4	60	35	1:40	20.82	21.23
17	6	60	35	1:27.5	29.49	28.52
18	4	30	10	1:27.5	41.34	42.48
19	4	30	35	1:40	25.80	25.14
20	2	45	35	1:15	61.38	62.17
21	6	45	60	1:27.5	29.54	27.79
22	4	45	10	1:40	23.26	23.90
23	4	45	35	1:27.5	34.98	35.46
24	4	60	35	1:15	56.08	57.20
25	4	45	60	1:15	58.70	56.14
26	6	45	35	1:40	23.23	23.90
27	4	45	35	1:27.5	32.04	35.46

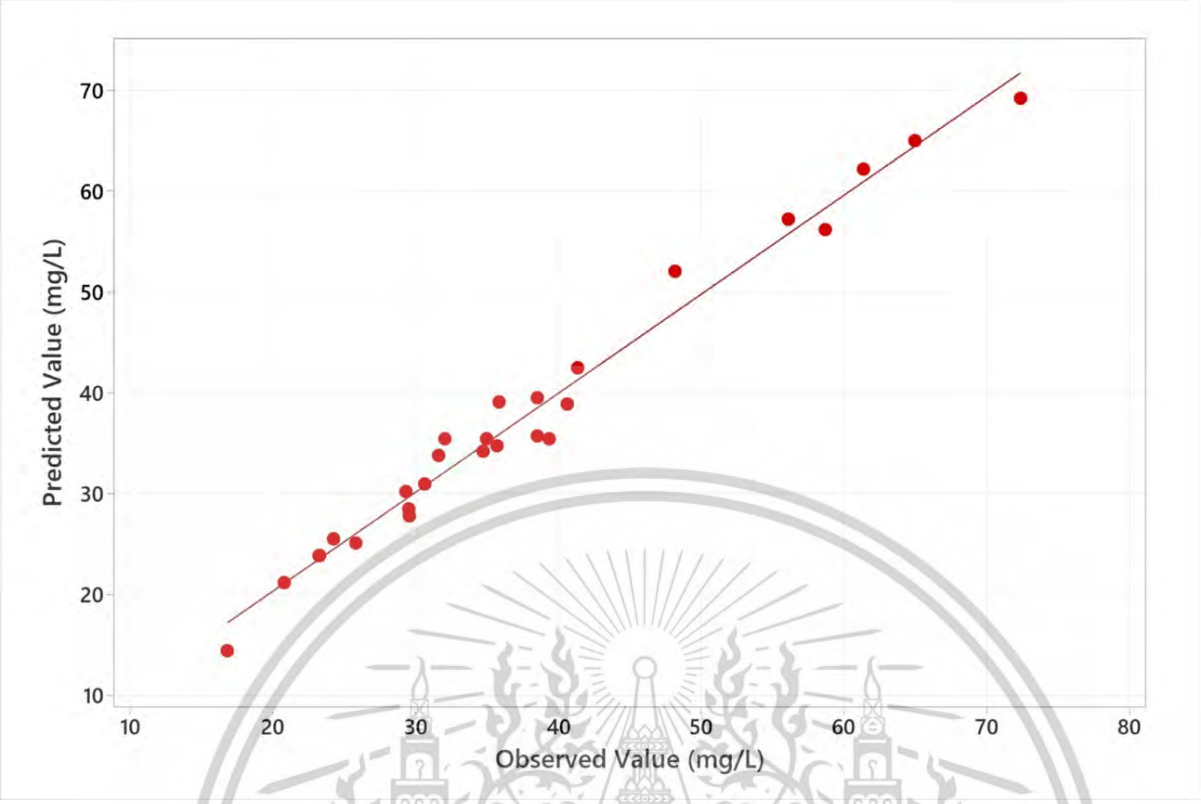

Figure 8 Experimental results of betacyanin extraction versus model results.

The model-fitting findings demonstrate that the data are best described by a second-order polynomial equation that includes the interaction terms. The equations of the model are as follows.

Betacyanin yield (mg/L) = 136.0 + 4.80 X_1 - 0.313 X_2 - 0.278 X_3 - 5.150 X_4 - 0.897 X_1*X_1 + 0.00188 X_2* X_2 + 0.00314 X_3*X_3 + 0.04008 X_4*X_4 - 0.0221 X_1*X_2 - 0.0604 X_1*X_3 + 0.1963 X_1*X_4 - 0.00301 X_2*X_3 + 0.00519 X_2*X_4 + 0.01172 X_3*X_4

R^2 = 0.98 (Eq. 8)

where X_1, X_2, X_3, and X_4 are pH, temperature, time, and ratio, respectively.

The regression coefficients, standard errors, and P-values for Eq. 7 were calculated (Table 4). The quadratic model had an R^2 of 0.98, indicating that the model fits the data (Sriprom et al., 2015). The linear model term of the solid-liquid ratio (X_4) and the quadratic model term of pH (X_1^2) were found to have a significant effect on betalain extraction (95% confidence level,

P-value <0.05). In the model analyzing the interaction effect, pH, ratio (X_1X_4), and time and ratio (X_3X_4) were found to have significant interaction effects.

Statistical analysis using analysis of variance (ANOVA) showed that the model had a high R^2 value of 98.01% and an adjusted R^2 value of 95.69%. This indicates that the model fits the data. The coefficient of determination (R^2) measures how well the model explains the variance in the response (Tekin et al., 2023). At the same time, the adjusted R^2 is a modified R^2 that considers the number of predictors in the model, the value may be smaller than R^2, and the gap should not exceed 0.2 (Czyrski & Sznura, 2019). This result suggests that the quadratic model best fits the data, with the highest adjusted R^2 value.

Table 5 Regression coefficient and P-values for the model of extraction yield

Term	Coefficient	Standard Error Coefficient	P-Value
Constant	136.0	24.4	0.000
PH	4.80	3.90	0.242
Temperature (°C)	-0.313	0.606	0.614
Time (minutes)	-0.278	0.289	0.354
Ratio (w/v)	-5.150	0.643	0.000
PH*PH	-0.897	0.319	0.016
Temperature (°C)*Temperature (°C)	0.00188	0.00566	0.745
Time (minutes)*Time (minutes)	0.00314	0.00204	0.150
Ratio (w/v)*Ratio (w/v)	0.04008	0.00816	0.000
PH*Temperature (°C)	-0.0221	0.0490	0.661
PH*Time (minutes)	-0.0604	0.0294	0.063
PH*Ratio (w/v)	0.1963	0.0589	0.006
Temperature (°C)*Time (minutes)	-0.00301	0.00392	0.457
Temperature (°C)*Ratio	0.00519	0.00785	0.521
Time (minutes)*Ratio	0.01172	0.00471	0.028

The analysis of variance in Table 5 also shows that the quadratic model is the most statistically significant, with a p-value of 0.000 and an F-value of 11.98. This suggests that the quadratic model fits the data better than the linear and 2-Way interaction models do. The lack

of fit was insignificant (p=0.779), indicating that the model adequately fitted the data and captured major trends (Sriprom et al., 2023).

Table 6 ANOVA for experimental data fitting to the response surface

Source	Degree of Freedom	Adjusted Sum of Square	Adjusted Mean Square	F-Value	P-Value
Model	14	5124.65	366.046	42.27	0.000
Linear	4	713.24	178.310	20.59	0.000
Square	4	414.88	103.721	11.98	0.000
2-Way Interaction	6	197.12	32.853	3.79	0.024
Error	12	103.92	8.660		
Lack-of-Fit	10	76.86	7.686	0.57	0.779
Pure Error	2	27.06	13.529		
Total	26				

The response model was used to verify that the residuals were computed by measuring the differences between the experimental and predicted values and analyzed through graphical analysis. Residual plots for the quadratic regression model are shown in Figure 9(a-d). A residual probability plot (Figure 9a) was used to verify the assumption of normality. The tendency of the normal probability plot to slope somewhat higher on the right side of Figure 9b indicates that the tail of the error distribution is slightly narrower than expected for a normal distribution; however, this plot is not obviously non-abnormal. The betalain extraction optimization had a residual value lower than ± 4, as shown in Figure 9b, demonstrating that the data exhibited a relatively constant variation across the predicted values and lacked influential outliers. The histogram in Figure 9c shows a normal distribution. The fluctuation depicted in Figure 9d around the middle line indicates that the data were evenly distributed. All these plots indicated that the data were adequate and reliable, demonstrating that the model could accurately describe the optimization of betalain extraction from dragon fruit peels (Sriprom et al., 2015).

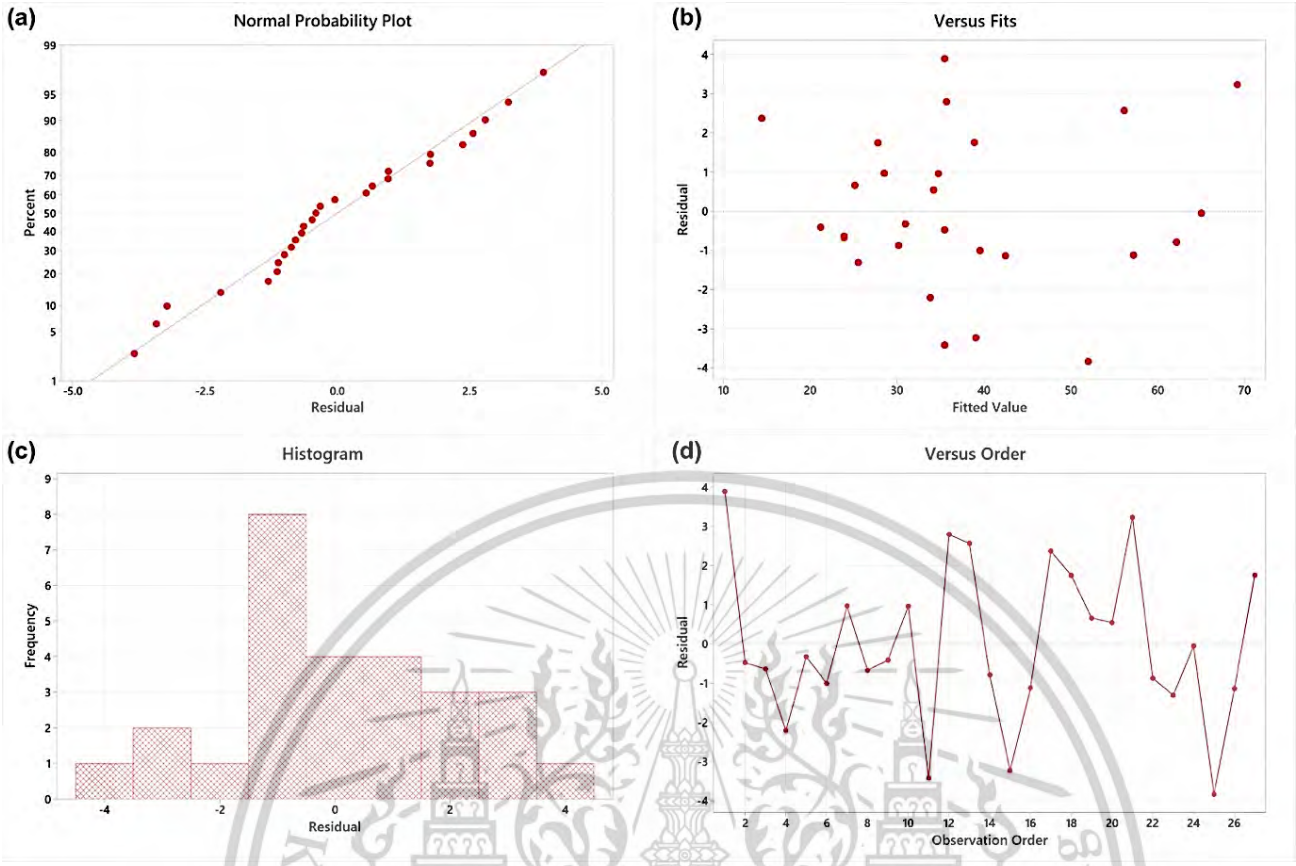

Figure 9 Internal standardized residual plots (a) normal probability plot, (b) versus fits, (c) histogram, and (d) versus observation order for betacyanin content.

4.1.2 Main Effect of Extraction Variables on Betalain Yield

Figure 10 shows the main effects of the four independent variables on the betalain extraction. This indicates that the extraction yield decreased with increasing time, temperature, and ratio. The solid-to-liquid extraction ratio significantly affected betalain extraction, as indicated by the data presented in Table 4. The table shows that the solid-to-liquid ratio was the most significant factor influencing these two variables ($p < 0.05$) at both the linear and quadratic levels.

The pH level (Figure 10a) significantly affected the betalain extraction, although the result was not statistically significant. Altering the pH of the extraction medium affected the betalain content. Specifically, raising the pH to above 4.0 decreased the betalain content, whereas lowering the pH to below 3.0 did not necessarily increase the betalain content. The finding that betalain yield decreases with increasing pH is consistent with previous research showing that betalain stability decreases at higher pH (H. M. C. Azeredo, 2009; Kushwaha et al., 2018).

Temperature negatively impacted betalain extraction (Figure 10b). Higher temperatures decreased the extraction yield because heat could degrade betalain. Although higher temperatures may increase cell permeability and extractability (Maran & Priya, 2016), degradation of betalain outweighs this effect. This is in agreement with the findings that increasing the temperature decreased the betalain extraction, reported by Basavaraja et al., (2022). The highest betalain yields at 30°C and 60°C was also obtained by (López et al., 2009). Another report by Chandran et al., (2014)showed that betalain degradation is related to temperature. This difference in efficiency can be explained by the fact that higher temperatures can cause pigment degradation reactions, which can decrease the overall yield of the betalain extraction. This may be due to the temperature-sensitive characteristics of betalain.

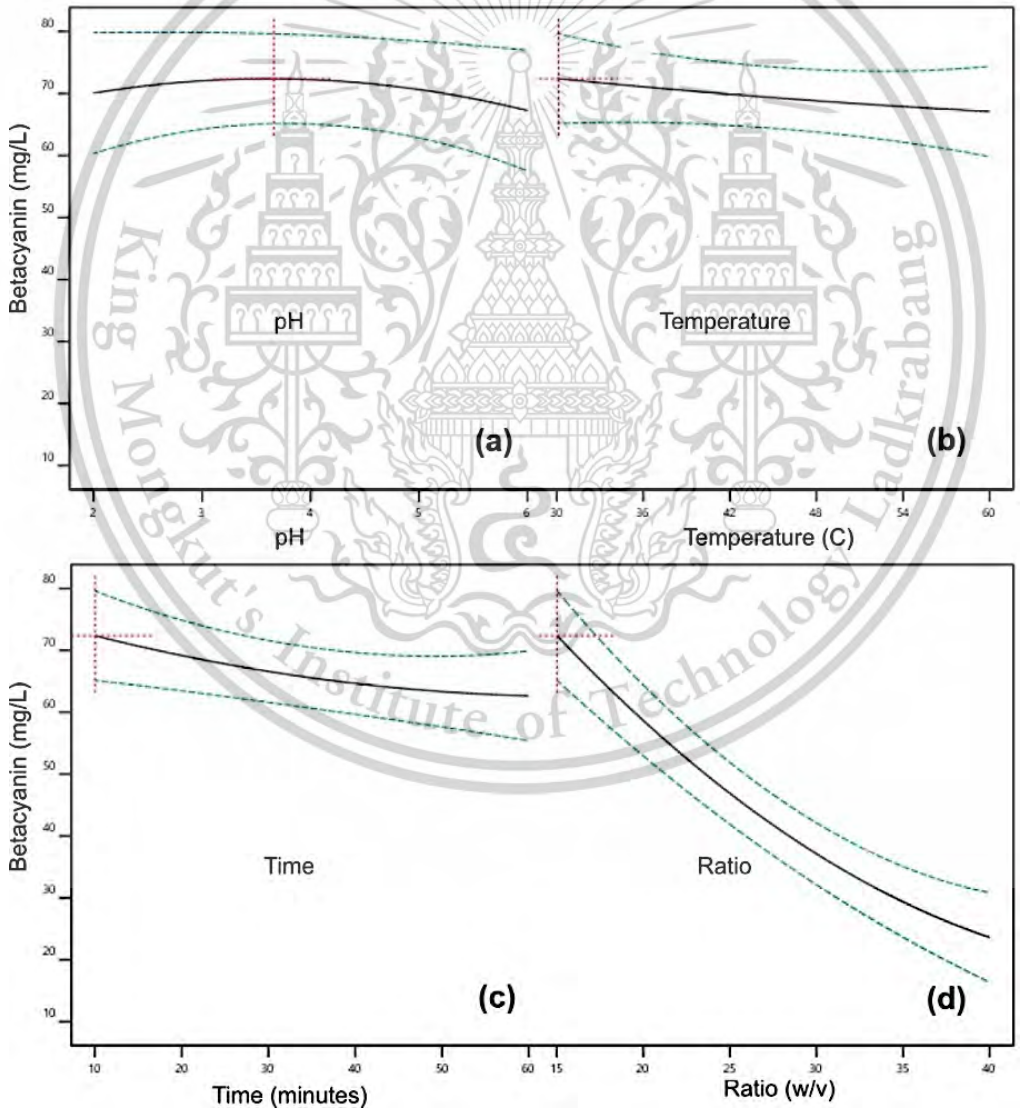

Figure 10 The main effect plots betacyanin extraction by different variables (a) effect of pH on betacyanin yield; (b) effect of temperature on betacyanin yield; (c) effect of time on betacyanin yield; (d) effect of solid-to-liquid ratio on betacyanin yield.

Similarly, the extraction time had a detrimental effect on the process as its value increased (Figure 10c). However, the extraction time did not significantly affect the betalain extraction (Table 4). Longer times did not increase the yield, likely because of pigment degradation. This also corresponds to the results of other studies, where the extraction time did not significantly affect betalain yield from beetroot by-products (Lazăr et al., 2021).

Increasing the solid-to-liquid ratio significantly decreased the betacyanin yield (Figure 10d). Similar findings during the extraction of betalain from beetroot pomaces was also reported by Kushwaha et al., (2018). This is because an increase in the solid-to-liquid ratio results in more source material being available for extraction, leading to a higher concentration of these compounds.

4.1.3 Interaction Effect of Extraction Variables on Betalain Yield

Main effect plots were used to represent the effect of these variables on the extraction of betalain from dragon fruit peels. The plots show the relative effects of any two variables when the remaining variables were kept constant. The response surface plots estimating the specific surface area of betalain extraction versus independent variables are presented in Figure 11.

The solid-to-liquid ratio significantly affected betalain extraction from dragon fruit peel (Table 4). A lower ratio increased the betalain yield. The extraction time and solid-to-liquid ratio also positively affected betalain at $p < 0.05$. The betalain yield increased with decreasing extraction time and solid-to-liquid ratio (Figure 11a). Longer times did not increase the product yield, as betalain degraded over time. Thus, minimizing the time and using a lower solid-to-liquid ratio are critical for maximizing betalain extraction.

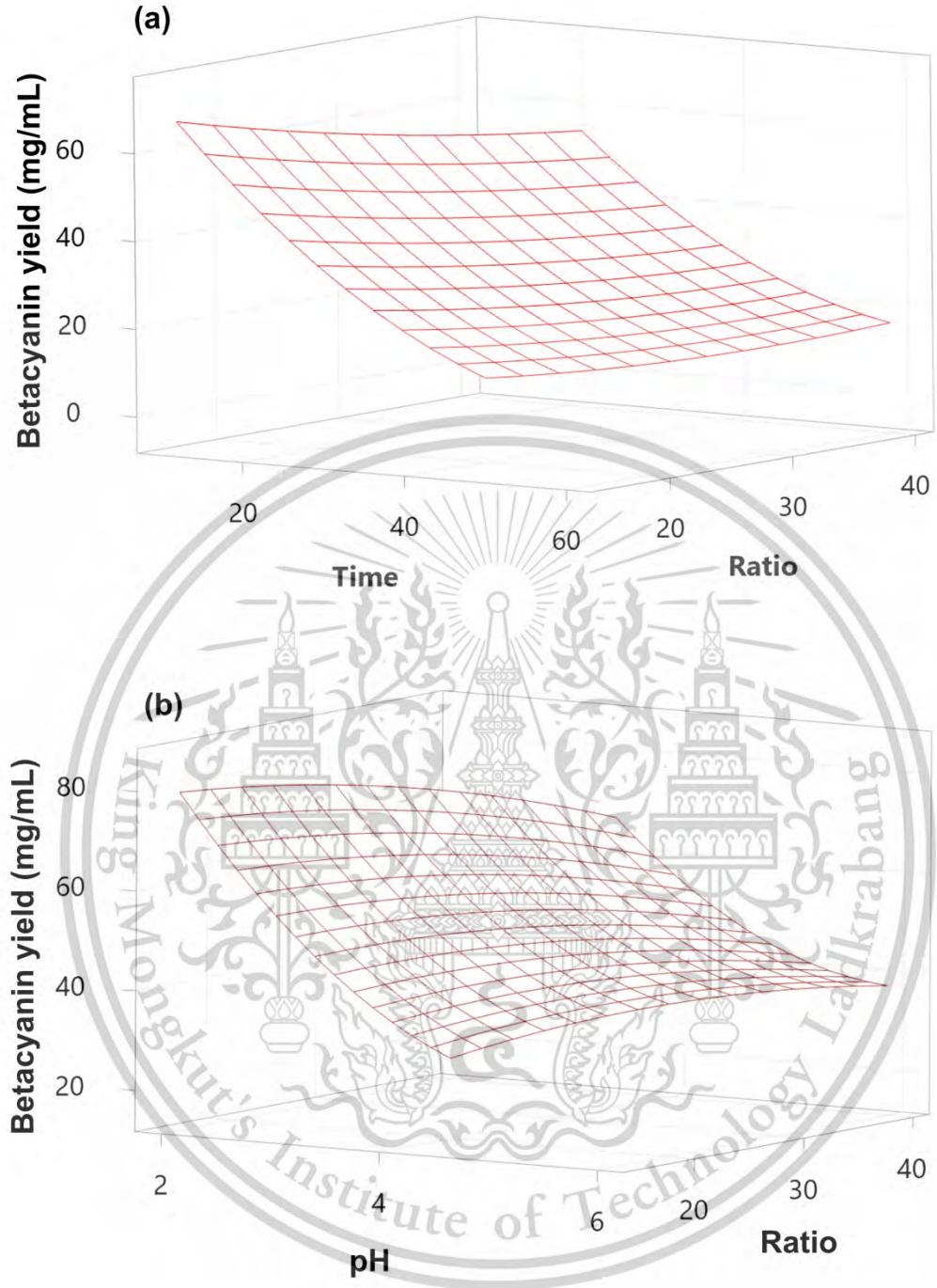

Figure 11 Surface plot showing the effect of process variable on betalain (a) effect of time and solid-to-liquid ratio on betacyanin yield; (b) effect of pH and solid-to-liquid ratio on betacyanin yield.

The pH and solid-to-liquid ratio significantly affected betalain extraction from dragon fruit peels ($p < 0.05$) (Table 4). A lower pH and solid-to-liquid ratio increased the yield, as these conditions minimized betacyanin degradation. However, extremely low pH levels should be avoided because they can break down the betalain (Esteves et al., 2018). The interaction

between pH and solid-to-liquid ratio also affected yield, with pH having a more significant effect at higher solid-to-liquid ratios. Optimizing these two factors is critical for maximizing betalain extraction. Balancing their effects to maximize yield while avoiding betalain degradation is important for efficient industrial extraction of betalain from dragon fruit peels.

4.1.4 The Optimum Condition for Betalain Yield Extraction from The Dragon Fruit Peels

The optimum levels of various factors were obtained by applying the desired functional methodology. These optimum levels indicate that an extraction pH of 3.6, a temperature of 30 °C, an extraction time of 10 minutes, and a solvent ratio at 1:15 will result in 72.47 mg/L of betacyanin content.

Using RSM optimization, this set of conditions was proven to be the most effective. The validity of these optimized settings was validated, and experiments were conducted to compare the experimental results with the projected response values of the model equation. Under optimal conditions, it was determined that the extraction efficiency of betalain under these conditions was 73.09 ± 1.79 mg/L after performing experiments in triplicate. It should be emphasized that these ideal values are applicable within a given range of process parameters.

Optimization of betalain extraction from dragon fruit peels resulted in a greater yield than that previously reported (Pichayajittipong & Thaiudom, 2014). Although we successfully extracted betalain from dragon fruit peels using safe and eco-friendly solvents and methods, our results were not as impressive as those of a study using ultrasound-assisted extraction (Bhagya Raj & Dash, 2020).

4.1.5 The Effect of pH on Betalain Extracted from The Dragon Fruit Peels

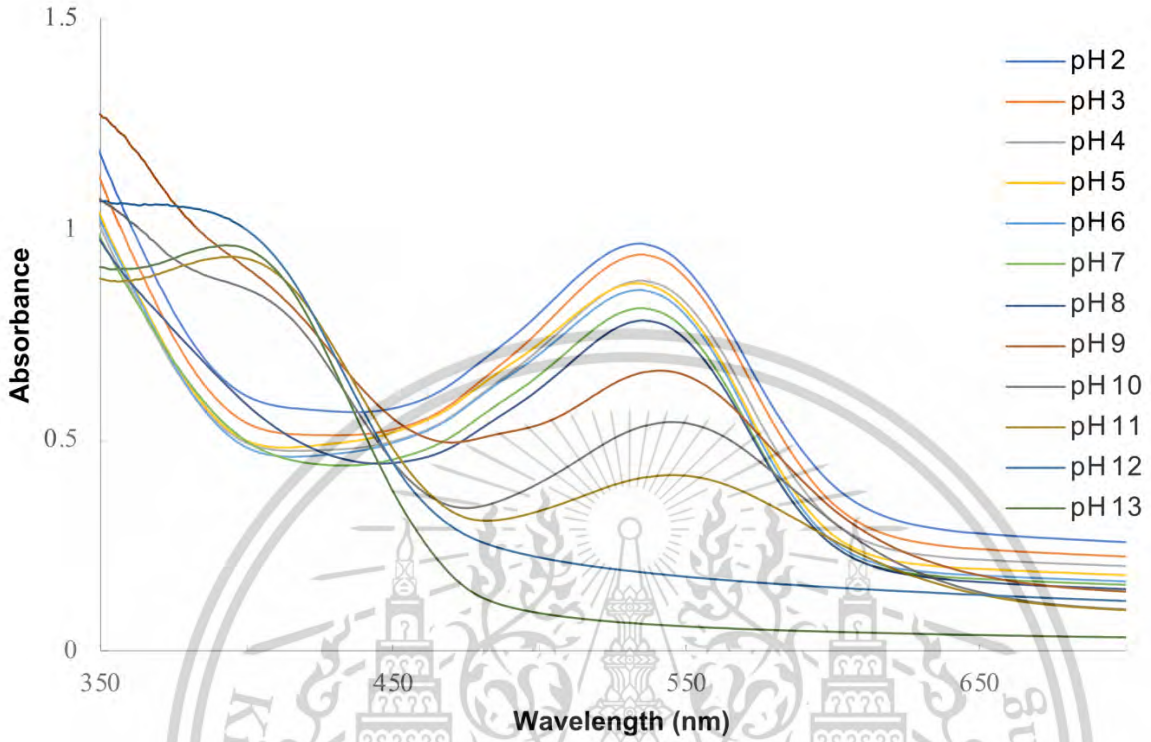

Figure 12 Absorption spectra of dragon fruit peel extract at different pH values

Table 6 shows that pH affects the color of the betalain extract. The pH levels affected the L*, a*, b*, and ΔE* values. The L* value slightly reduced as the pH decreased but increased significantly when the pH exceeded 11.0. Except for solutions with pH values of 12.0 and 13.0, which had higher L* values, the L* value generally decreased with increasing betacyanin content. The increase in pH had a significant effect on the lightness of the betalain extract solution, indicating the degradation of betalain to bright yellow betalamic acid, as confirmed by the maximum absorbance shown in Figure 12.

Table 7 relationship between the betalain content and CIELAB Color in different pH

pH	L*	a*	b*	ΔE*	Betacyanin (mg/L)	Color representative
2	50.36 ± 0.01	66.53 ± 0.04	-7.42 ± 0.04	10.8 ± 0.04	87.94±0.16	
3	51.6 ± 0.02	67.49 ± 0.02	-8.21 ± 0.03	11.31 ± 0.03	85.66±0.12	
4	52.92 ± 0.04	67.46 ± 0.04	-6.91 ± 0.03	9.86 ± 0.03	80.17±0.13	
5	53.03 ± 0.03	66.95 ± 0.04	3.21 ± 0.05	0.66 ± 0.06	79.37±0.18	
6†	53.12 ± 0.01	67.34 ± 0.03	3.73 ± 0.02	0	77.99±0.17	
7	54.23 ± 0.01	65.69 ± 0.04	0.15 ± 0.04	3.01 ± 0.03	74.25±0.13	
8	53.12 ± 0.01	62.33 ± 0.01	0.92 ± 0.04	4.8 ± 0.01	71.55±0.09	
9	47.75 ± 0.04	51.26 ± 0.04	4.45 ± 0.06	16.55 ± 0.04	60.71±0.07	
10	50.3 ± 0.01	33.6 ± 0.03	4.64 ± 0.04	33.28 ± 0.04	49.36±0.13	
11	53.11 ± 0.02	24.01 ± 0.03	12.35 ± 0.02	43.7 ± 0.03	37.86±0.08	
12	85.75 ± 0.03	-2.35 ± 0.04	49.56 ± 0.04	89.33 ± 0.06	17.01±0.06	
13	87.14 ± 0.02	-8.74 ± 0.02	57.71 ± 0.02	99.1 ± 0.02	5.84±0.04	

†pH 6.0 was used to compare the color of the betacyanin extract at each pH.

The a* value of the betalain extract remained constant at pH 2.0-8.0, supported by the maximum absorbance of the solution around 533-535 nm in the betacyanin extract within the same range. The absorbance decreased from 0.959 (at pH 2.0) to 0.781 (at pH 8.0), which affected the betalain content and L* and a* values in this pH range. This result is consistent with other studies, where betalain was relatively stable at pH 3.0-7.0 with optimum pH 5.0-6.0 (Herbach et al., 2006a).

In contrast, the a* value significantly decreased as the pH increased and the betalain content decreased. The disappearance of the reddish color with increasing pH indicated the degradation of betacyanin. Conversely, the b* value increased with increasing pH and became yellow at pH 10.0. Increasing the pH to 9.0 and above, resulted in the disappearance of the band at approximately 530 nm and the appearance of a 390-410 nm absorbance. This absorbance, which was only found at pH 12.0 and 13.0, may be due to the degradation of betacyanin through hydrolytic cleavage, resulting in the formation of bright yellow betalamic acid (Herbach et al., 2005, 2006b). Hydrolysis promoted by higher pH degrades the aldimine bond between betalamic acid and cyclo-DOPA from betacyanin (Ciriminna et al., 2018).

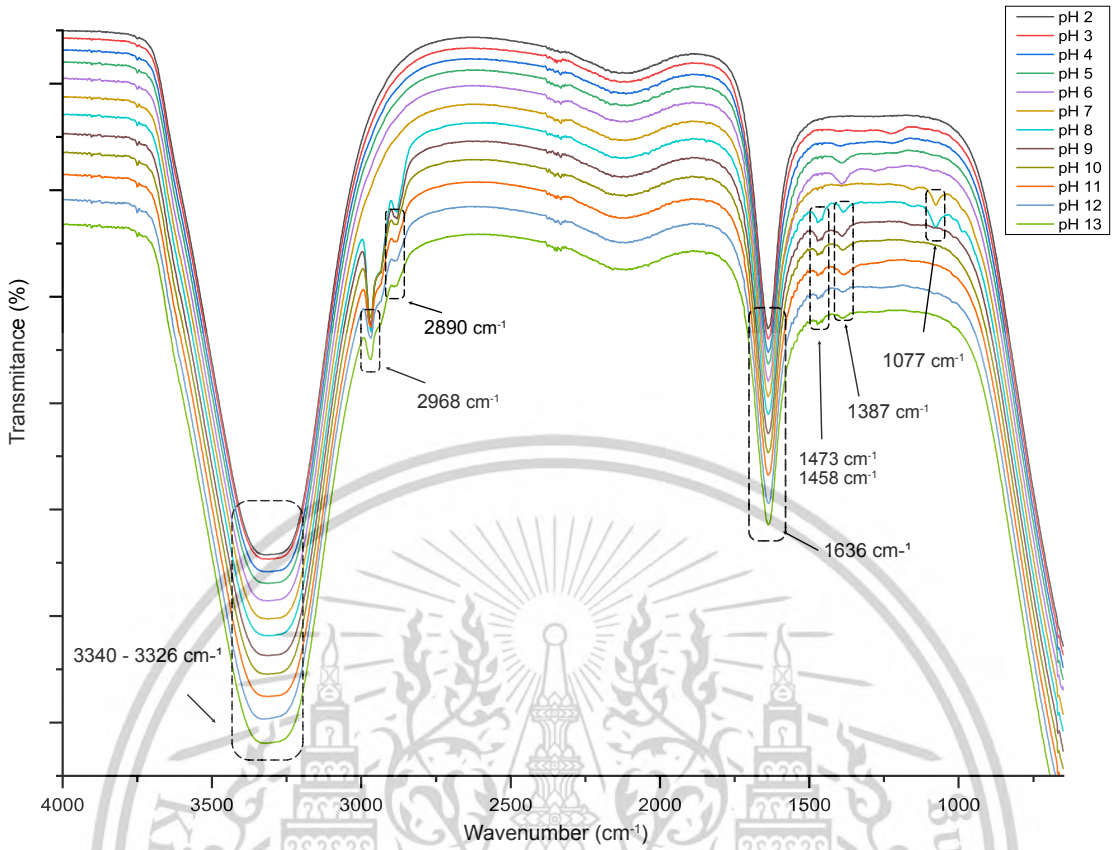

Figure 13 FT-IR Spectrum of betalain from dragon fruit peel extracts at various pH values.

The ΔE* value of the betacyanin extract remained stable at pH 5.0 – 7.0 but changed under acidic conditions and showed different colors at pH values above 7.0. Increasing the pH will increase the ΔE* value, indicating a significant effect of increasing pH on the stability of the betalain extract, resulting in a color change from red to yellowish. High pH influences the cleavage of betacyanin into bright yellow betalamic acid and colorless cyclo-DOPA (Esteves et al., 2018; Schwartz & von Elbe, 1983).

A comprehensive chemical and structural analysis of the effect of pH on betalain is beyond the scope of this study. Functional group analysis was performed using FTIR to determine the influence of pH on the original chemical structure of betacyanin. In all solutions, a strong and wide band from 3340 to 3290 cm^{-1}, which corresponds to O-H stretching(Gao et al., 2022), was observed (Figure 13), which sometimes overlapped with the stretching of the aromatic (N-H-containing) group (Barkociová et al., 2021). The band at 1636 cm^{-1} found in all pH solutions is attributed to a carbonyl double bond (C=O) (Chang et al., 2013; Janiszewska-

Turak et al., 2022). These two bands remained unchanged, possibly because the aromatic ring and heterocyclic in the solution remained.

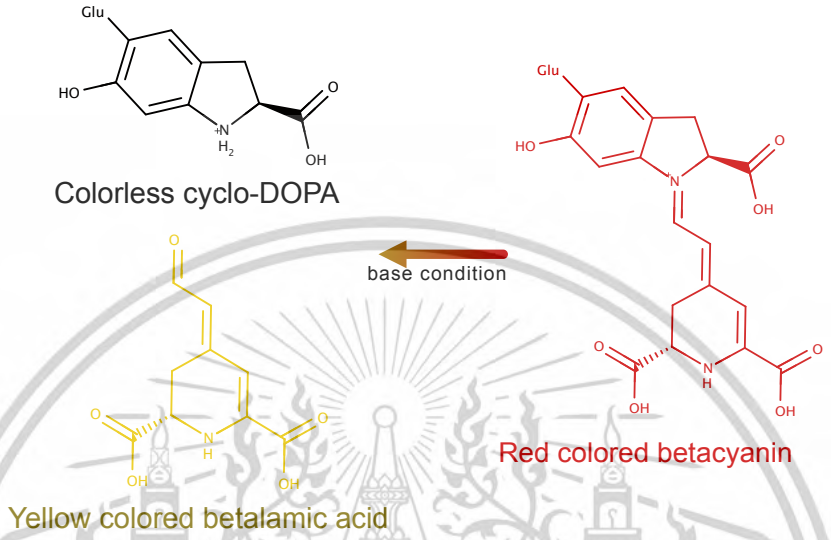

Figure 14 Structure of betacyanin, betalamic acid, and cyclo-DOPA

pH 7.0 and 8.0, showed a characteristic band at 1077 cm^{-1} corresponding to C-O stretching, indicating the involvement of the carboxyl group (Qin et al., 2020a). This indicates the involvement of carboxylate groups (-COO-) in the chemical reactions of the solution at that pH. Bands at 1387, 1458, and 1473 cm^{-1}, representing the bending vibrations of -OH and C=C aromatic bonds, respectively, were observed at pH 8.0 and above (Ezati et al., 2019; X. Li et al., 2022). Additionally, the bands at 2890 cm^{-1} and 2968 cm^{-1} refer to C-H absorption (Gao et al., 2022; Gnanasambandam & Proctor, 2000). However, these bands only appeared for betalain in the alkaline solution and did not occur at different pH values. The bending vibration of -OH and C=C aromatic bonds under alkaline conditions could be attributed to the ionization of hydroxyl and carboxylate groups, which led to changes in the molecular conformation of the betacyanin structure. Betacyanin undergoes a structural shift under alkaline conditions due to the formation of betalamic acid and cyclo-DOPA as shown in Figure 14.

Several studies have reported the stability of betalain at an optimal pH range of 3.0-7.0 (Jackman & Smith, 1996). However, pH plays a crucial role in determining the stability of betalain, with betacyanin being stable at pH 5.0-6.0, while betaxanthin shows higher stability at pH 7.0 (Castellar et al., 2003; A. S. Huang & Elbe, 1987). Although betacyanin exhibits a

wide range of pH stabilities, degradation can occur outside this range. The aldimine bond of betacyanin is hydrolyzed under alkaline conditions, resulting in the degradation of betalamic acid and colorless cyclo-dopa, which can occur through heating and alkaline conditions (Schwartz & von Elbe, 1983; von Elbe & Attoe, 1985). Visual color deterioration has also been observed during the thermal degradation of betacyanin, which follows first-order kinetics as reported by Chandran (Chandran et al., 2014). The decomposition of betanin into betalamic acid by a base is due to hydrolysis, which is subject to general base catalysis by HPO_2^{-4} and specific base catalysis by -OH, as reported by (Esteves et al., 2018).

The pH-dependent behavior of betalain extracts, as unveiled by FTIR analysis and color changes, holds significant promise with diverse practical applications. Understanding how pH impacts betalain structures can pave the way for innovative solutions in various industries. For instance, in the realm of smart packaging, this knowledge can be harnessed to design indicators that change color in response to pH variations, offering real-time freshness monitoring for food products (Qin et al., 2020a; Said & Sarbon, 2023; Yao et al., 2022). Controlling pH during processing can help preserve the vibrant hues of natural betalain-based colorants, reducing the need for synthetic additives in food (Fernández-López et al., 2023; Jiang et al., 2021b). Furthermore, betalain-rich extracts can find utility as natural food colorants, offering a pH-sensitive alternative to synthetic dyes. This nuanced understanding of pH's influence on betalain equips industries with the tools to enhance product stability and visual appeal while meeting the demands for sustainable and health-conscious solutions.

4.2 Mechanism Interaction of Xyloglucan, Chitosan, and Betalain

In this study, we examined the interaction between xyloglucan-chitosan and betalain to modify a stable film from Adair et al. (2023). Their findings revealed that xyloglucan forms a stable complex with chitosan via covalent bonding between the aldehyde group at the first carbon of xyloglucan and the amino group of chitosan.

As shown in Table 7, chitosan exhibited a positive zeta potential of +49.70 mV, xyloglucan had a neutral zeta potential of +0.12 mV and betalain had a negative zeta potential of -26.37 mV. Upon mixing xyloglucan-chitosan with betalain, a significant reduction in zeta potential was observed, with the value shifting to -0.912 mV for XC-EB5. The reduction in zeta potential indicated that the carbonyl group of betalain binds to the amino group of chitosan, partially neutralizing the charges of chitosan and suggesting a primarily ionic interaction (Alemu et al., 2023). The positive charge of chitosan enables it to interact with betalain and

other molecules with negatively charged molecules, such as proteins, lipids, and ions (Sahoo et al., 2009).

Table 8 Zeta potential of xyloglucan, chitosan, betalain, and xyloglucan-chitosan

Samples	Zeta Potential (mV)
Xyloglucan	$+0.12 \pm 0.43^{b}$
Chitosan	$+49.70 \pm 0.96^{c}$
Betalain	-26.37 ± 2.04^{a}
Xyloglucan-chitosan	$+49.76 \pm 0.64^{c}$
XC-EB3	$+4.15 \pm 2.40^{d}$
XC-EB5	-0.912 ± 0.42^{e}
XC-EB7	$+0.117 \pm 0.04^{b}$

Values are presented as mean ± SD (n = 3). Different superscript letters in the same column indicate significant differences ($p < 0.05$).

The FTIR analysis, shown in Figure 15 provides further insight into the interaction between XC and EB. A sharp peak at 1639 cm^{-1} that appears in the XC spectrum indicates the C=O peak of aliphatic secondary amides (Adair et al., 2023). However, the addition of EB resulted in the disappearance of this peak, indicating a strong interaction between EB and XC. As the EB increases, the nitrogen-containing groups in betalain competed for protonation with the amine groups in chitosan, leading to a reduction in the number of free protonated amines. These changes resulted in decreased intensity of the peak of the 1638 cm^{-1} and a shift to 1575 cm^{-1}, which corresponds to enhanced N-H bending vibrations of protonated amines in chitosan. This shift suggest the formation of hydrogen bond between the protonated amines of chitosan and the hydroxyl (-OH) or carboxylate group of betalain. The peak of 1575 cm-1 also associated with N-H bending vibrations (Lawrie et al., 2007). Additionally, the peaks at 2885 cm^{-1} and 2928 cm^{-1} can be attributed to C-H symmetric and asymmetric stretching, respectively, which are characteristics of polysaccharides (Manamoongmongkol et al., 2024; Prajapati & Jadeja, 2024). The peak at 1024 cm^{-1} mi corresponds to the C–O bond of betalain or xyloglucan (Fu et al., 2017; Qin et al., 2020b). A broad band at 3200-3300 cm^{-1} corresponds to O-H and N-H stretching vibrations that are indicative of hydroxyl and amino groups, which may indicate the interaction between the hydroxyl group of xyloglucan, the amino group of chitosan, as well as the hydroxyl group of betalain (Wiggers et al., 2022).

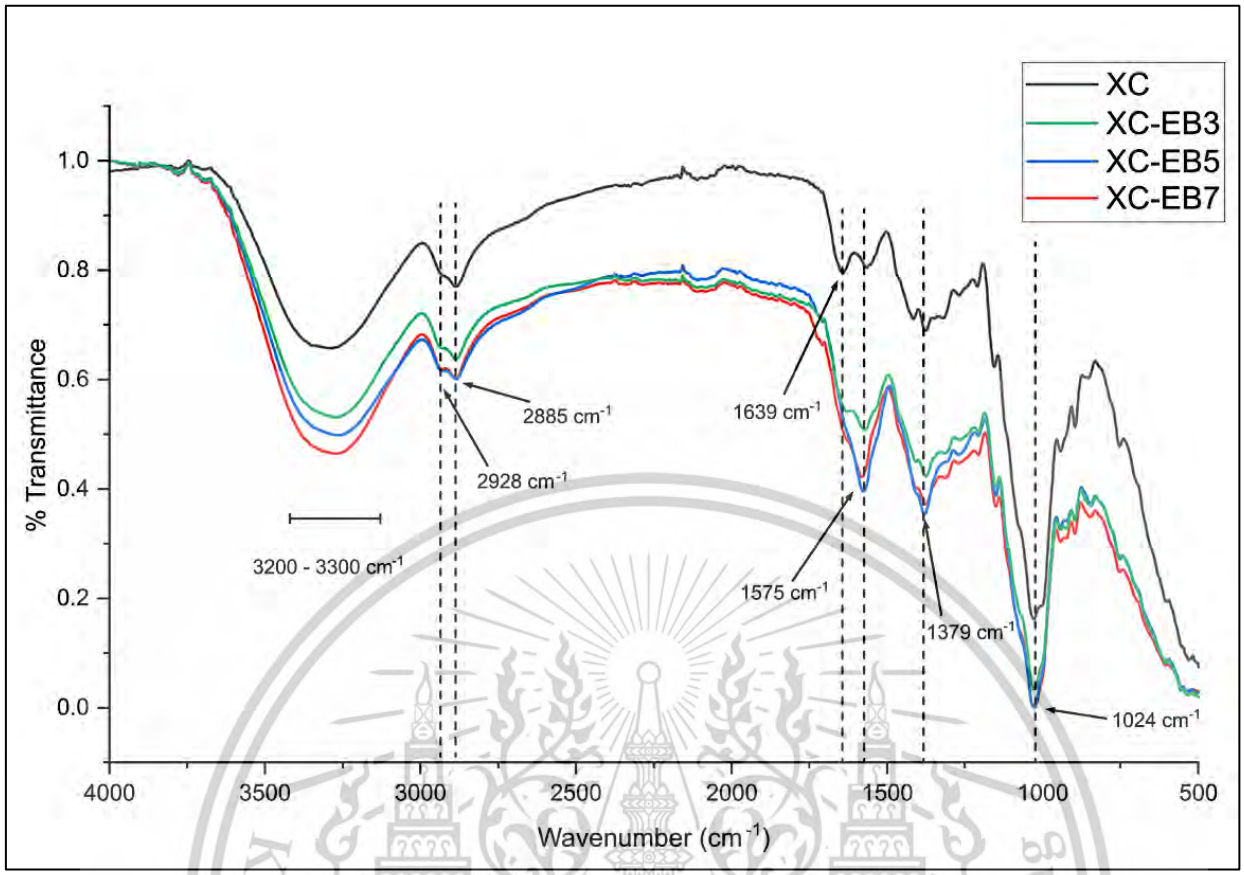

Figure 15 FTIR of xyloglucan-chitosan and betalain film

When EB was incorporated into the XC matrix, the zeta potential shifted from a positive value to nearly neutral, indicating that betalain interacted with both xyloglucan and chitosan through ionic interactions and hydrogen bonding mechanisms, as depicted in Figure 16. This interaction neutralizes the positive charge of chitosan and disrupts its ionic interactions with xyloglucan. The nearly neutral zeta potential suggests competitive binding between betalain and the polymers, which disrupts the ionic interactions between xyloglucan and chitosan.

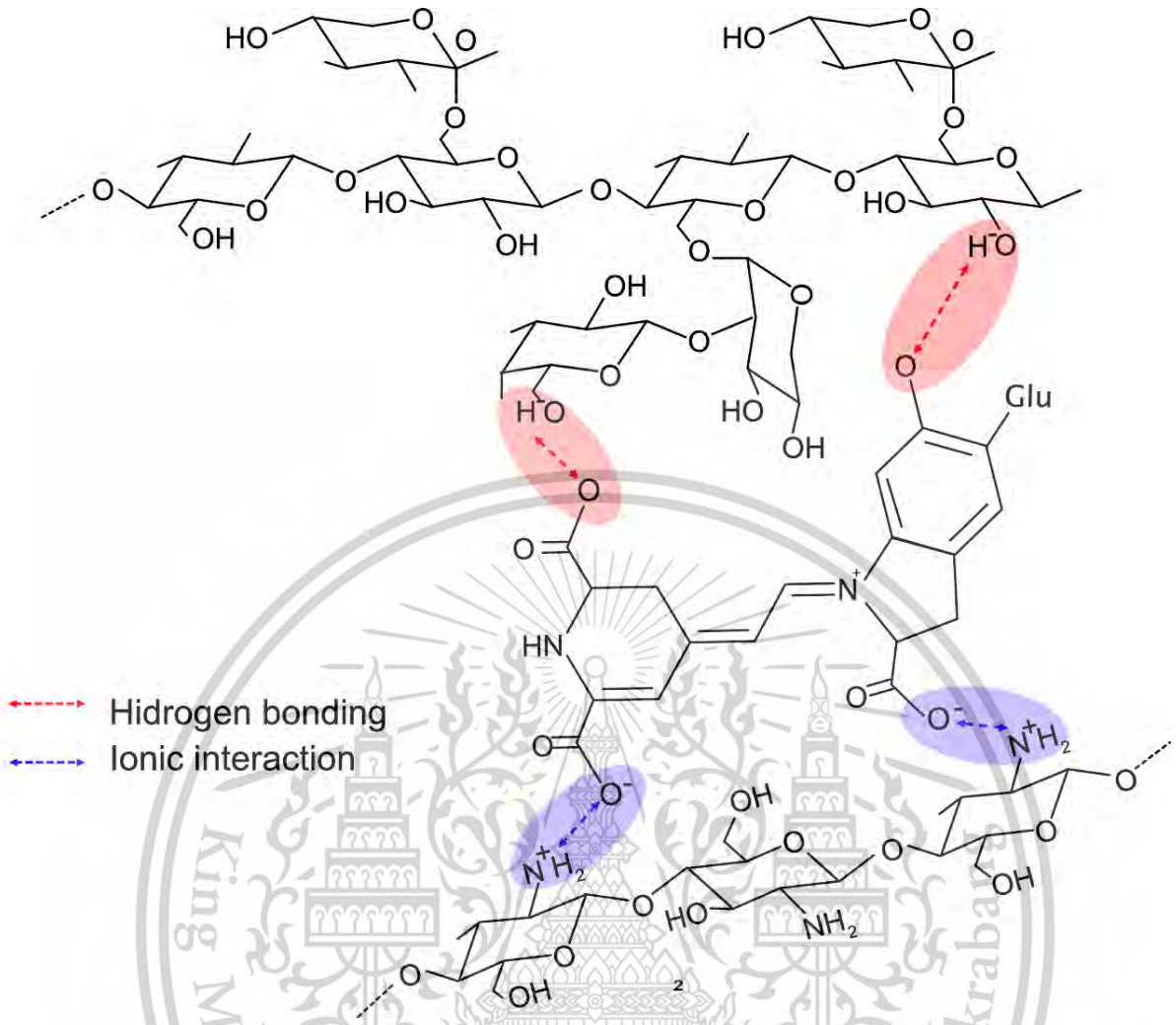

Figure 16 Mechanism of interaction between xyloglucan, chitosan, and betalain in film

4.3 Rheological Property

The rheological properties of XC films with varying concentrations of betalain demonstrated distinct viscoelastic behaviors, as illustrated in Figure 17. The storage modulus (G′) signifies the elastic behavior, while the loss modulus (G″) denotes the viscous behavior, both as functions of angular frequency.

All samples exhibited an increase in G′ and G″ as the angular frequency increased (from 0 to 100 rad/s), demonstrating frequency-dependent behavior. The XC film-forming solution displayed higher G′ and G″ values than the other samples, suggesting a predominantly viscous behavior (Manamoongmongkol et al., 2024). However, with the incorporation of betalain into the film-forming solution, a noticeable decrease in both the G' and G" values was observed, with G" consistently higher than G'. This observation aligns with previous studies that demonstrated that the addition of active substances such as EB can plasticize the polymer matrix network, resulting in decreased elasticity and increased viscosity (Guo et al., 2023; Liang et al., 2019; Wu et al., 2019). Increasing the concentration of EB further elevated the G" value in the film-forming solution, implying that EB was integrated into the XC matrix network, forming hydrogen bonds and enhancing the viscosity of the film-forming solution.

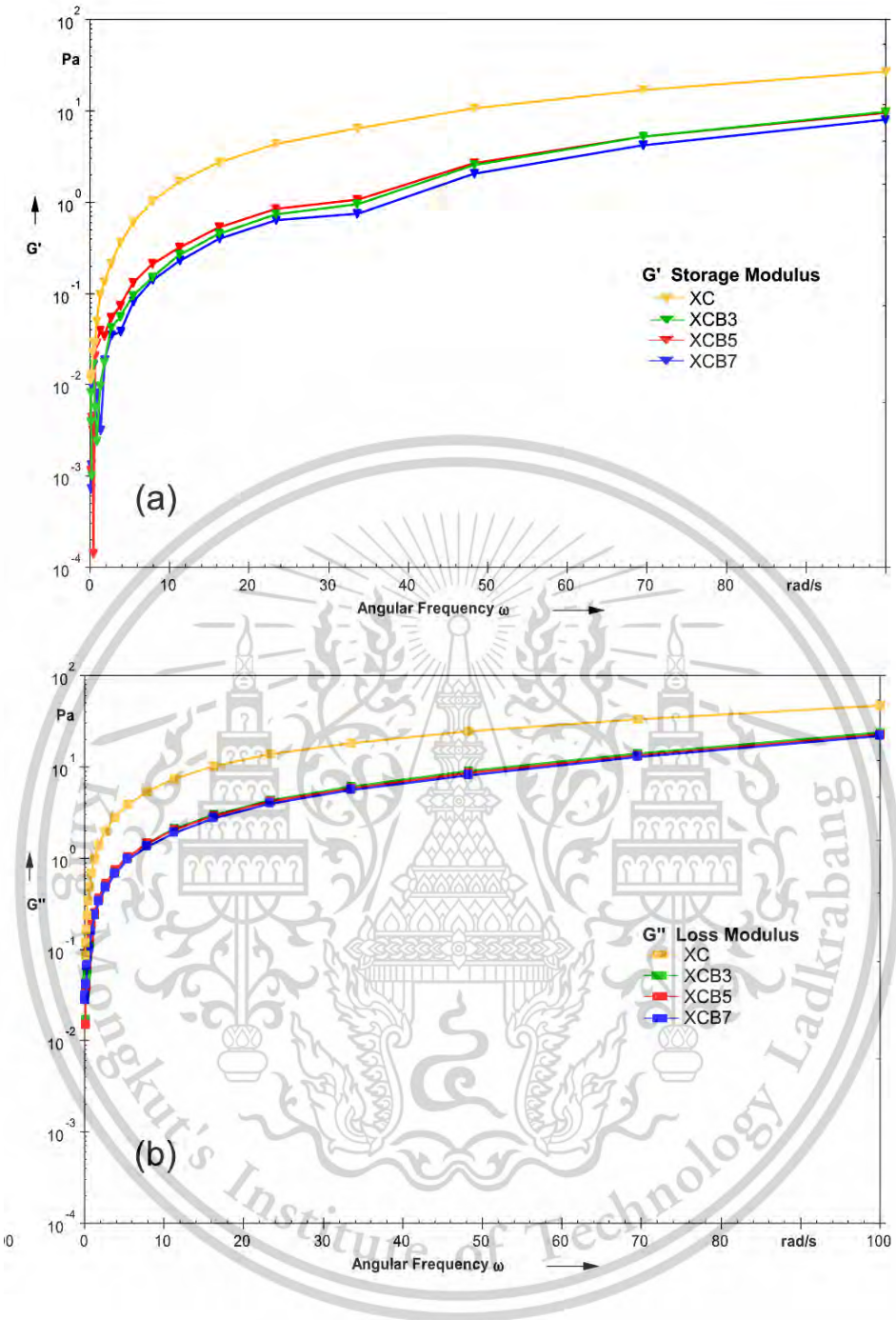

Figure 17 Rheological properties of the intelligent packaging film solution. (a) Storage modulus; (b) loss modulus.

4.4 Antibacterial Properties of Film-forming Solution

The MIC results for the film-forming solution against *E. coli* and *S. aureus* are shown in Table 8. For E. coli, the MIC values for all XC-EB3, XC-EB5, and XC-EB7 film-forming solution were consistently 1.25% (w/v), whereas for XC, the MIC was 0.625% (w/v). In the case of *S. aureus,* the MIC values for XC-EB3, XC-EB5, and XC-EB7 film-forming solution were 2.5% (w/v) and for XC was 0.313% (w/v). These findings revealed that the antimicrobial agent exhibited inhibitory effects against the tested bacterial strains, indicating that the film-forming solution were effective in suppressing microbial growth. However, it was found that the XC film-forming solution exhibited a stronger inhibitory effect against both bacteria compared to other samples that contain betalain. The higher MIC suggests that the presence of EB might reduce the efficacy of the XC film-forming solution, possibly due to interference with the ionic interactions between the positively charged amino groups of chitosan and the negatively charged microbial cell surfaces (Tao et al., 2011).

This phenomenon can be explained by the complex interplay of electrostatic interactions occurring at the molecular level. The antimicrobial properties of chitosan primarily originate from its cationic nature, where the positively charged chitosan interacts electrostatically with the negatively charged microbial cell surface (Helander et al., 2001). This electrostatic interaction disrupts the integrity of the microbial cell, ultimately leading to cell death(Han et al., 2024). The addition of betalain to the xyloglucan-chitosan solution reduces the zeta potential, making the charge nearly neutral. When the zeta potential decreases, the effectiveness of the chitosan's positive charge is diminished, weakening its ability to interact with microbial cell surfaces (Chen et al., 2010). Consequently, incorporating betalain into the xyloglucan-chitosan film alters the zeta potential of the film-forming solution, which may affect its antimicrobial activity.

.

Table 9 Minimum inhibitory concentration (MIC) and minimum bactericidal concentration (MBC) of film film-forming solution against *E. coli* and *S. aureus*

Sample Code	MIC (%)	MBC (%)	MIC (%)	MBC (%)
	E. coli		*S. aureus*	
XC	0.625	5	0.313	>10
XC-EB3	1.25	10	2.5	>10
XC-EB5	1.25	10	2.5	>10
XC-EB7	1.25	10	2.5	>10

The MBC results provide more insight into the bacterial limitation of both XC films and betalain added film. As shown in Table 8, the MBC values for *E. coli* were 5% for the XC sample and 10% for the XC-EB3, XC-EB5, and XC-EB7 samples. Doubling the MBC values correlates with the interference of betalain in the charge-mediated's bactericidal mechanism of chitosan. While XC film-forming solution has stronger bactericidal effects to *E. coli*, by disrupts the *E. coli* outer membrane through electrostatic interaction, the addition of betalain lead to the reduction of chitosan ability to disrupt the cell membrane. This probably due to competitive bidning between betalain and microbial surface for amino group of chitosan. This finding aligns with the observed zeta potential reduction (Table 7), as a diminished positive charge density weakens chitosan's ability to penetrate the lipopolysaccharide layer of Gram-negative bacteria

For *S. aureus*, the MBC values were greater than 10% for all samples, highlighting the fundamental limitation in activity of chitosan against Gram-positive bacteria, potentially due to their thicker peptidoglycan layer that resist electrostatic disruption. The disparity between MIC and MBC value, points out that while charge-mediated growth inhabitation occurs at lower concentration, complete bacterial destruction required a sufficient amount of chitosan. This requirement seems to be strongly affected by betalain, which reduces chitosan's positive charge. As a result, the modified films' MBC values remain at 10% regardless of the betalain concentration, suggesting that betalain reaches a limit in how much it interferes with chitosan's antibacterial effect

4.5 Intelligent-Film Packaging Formation: Develop and Characterize Intelligent-Film Packaging Based on The Xyloglucan-Chitosan-Betalain Complex and Its Application.

4.5.1 Physical Properties of Intelligent Packaging Film

4.5.1.1. Moisture Content and Thickness

The moisture content of XC film show negligible variation from 15.45 ± 0.22% to 15.27 ± 0.43%. despite incremental EB incorporation (Table 9). As a hemicellulose with abundant hydroxyl groups, xyloglucan typically forms film with moisture sensitivity due to these hydrophilic groups (G. Liu et al., 2023). This suggests that the addition of EB had no significant impact on the moisture content of the XC films, as the tight microstructure remained unchanged (Jiang et al., 2023). This stability in moisture content contrasts with finding reported by Naghdi

et al. (2021) and Qin et al. (2020b), who observed that the moisture content decreased more substantially with addition of betalain from red pitaya peel. Similarly, another study demonstrated that the incorporation of red beetroot betalain significantly affected the moisture content of the film. Specifically, an increase in betalain concentration results in a reduction in moisture content (Abdolmaleki et al., 2024).

The significant increase in film thickness with increasing betalain content from 0.038 ± 0.0038 mm in control film to 0.060 ± 0.003 mm in XC-EB7 indicates a structural modification within polymer matrix. This increase in thickness suggests that betalain incorporation fundamentally alters the spatial arrangement of polymer chain. This can be attributed to the intermolecular bridges form between betalain and polymer chains through hydrogen bonding or other interactions, resulting in a more expanded three-dimensional network (Canizales-Rodríguez et al., 2024). This finding align with observation by Qin et al. (2024), who noted thickness increases in chitosan film with the addition of anthocyanin, owing to the strong hydrogen bond between anthocyanin and the polymer matrix. Similar structural expansion has been observed in other bio-polymer natural pigment system, such as in the incorporation of pomegranate extract into chitosan-based edible film (N. Kumar et al., 2021), suggesting a common mechanism regardless of the specific pigment.

Table 10 Moisture content, thickness, and swelling index of intelligent packaging film

Samples	Moisture content (%)	Thickness (mm)	Swelling (%)
XC	15.45 ± 0.22^{a}	0.038 ± 0.003^{a}	493.73 ± 20.91^{a}
XC-EB3	15.42 ± 0.46^{a}	0.047 ± 0.002^{b}	687.32 ± 14.94^{b}
XC-EB5	15.29 ± 0.19^{a}	0.051 ± 0.003^{c}	726.88 ± 25.50^{bc}
XC-EB7	15.27 ± 0.43^{a}	0.060 ± 0.003^{d}	747.45 ± 21.71^{c}

Values are given as mean ± SD. Different superscript letters in the same column indicate significantly different ($p < 0.05$).

4.5.1.2. Surface Morphology By Scanning Electron Microscopy

The appearance of the films as observed through scanning electron microscopy (SEM), is shown in Figure 18. The XC film, depicted in Figure 18(a), exhibited a smooth and uniform surface, indicating a homogeneous polymer blend. In contrast, the addition of EB led to a more textured and a coarser film surface, as shown in Figure 18(b-d), suggesting increased

aggregation. This structural change may be attributed to the complexation between chitosan and betalain. The addition of betalain resulted in the surface of the film becoming coarser than the film without betalain. Our finding aligns with the study with those of Jiang et al. (2023), who reported that incorporating of betacyanin extracted from pitaya peel waste into a pectin-based film resulted in a more heterogeneous structure. Similarly, Yao et al. (2020) found that the cross-section of quaternary ammonium chitosan (QAC)/polyvinyl alcohol (PVA) film became rougher when cactus pear betalain extract (CPE) was excessively incorporated into the film. These morphological differences in the film surface may influence other properties, such as thickness and mechanical strength.

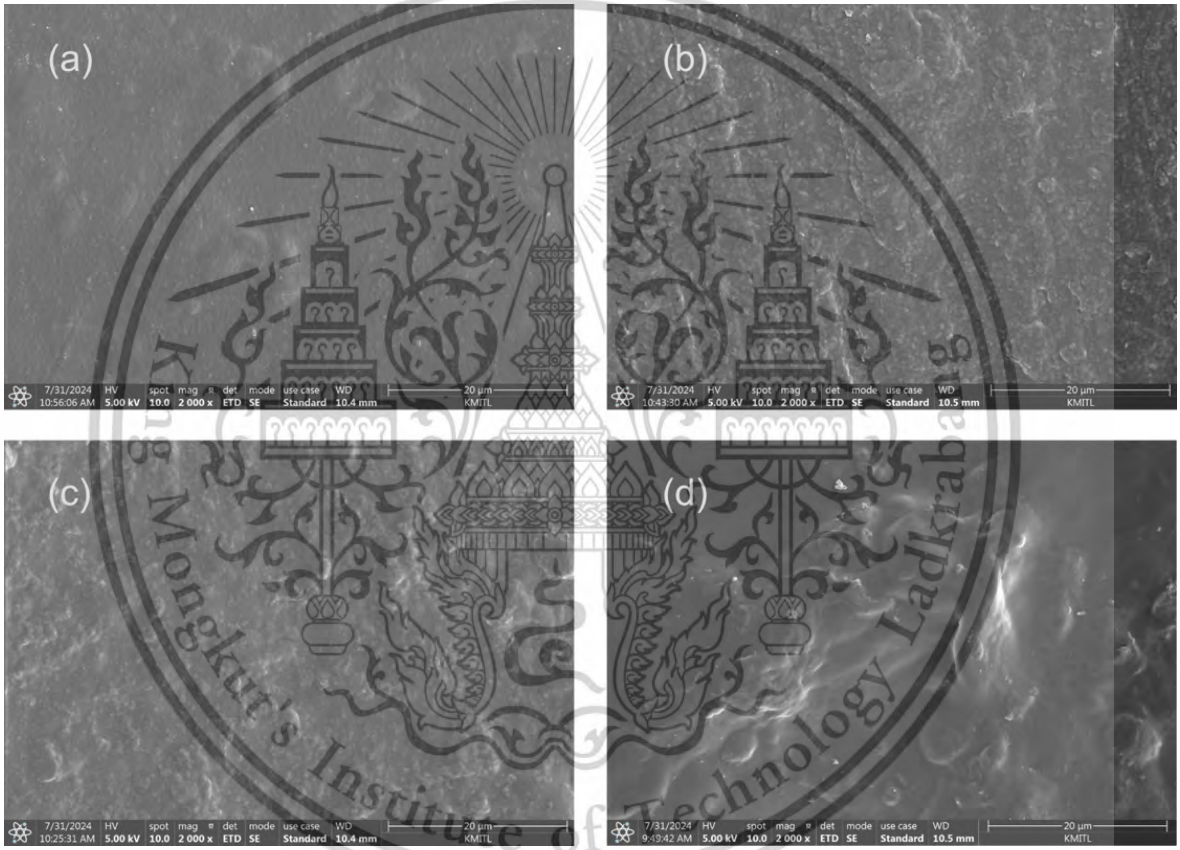

Figure 18 SEM micrographs on surface of of intelligent packaging film different betalain concentration extracts. Magnifications was 2,000 ×. (a) XC, (b) XC-EB3, (c) XC-EB5, and (d) XC-EB7

4.5.1.3. Film Color

Table 11 Color parameters (L*, a*, and b*) and visual image of intelligent packaging film

Samples	L*	a*	b*	ΔE	Visual image
XC	90.17 ± 0.13[a]	0.12 ± 0.05[a]	0.47 ± 0.42[a]	4.00 ± 0.37[a]	
XC-EB3	83.99 ± 0.66[b]	9.59 ± 0.82[b]	-0.46 ± 0.21[b]	12.08 ± 1.01[b]	
XC-EB5	78.84 ± 0.63[c]	17.15 ± 0.91[c]	-1.92 ± 0.40[c]	20.93 ± 1.08[c]	
XC-EB7	76.49 ± 1.58[d]	21.68 ± 2.15[d]	-4.44 ± 0.28[d]	25.96 ± 2.68[d]	

Values are given as mean ± SD. Different superscript letters in the same column indicate significantly different ($p < 0.05$).

The color parameters (L, a*, b*, and ΔE) and images of the films are presented in Table 10. The XC film exhibited high lightness (L* = 90.17 ± 0.13) with minimal red-green (a* = 0.12 ± 0.05) and yellow-blue (b* = 0.47 ± 0.42) components. This result aligns with previous studies on chitosan-based films, which are typically display highly transparency and minimal coloration (Souza et al., 2015). The slight yellow tint observed in the control film can be attributed to the inherent color of chitosan, which impart a pale yellow hue to the films (Elsabee & Abdou, 2013). Significant changes in color parameters were observed upon the addition of EB. The lightness (L*) values decreased progressively with increasing EB concentration, from 83.99 ± 0.66 to 76.49 ± 1.58. This reduction in lightness were expected due to the intense pigmentation of betalains, which contribute to the vibrant coloration of dragon fruit peels (Sen & Baruah, 2023). Concurrently, the a* values, representing the red-green axis, increased with EB incorporation (9.59 ± 0.82 to 21.68 ± 2.15), indicating a pronounced shift towards the red spectrum. This trend is characteristic of betacyanins, the red-violet pigments predominant in dragon fruit peels (Sadowska-Bartosz & Bartosz, 2021a). The increasing a* values with higher

EB concentrations suggest a dose-dependent relationship between the amount of extract added and the intensity of red coloration in the films.

The total color difference (ΔE) provides a comprehensive measure of the overall color variation relative to the control sample (XC). The ΔE values increased significantly with higher EB concentrations (12.08 ± 1.01 to 25.96 ± 2.68). A ΔE greater than 5 indicates that the film is visually distinguishable to the average observer, as established in prior research on colorimetric sensors (Cejudo-Bastante et al., 2014). Accordingly, all betalain-incorporated films in this study exhibited visually distinct coloration compared to the control, with XC-EB7 showing the most pronounced color difference. The interaction between EB and the XC matrix likely influenced color development. As a cationic polymer, chitosan forms ionic complexes with anionic betalain molecules. This interaction potentially altering the spectral properties and stability of the complex (S. Liu et al., 2022).

4.5.1.4. Swelling Index

The swelling index of the XC film was significantly lower (493.73 ± 20.91%) than that of the XC-EB3-7 films ($p < 0.05$), as shown in Table 9. The addition of EB to the XC film significantly increased its swelling. This affect may be attributed to the presence of hydroxyl (-OH) and carboxyl (-COOH) functional groups in betalains from dragon fruit peels, which can form hydrogen bond with water molecule (H. M. Azeredo, 2009). The increased hydroxyl content in the film along with intensified interaction between betalain and xyloglucan intensified at higher concentration of EB added, enhanced the film's water retention capacity, leading to a higher swelling index. A similar trend was observed in films based on purple purple-fleshed sweet potato starch and sweet potato peel, where the incorporated of higher anthocyanin extract leading to a greater swelling capacity (Sohany et al. 2021). Likewise, Daei et al. (2022) reported that films made from carrageenan gum with *Plantago psyllium* mucilage, exhibited an increased swelling index upon incorporated of red beet extracts. However, an opposite trend was reported by Cheng et al. (2022), where increasing amount of red cabbage anthocyanin extract (RCAE) led to a lower swelling index of the film. This reduction was attributed to the formation of a denser composite structure between anthocyanin and the film-forming polymer, which restricted water uptake.

4.5.1.5. Water Contact Angle (WCA)

Water contact angle (WCA) measurement is a crucial parameter for determining the hydrophobic or hydrophilic nature of biopolymer film surfaces. A WCA value below 90° indicates a more hydrophilic surface, whereas a value exceeding 90° signifies a hydrophobic surface (Zhang et al., 2020).

As shown in Figure 19, the WCA values of the films were recorded as 92.48 ± 1.21°, 92.06 ± 0.66°, 70.12 ± 1.62°, and 73.68 ± 1.62° ($p < 0.05$), for XC, XC-EB3, XC-EB5, and XC-EB7 respectively. The WCA of XC (92.48 ± 1.21°) confirmed that the xyloglucan-chitosan film was hydrophobic, indicating a higher resistance to water penetration. A larger contact angle, indicative of greater hydrophobicity, correlates with enhanced resistance to water penetration in thin films (Tanpichai et al., 2022). However, the addition of EB led to a significant reduction in WCA, with values decreasing to 70.12 ± 1.62° and 73.68 ± 1.62° ($p < 0.05$) for XC-EB5 and XC-EB7, respectively. This trend indicates an increase in the hydrophilicity of the film surfaces with higher betalain content. The observed results can be attributed to the hydrophilic nature of betalain, which contains hydroxyl groups that enhance the affinity of the film for water (Halloub et al., 2023).

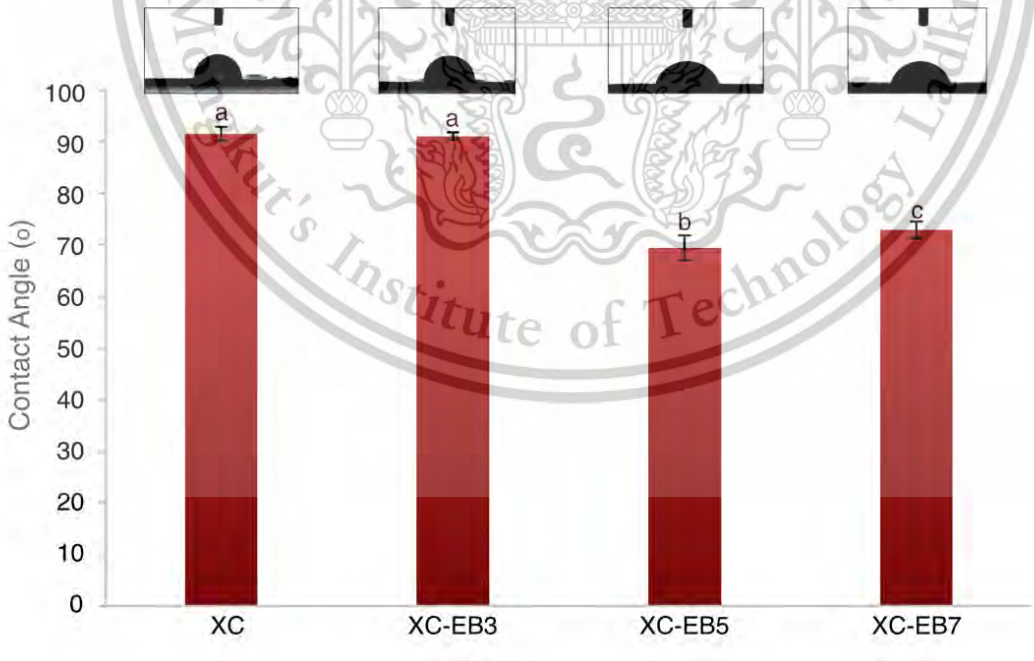

Figure 19 Water contact angle of intelligent films

4.5.1.6. Water Vapor Transmission Rate (WVTR) and Water Vapor Permeability (WVP)

Water Vapor Transmission Rate (WVTR) and Water Vapor Permeability (WVP) are critical parameters in evaluating the barrier properties of films, especially the effectiveness in preventing moisture transfer. WVTR measure the amount of water vapor passes through a unit area over specific time period, while WVP measure the rate of which water vapor permeates through a film, relative to the difference of pressure across it. These parameters are influenced by the polymer molecular structures and the presence of hydrophilic or hydrophobic group (Ghanbarzadeh et al., 2007).

The addition of EB significantly influenced the barrier properties of the films, as evidenced by the observed increases in both WVTR and WVP (Figure 20). For instance, XC-EB3 shows a WVTR of 1.551 ± 0.02 $g \cdot h^{-1} \cdot m^{-2}$ and a WVP of 4.410 ± 0.15 × $10^{-10} \cdot g \cdot h^{-1} \cdot m^{-1} \cdot pa^{-1}$, which are slightly higher than those of the control XC film (1.482 ± 0.059 $g \cdot h^{-1} \cdot m^{-2}$ for WVTR and 3.473 ± 0.14 × $10^{-10} \cdot g \cdot h^{-1} \cdot m^{-1} \cdot pa^{-1}$ for WVA). Further increases in betalain concentration (XC-EB5 and XC-EB7) resulted in more pronounced increases in WVTR and WVP, with the XC-EB7 showing the highest values of 1.814 ± 0.05 02 $g \cdot h^{-1} \cdot m^{-2}$ and 5.923 ± 0.15 × $10^{-10} \cdot g \cdot h^{-1} \cdot m^{-1} \cdot pa^{-1}$ for WVTR and WVP, respectively. This trend suggests that the addition of EB to the XC films affected their barrier properties, likely due to the hygroscopic nature of betalain.

The control XC films exhibited hydrophobic behaviour, evidenced by its higher WCA (92.48 ± 1.21°), which corelated with lower WVTR and WVP (Cui et al., 2023). Hydrophobicity reduces surface wettability, thereby limiting water vapor transmission. However, EB incorporation reduce WCA, indicating increasing hydrophilicity due to betalain's hydroxyl (-OH) and carboxyl (-COOH) groups (Sadowska-Bartosz & Bartosz, 2021b). These groups enhance water affinity, facilitating water vapor permeation. This observation aligns with the hydrophobicity of the film, where an increase in betalain concentration corresponded to a decrease in the hydrophobicity, as shown in Fig 20, thereby affecting the WVTR and WVP of the film. Structural disruptions in the polymer matrix, caused by hydrophilic EB, further amplify WVP (Delgado et al., 2022). Similar findings were reported by Kanatt (2020), who demonstrated that the addition of betalain from Amaranthus leaf extract influenced the physical properties of biopolymer films.

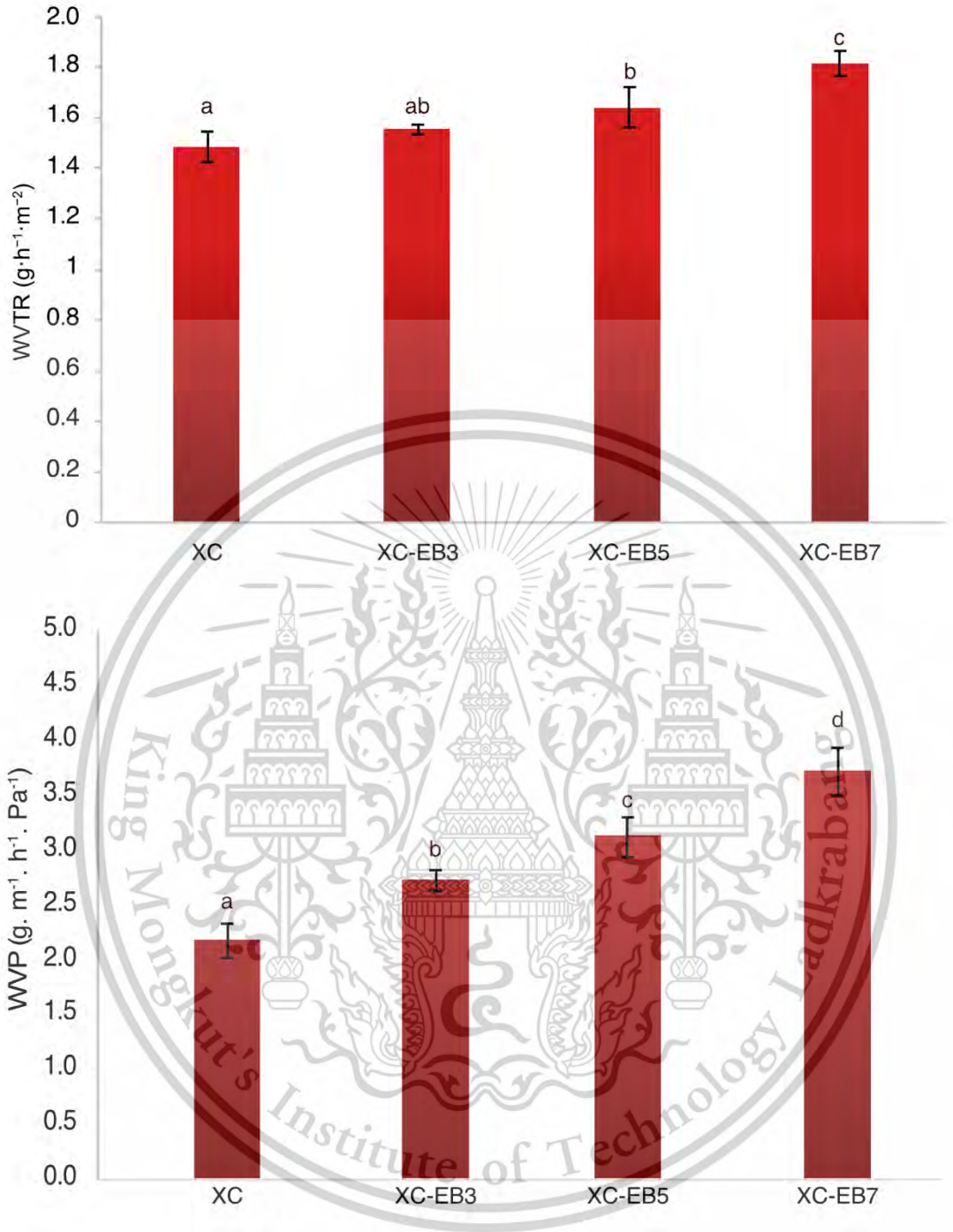

Figure 20 Water vapor transmission rate (WVTR) and Water vapor pressure (WVP) of intelligent packaging film. Values are given as mean ± SD. Different superscript letters in the above bar indicate significantly different ($p < 0.05$)

4.5.2 Mechanical Property of Film

Tensile strength and elongation at break are critical indicators of a film's mechanical performance under stress (Dirpan et al., 2023). As shown in Figure 21, a significant difference ($p < 0.05$) in tensile strength was observed among the films, ranging from 32.47 ± 1.46 to 16.73 ± 0.81 MPa. The XC film exhibited the highest tensile strength among the samples (32.47 ± 1.46 MPa) but this decreased significantly to 16.73 ± 0.81 MPa with increasing EB concentration. This reduction in tensile strength might be attributed to the plasticizing effect of betalain, which disrupts intermolecular interactions between xyloglucan and chitosan. Betalain, due to their hydrophilic nature, may enhance the polymer chains mobility, thereby reducing the overall rigidity of the film (Khan et al., 2024). A similar phenomenon was reported in the polyvinyl alcohol/sodium carboxymethyl cellulose film incorporated with red cabbage anthocyanin, where anthocyanin weakened the polymer network (Liu et al. 2021). However, contrasting finding by Yao et al. (2021) found that the addition of betalain from various sources into starch/polyvinyl alcohol films significantly enhanced tensile strength of the films.

In contrast to tensile strength, increasing EB concentration significantly increased the elongation at break of the films. The lowest elongation at break (144.67 ± 3.53%) was observed for the control XC film, while XC-EB7 demonstrated the highest (190.33 ± 3.91%). This observation aligns with the findings of Yao et al. (2022), who reported similar effects when betacyanin extract from red pitaya flesh was incorporated into polysaccharides and polyvinyl alcohol films. Likewise, other findings by Hu et al. (2020) noted that betalain enhanced the elasticity of chitosan/fish gelatine blend films. This enhancement suggests that the addition of EB into the film may impart a plasticizing effect on the films, enhancing the flexibility and extensibility of film. This effect may be attributed to the abundance of hydroxyl groups in betalain, which promote intermolecular hydrogen bonding with the xyloglucan matrix, thereby reducing polymer rigidity (Etxabide et al., 2021).

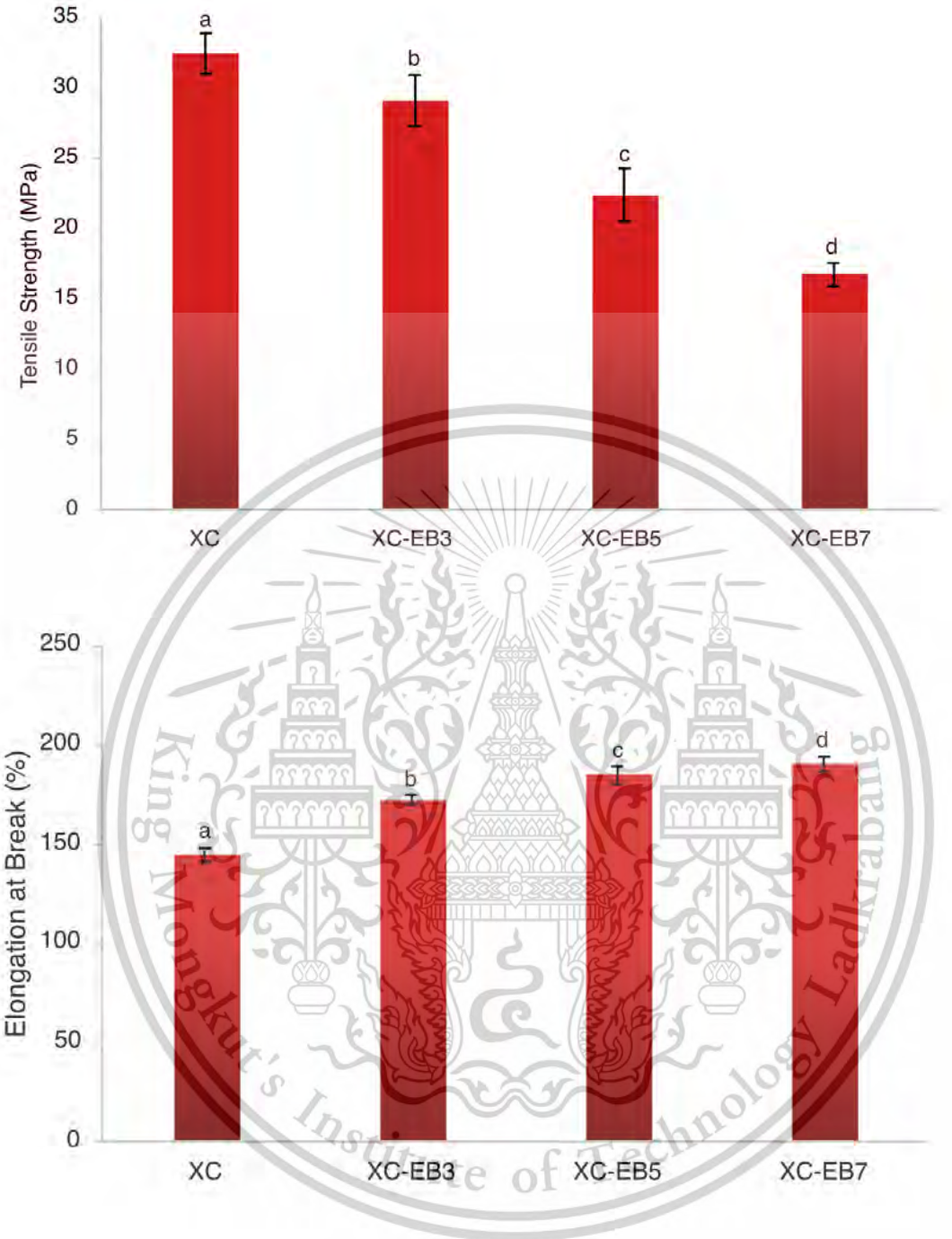

Figure 21 Mechanical properties of intelligent packaging film. (a) Tensile Strength; (b) Elongation at Break. Values are given as mean ± SD. Different superscript letters in the above bar indicate significantly different ($p < 0.05$).

4.5.3 Ammonia-Sensitivities of Film

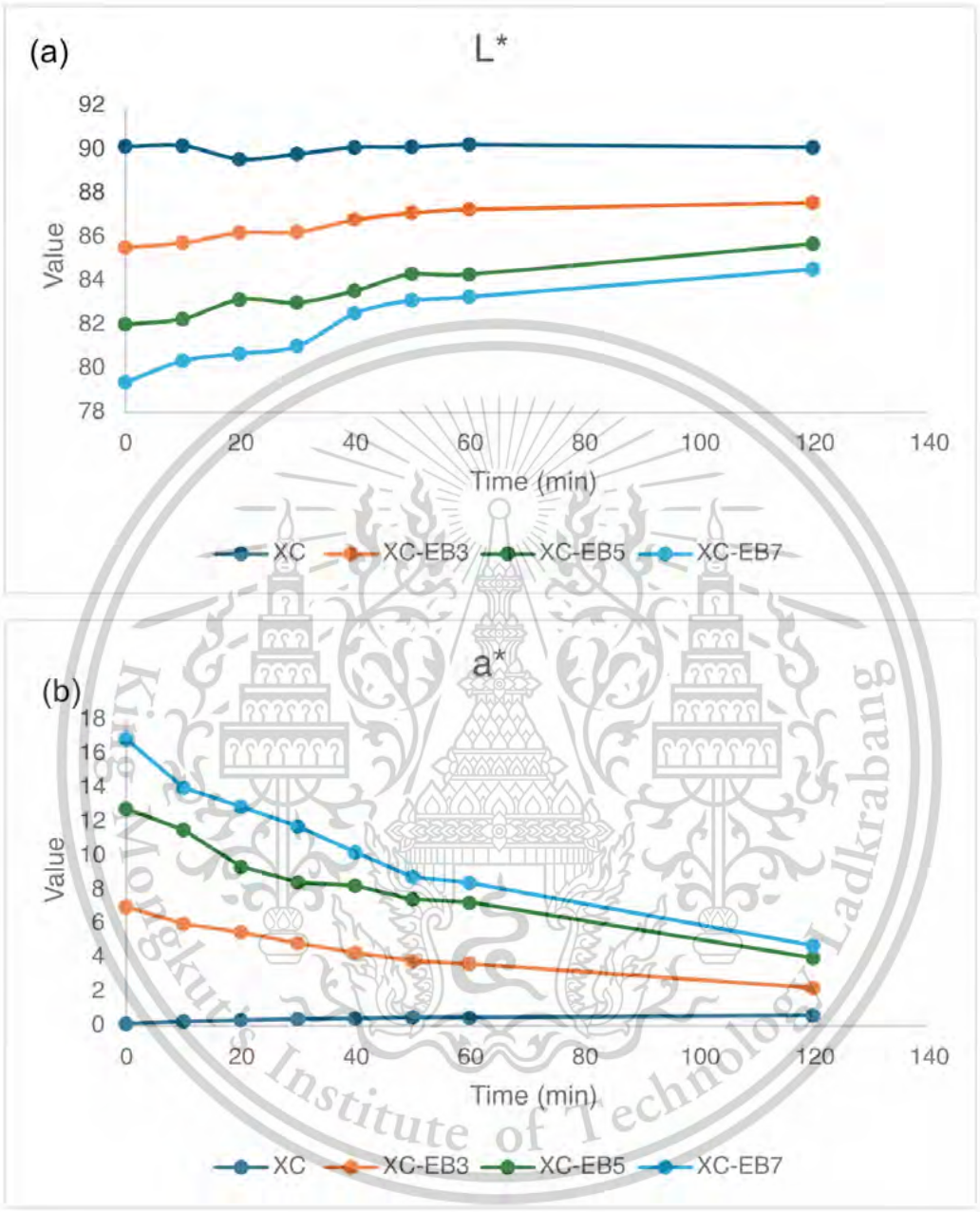

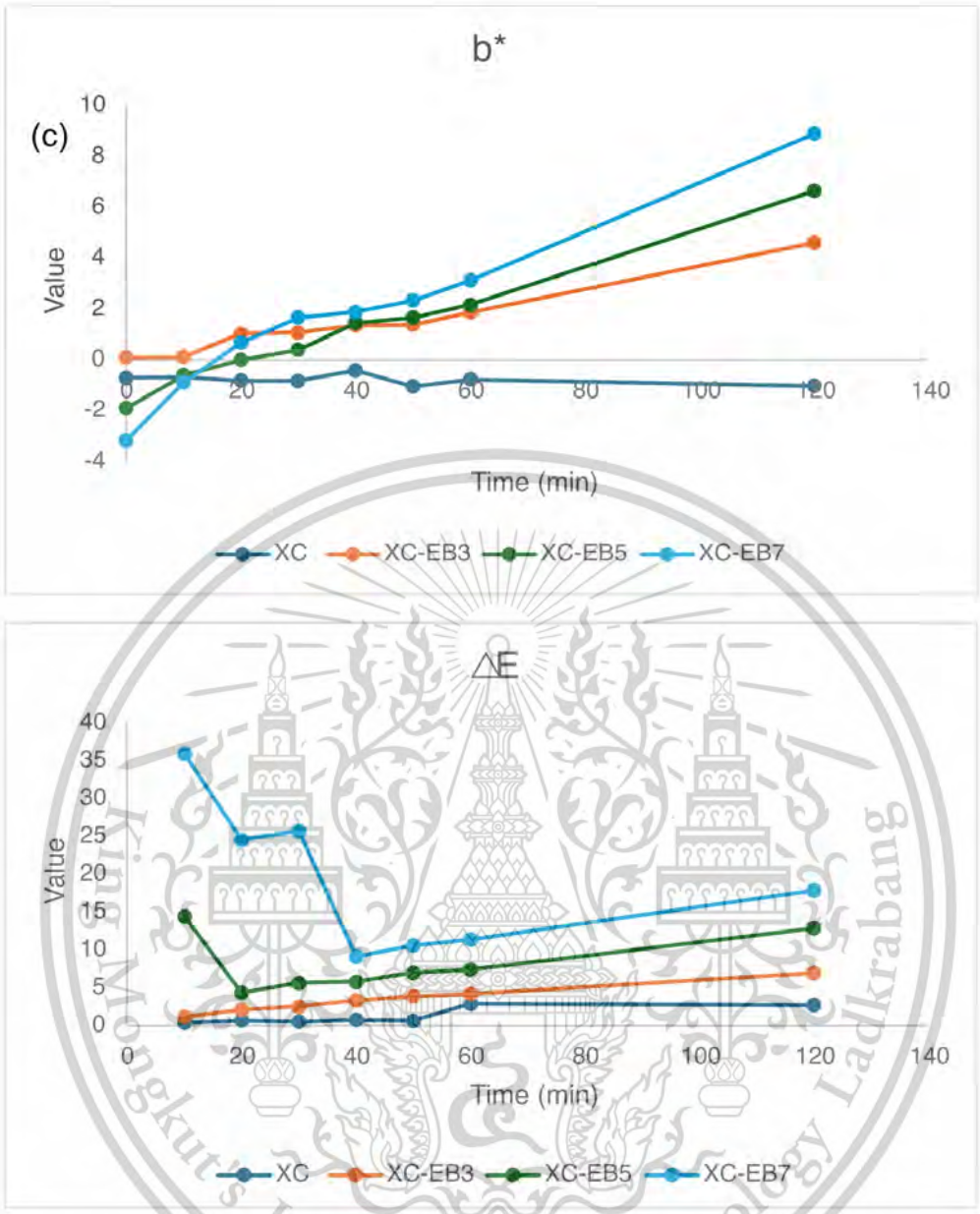

Figure 22 Changes in the color values of intelligent packaging film containing different betalain content for 120 mins. (a) Lightness (L*) value; (b) Redness/greenness (a*) value; Yellowness/blueness (b*) value; and Total color difference (ΔE) value

One of the key volatile nitrogen compounds produced during the microbial food spoilage of protein-rich food is ammonia. Microbial activity not only deteriorates protein-rich food but also alter their pH, and generates volatile nitrogen compounds, such as ammonia, dimethylamine, and trimethylamine (Esposito et al., 2018). The ammonia sensitivity test is commonly used as an indicator of food degradation. The result of ammonia sensitivity test for

the films revealed significant changes in colorimetric parameters over time, demonstrating their potential as ammonia-responsive indicators.

The incorporation of EB into the XC matrix influence the film's responses to ammonia exposure. As observed in the L* values (Figure 22a), the XC film maintained a relatively stable lightness, likely due to the resistance of chitosan and xyloglucan to ammonia-induced structural changes. In contrast, the XC-EB films exhibited a gradual increase in L*, indicating a lightening effect upon ammonia interaction. This phenomenon can be attributed to alkaline-induced structural modification in betalain molecules, which alter their light absorption properties (Herbach et al., 2006c).

The a* values of XC-EB films exhibited a pronounced decrease, signifying a loss of redness. While the b* value increased, indicating a shift toward yellow, particularly in film with higher betalain concentrations (XC-EB5 and XC-EB7). This color transition is likely caused by the deprotonation of betalain chromophores in the presence of ammonia, which increase the pH of the environment, and leads to the formation of degradation products of betalain, such as betalamic acid and cyclo-DOPA derivatives (Ciriminna et al., 2018). Similar finding was reported by Jiang et al. (2023), who demonstrated the ammonia sensitivity of films incorporated with betalain.

A ΔE value exceeding 5, indicates a noticeable color difference detectable by the human eyes, confirm that the film underwent visually perceptible change (Canizales-Rodríguez et al., 2024). For example, ammonia-sensitive films incorporating dragon fruit betacyanins exhibited faster color changes (within 10 minutes) compared to those containing beetroot-derived pigments, emphasizing the practical significance of ΔE in real-time freshness monitoring (Le et al., 2024). The overall color change (ΔE) further highlights those films with higher betalain content (XC-EB5 and XC-EB7) demonstrated greater sensitivity to ammonia, as evidenced by the larger ΔE values (Figure 22d). This increased responsiveness can be attributed to the higher availability of betalain molecules for interaction with ammonia molecules, resulting in a more pronounced color shift. The observed colorimetric variations suggest that film with higher betalain concentrations have strong potential applications as visual indicators in food packaging systems, enhancing real-time monitoring of food freshness.

4.5.4 Application of Films to Shrimp Spoilage Detection

Table 12 The TVB-N level changes of shrimp during storage at 4 °C for 8 days and the color changes of xyloglucan/chitosan film with betalain extract from dragon fruit peels

Time (day)	TVB-N Level (mg/100 g)	ΔE			
		XC	XC-EB3	XC-EB5	XC-EB7
Day 0	14.88 ± 0.32[a]	-	-	-	-
Day 2	20.11 ± 0.09[b]	8.03 ± 0.88	11.53 ± 1.55	8.26 ± 1.13	8.57 ± 0.13
Day 4	25.87 ± 0.29[c]	7.39 ± 0.58	12.75 ± 1.63	8.80 ± 1.29	10.77 ± 0.65
Day 6	43.41 ± 0.33[d]	8.06 ± 1.03	12.40 ± 1.22	17.82 ± 1.26	20.75 ± 0.22
Day 8	70.83 ± 0.45[e]	8.01 ± 1.38	12.81 ± 1.40	21.99 ± 0.74	27.11 ± 0.58

Values are given as mean ± SD. Different superscript letters in the same column indicate significantly different ($p < 0.05$).

Meat and fish, as protein-rich foods, are highly susceptible to spoilage during storage due to lipid oxidation and microbial proliferation. These foods are typically stored under refrigerated or frozen conditions to maintain their quality and characteristic properties (Mutwakil, 2011; Wazir et al., 2019). Shrimp, one of the most perishable seafoods due to the presence of water, fatty acids, and proteins, is prone to microbial contamination during transportation and storage, and subsequently produces several volatile amines such as ammonia, dimethylamine, and trimethylamine (Kanatt, 2020). Ammonia, a key component of Total Volatile Base Nitrogen (TVB-N), is generated through proteolysis in meat or fish during storage and serves widely recognized indicator of seafood freshness. Initially, in the total TVB-N of the fresh shrimp was determined to be 14.88 ± 0.32 mg/100 g (Table 11).

The results showed that, the amount of TVB-N of shrimp stored in 4 °C increased significantly, with values 14.88 ± 0.32, 20.11 ± 0.09, 25.87 ± 0.29, 43.41 ± 0.33, and 70.83 ± 0.45 (mg/100 g shrimp) for each 2 days periods ($p < 0.05$) as shown in Table 11. This increase in TVB-N corresponded with a visible color change in the XC-EB3, XC-EB5, and XC-EB7 films over the observation period. Notably, the XC-EB3 film exhibited an obvious color shift by the 4th day of observation, while all EB-containing films showed distinct color changes by the 6th day.

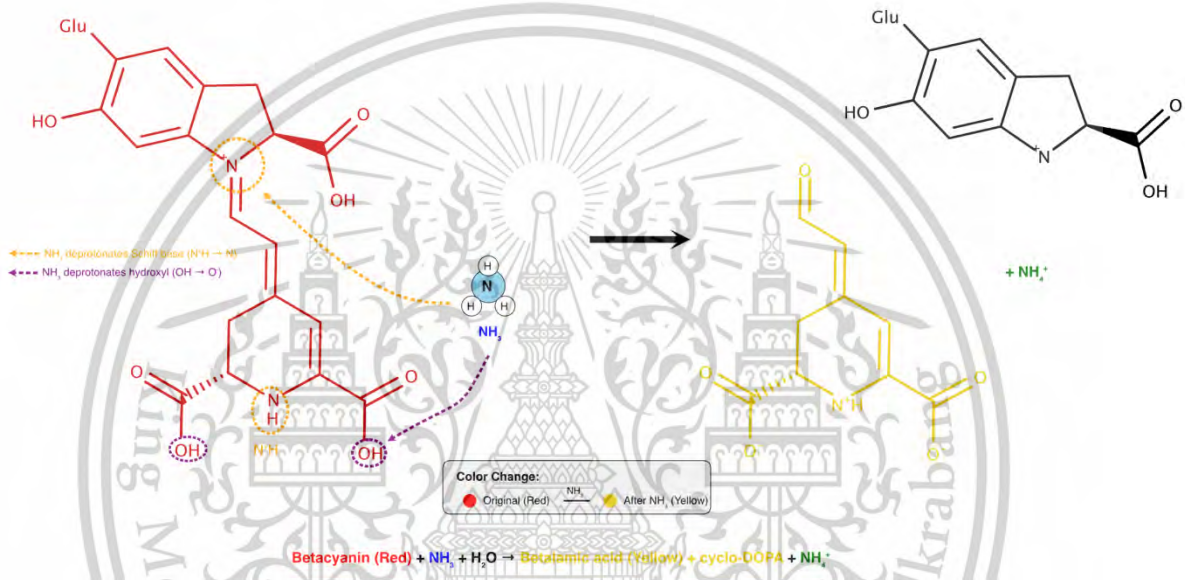

Figure 23 Mechanism of interaction between betalain and ammonia

The color change in the EB-containing film occurs due to interaction with ammonia released by shrimp during storage. Stored shrimp release compounds such as ammonia, trimethylamine (TMA), and dimethylamine (DMA), formed through enzymatic activity and microbial growth (Parlapani et al., 2024). Ammonia serves as the primary compound detected by the EB-containing film. The presence of ammonia, a volatile base, increases the film's pH. Increased ammonia levels, indicated by rising TVB-N values, cause structural changes where betacyanin breaks down into yellow betalamic acid, as previously described in Figure 23. Ammonia molecule act as a base and abstracts a proton (H^+) in betacyanin, particularly from the nitrogen atom. This creates NH_4^+ (ammonium ion) and leaves the betacyanin structure with a negative charge. The loss of the proton triggers structural rearrangement within the betacyanin molecule, specifically affecting the dihydropyridine ring and adjacent carbon-

nitrogen bonds. As a result of this structural transformation, the absorption spectrum of betacyanin shifts, causing the observable color change from red-violet to yellow(Naghdi et al., 2021). Consequently, the rise in TVB-N positively correlates with increased ammonia levels, leading to structural changes in betalain within the XC-EB film and resulting in a color shift to yellow.

These finding suggest that shrimp spoilage progressed over time during storage and that the intelligent film effectively detected shrimp deterioration as TVB-N level increases. Similar observations were reported by Abdolmaleki et al. (2024), who demonstrated film based on gelatin/hydroxymethyl cellulose films containing red beetroot extract successfully detected shrimp and meat spoilage during storage. Additionally, Zou et al. (2024) also found that alizarin-based colorimetric nanofibrous films exhibited visible color change corresponding to TVB-N levels, further validating the effectiveness of colorimetric indicator for seafood freshness monitoring.

CHAPTER 5
CONCLUSION

5.1 Conclusion

This study successfully optimized the extraction of betalain from dragon fruit peel waste using BBD (Box-Behnken Design). The solid-to-liquid extraction ratio significantly influenced the yield, with optimal conditions identified as pH 3.6, a temperature of 30°C, an extraction time of 10 minutes, and a solid-to-liquid ratio of 1:15. Under these conditions, the betalain yield reached 73.09 ± 1.79 mg/L, closely matching the expected value of 72.37 mg/L. Acidic conditions and lower solid-to-liquid ratios were found to enhance betacyanin extraction, while pH changes were shown to affect the extract's color parameters (L*, a*, b*) due to betacyanin degradation into betalamic acid and cyclo-DOPA, as confirmed by FTIR analysis. These findings highlight the potential of betalain extract from dragon fruit peel as a natural colorant, supporting sustainability by reducing agro-industrial waste.

Furthermore, this research demonstrated the integration of agricultural waste materials, such as xyloglucan from tamarind seed kernel waste and betalain from dragon fruit peels, to develop intelligent packaging films. The interaction between xyloglucan, chitosan, and betalain revealed a combination of electrostatic forces and hydrogen bonding, influencing colloidal stability and the hydrogels' elasticity and viscosity. The incorporation of betalain significantly affected the structural, mechanical, and functional properties of the films. Among the tested formulations, XC-EB5 was identified as the most suitable for intelligent packaging, offering superior sensitivity to TVB-N for monitoring the freshness of protein-rich foods. This study underscores the potential of xyloglucan-chitosan films containing betalain as intelligent packaging solutions, promoting food safety, quality, and sustainability.

5.2 Suggestion

In this study, betalain was successfully extracted from dragon fruit peels. This betalain was subsequently utilized as an intelligent film for indicating spoilage in shrimp freshness by incorporating it into xyloglucan-chitosan film. The film was effectively applied to detect shrimp spoilage in a trial experiment. However, further improvements can be implemented to enhance the application of this intelligent film, such as increasing the film's strength and hydrophobicity to prevent damage due to water vapor produced by the food products.

Application to other food materials is necessary to comprehensively understand the function of betalain as a freshness indicator. Furthermore, the film can also be used for detecting formaldehyde in food products.

REFERENCES

Abdolmaleki, K., Rezaei, F., Mohammadi, R., Zare, L., & Shahmoradi, S. (2024). The application of film based on gelatin/hydroxymethyl cellulose and red beetroot betalain in smart food packaging. *Food Science and Technology International*, 10820132241266112. https://doi.org/10.1177/10820132241266112

Abirami, K., Swain, S., Baskaran, V., Venkatesan, K., Sakthivel, K., & Bommayasamy, N. (2021). Distinguishing three Dragon fruit (Hylocereus spp.) species grown in Andaman and Nicobar Islands of India using morphological, biochemical and molecular traits. *Scientific Reports*, *11*(1), 2894. https://doi.org/10.1038/s41598-021-81682-x

Adair, P., Sriprom, P., Narkrugsa, W., Phumjan, L., Manamoongmongkol, K., Permana, L., & Assawasaengrat, P. (2023). Preparation, characterization, and antimicrobial activity of xyloglucan-chitosan film from tamarind (tamarind indica L.) seed kernel. *Progress in Organic Coatings*, *179*, 107486. https://doi.org/10.1016/j.porgcoat.2023.107486

Ahmad, A., Alkharfy, K. M., Wani, T. A., & Raish, M. (2015). Application of Box–Behnken design for ultrasonic-assisted extraction of polysaccharides from Paeonia emodi. *International Journal of Biological Macromolecules*, *72*, 990–997. https://doi.org/10.1016/j.ijbiomac.2014.10.011

Alemu, D., Getachew, E., & Mondal, A. K. (2023). Study on the Physicochemical Properties of Chitosan and their Applications in the Biomedical Sector. *International Journal of Polymer Science*, *2023*(1), 5025341. https://doi.org/10.1155/2023/5025341

Amnuaikit, T., Khakhong, S., & Khongkow, P. (2019). Formulation Development and Facial Skin Evaluation of Serum Containing Jellose from Tamarind Seeds. *Journal of Pharmaceutical Research International*, *31*(4), Article 4. https://doi.org/10.9734/jpri/2019/v31i430306

Azeredo, H. M. (2009). *Betalains: Properties, sources, applications, and stability—A review*. https://doi.org/10.1111/J.1365-2621.2007.01668.X

Azeredo, H. M. C. (2009). Betalains: Properties, sources, applications, and stability - A review. *International Journal of Food Science and Technology*, *44*(12), 2365–2376. https://doi.org/10.1111/j.1365-2621.2007.01668.x

Badan Standardisasi Nasional. (2009). *Cara uji kimia-Bagian 8: Penentuan kadar Total Volatil Base Nitrogen (TVB-N) dan Trimetil Amin Nitrogen (TMA-N) pada produk perikanan* (No. SNI 2354.8:2009). Badan Standardisasi Nasional.

Bagul, M. B., Sonawane, S. K., & Arya, S. S. (2018). Bioactive characteristics and optimization of tamarind seed protein hydrolysate for antioxidant-rich food formulations. *3 Biotech*, *8*(4), 218. https://doi.org/10.1007/s13205-018-1240-0

Bakar, J., Ee, S. C., Syed Muhammad, S. K., Mat Hashim, D., & Mohd Adzahan, N. (2011). Physico-chemical characteristics of red pitaya (Hylocereus polyrhizus) peel. *International Food Research Journal*, *18*(1), Article 1.

Barkociová, M., Tóth, J., Sutor, K., Drobnicka, N., Wybraniec, S., Dudík, B., Bilková, A., & Czigle, S. (2021). Betalains in Edible Fruits of Three Cactaceae Taxa—Epiphyllum, Hylocereus, and Opuntia—Their LC-MS/MS and FTIR Identification and Biological Activities Evaluation. *Plants*, *10*(12), 2669. https://doi.org/10.3390/plants10122669

Basavaraja, T., Joshi, A., Sethi, S., Arora, B., Tomar, B. S., Varghese, E., & Yadav, A. (2022). Extraction procedure of betalains pigments from hardy beetroot matrix and its stabilization. *Journal of Food Processing and Preservation*, *46*(10). https://doi.org/10.1111/jfpp.16844

Bayindirli, A., Yildiz, F., & Özilgen, M. (1988). Modeling of Sequential Batch Ultrafiltration of Red Beet Extract. *Journal of Food Science*, *53*(5), 1418–1421. https://doi.org/10.1111/j.1365-2621.1988.tb09290.x

Bhagya Raj, G. V. S., & Dash, K. K. (2020). Ultrasound-assisted extraction of phytocompounds from dragon fruit peel: Optimization, kinetics and thermodynamic studies. *Ultrasonics Sonochemistry*, *68*. https://doi.org/10.1016/j.ultsonch.2020.105180

Brun-Graeppi, A. K. A. S., Richard, C., Bessodes, M., Scherman, D., Narita, T., Ducouret, G., & Merten, O.-W. (2010). Study on the sol–gel transition of xyloglucan hydrogels. *Carbohydrate Polymers*, *80*(2), 555–562 . https://doi.org/10.1016/j.carbpol.2009.12.026

Calva-Estrada, S. J., Jiménez-Fernández, M., & Lugo-Cervantes, E. (2022). Betalains and their applications in food: The current state of processing, stability and future opportunities in the industry. *Food Chemistry: Molecular Sciences*, *4*, 100089. https://doi.org/10.1016/j.fochms.2022.100089

Canizales-Rodríguez, D. F., Rodríguez-Félix, F., Tapia-Hernández, J. A., Del-Toro-Sánchez, C. L., Ruíz-Cruz, S., Aubourg, S. P., Ocaño-Higuera, V. M., Silvas-García, M. I., Figueroa-Enríquez, C. E., & Álvarez-Moreno, M. G. (2024). Poly (Lactic Acid) Fibrous Film with Betalains from Pitaya (Stenocereus thurberi) by Electrospinning for Potential Use as Smart Food Packaging. *Coatings*, *14*(12), Article 12. https://doi.org/10.3390/coatings14121581

Cardoso-Ugarte, G. A., Sosa-Morales, M. E., Ballard, T., Liceaga, A., & San Martín-González, M. F. (2014). Microwave-assisted extraction of betalains from red beet (Beta vulgaris). *LWT - Food Science and Technology*, *59*(1), 276–282. https://doi.org/10.1016/J.LWT.2014.05.025

Castellar, R., Obón, J. M., Alacid, M., & Fernández-López, J. A. (2003). Color Properties and Stability of Betacyanins from *Opuntia* Fruits. *Journal of Agricultural and Food Chemistry*, *51*(9), 2772–2776. https://doi.org/10.1021/jf021045h

Cejudo-Bastante, M. J., Chaalal, M., Louaileche, H., Parrado, J., & Heredia, F. J. (2014). Betalain Profile, Phenolic Content, and Color Characterization of Different Parts and Varieties of Opuntia ficus-indica. *Journal of Agricultural and Food Chemistry*, *62*(33), 8491–8499. https://doi.org/10.1021/jf502465g

Chaari, M., Elhadef, K., Akermi, S., Ben Akacha, B., Fourati, M., Chakchouk Mtibaa, A., Ennouri, M., Sarkar, T., Shariati, M. A., Rebezov, M., Abdelkafi, S., Mellouli, L., & Smaoui, S. (2022). Novel Active Food Packaging Films Based on Gelatin-Sodium Alginate Containing Beetroot Peel Extract. *Antioxidants*, *11*(11), Article 11. https://doi.org/10.3390/antiox11112095

Chandran, J., Nisha, P., Singhal, R. S., & Pandit, A. B. (2014). Degradation of colour in beetroot (Beta vulgaris L.): A kinetics study. *Journal of Food Science and Technology*, *51*(10), 2678–2684. https://doi.org/10.1007/s13197-012-0741-9

Chang, H., Kao, M.-J., Chen, T.-L., Chen, C.-H., Cho, K.-C., & Lai, X.-R. (2013). Characterization of Natural Dye Extracted from Wormwood and Purple Cabbage for Dye-Sensitized Solar Cells. *International Journal of Photoenergy*, *2013*, e159502. https://doi.org/10.1155/2013/159502

Chen, L.-C., Kung, S.-K., Chen, H.-H., & Lin, S.-B. (2010). Evaluation of zeta potential difference as an indicator for antibacterial strength of low molecular weight chitosan. *Carbohydrate Polymers*, *82*(3), 913–919. https://doi.org/10.1016/j.carbpol.2010.06.017

Cheng, M., Yan, X., Cui, Y., Han, M., Wang, X., Wang, J., & Zhang, R. (2022). An eco-friendly film of pH-responsive indicators for smart packaging. *Journal of Food Engineering*, *321*, 110943. https://doi.org/10.1016/j.jfoodeng.2022.110943

Cheok, A., W. George, T., Rodriguez-Mateos, A., & W. Caton, P. (2020). The effects of betalain-rich cacti (dragon fruit and cactus pear) on endothelial and vascular function:

A systematic review of animal and human studies. *Food & Function*, *11*(8), 6807–6817. https://doi.org/10.1039/D0FO00537A

Ciriminna, R., Fidalgo, A., Danzì, C., Timpanaro, G., Ilharco, L. M., & Pagliaro, M. (2018). Betanin: A Bioeconomy Insight into a Valued Betacyanin. *ACS Sustainable Chemistry & Engineering*, *6*(3), 2860–2865. https://doi.org/10.1021/acssuschemeng.7b04163

Cui, C., Gao, L., Dai, L., Ji, N., Qin, Y., Shi, R., Qiao, Y., Xiong, L., & Sun, Q. (2023). Hydrophobic Biopolymer-Based Films: Strategies, Properties, and Food Applications. *Food Engineering Reviews*, *15*(2), 360–379. https://doi.org/10.1007/s12393-023-09342-6

Czyrski, A., & Sznura, J. (2019). The application of Box-Behnken-Design in the optimization of HPLC separation of fluoroquinolones. *Scientific Reports*, *9*(1), Article 1. https://doi.org/10.1038/s41598-019-55761-z

Daei, S., Mohtarami, F., & Pirsa, S. (2022). A biodegradable film based on carrageenan gum/Plantago psyllium mucilage/red beet extract: Physicochemical properties, biodegradability and water absorption kinetic. *Polymer Bulletin*, *79*(12), 11317–11338. https://doi.org/10.1007/s00289-021-04067-0

Day, B. P. F., & Potter, L. (2011). Active Packaging. In *Food and Beverage Packaging Technology* (pp. 251–262). John Wiley & Sons, Ltd. https://doi.org/10.1002/9781444392180.ch9

Delgado, J. F., Peltzer, M. A., & Salvay, A. G. (2022). Water Vapour Transport in Biopolymeric Materials: Effects of Thickness and Water Vapour Pressure Gradient on Yeast Biomass-Based Films. *Journal of Polymers and the Environment*, *30*(7), 2976–2989. https://doi.org/10.1007/s10924-022-02412-6

Delgado-Vargas, F., Jimenez, A. R., & Paredes-López, O. (2000). Natural pigments: Carotenoids, anthocyanins, and betalains—Characteristics, biosynthesis, processing,

and stability. *Critical Reviews in Food Science and Nutrition*, *40*, 173–289. https://doi.org/10.1080/10408690091189257

Deng, F., He, Y., Li, B., Song, Y., & Wu, X. (2018). Design of a slotted chipless RFID humidity sensor tag. *Sensors and Actuators B: Chemical*, *264*, 255–262. https://doi.org/10.1016/j.snb.2018.02.153

Di Donato, P., Poli, A., Taurisano, V., & Nicolaus, B. (2014). *Polysaccharides: Applications in Biology and Biotechnology/Polysaccharides from Bioagro-Waste New Biomolecules-Life* (pp. 1–29). https://doi.org/10.1007/978-3-319-03751-6_16-1

Dirpan, A., Ainani, A. F., & Djalal, M. (2023). A Review on Biopolymer-Based Biodegradable Film for Food Packaging: Trends over the Last Decade and Future Research. *Polymers*, *15*(13), Article 13. https://doi.org/10.3390/polym15132781

do Carmo Brito, B. de N., da Silva Pena, R., Santos Lopes, A., & Campos Chisté, R. (2017). Anthocyanins of Jambolão (Syzygium cumini): Extraction and pH-Dependent Color Changes. *Journal of Food Science*, *82*(10), 2286–2290. https://doi.org/10.1111/1750-3841.13847

Dutta, P., Giri, S., & Giri, T. K. (2020). Xyloglucan as green renewable biopolymer used in drug delivery and tissue engineering. *International Journal of Biological Macromolecules*, *160*, 55–68. https://doi.org/10.1016/j.ijbiomac.2020.05.148

Echegaray, N., Guzel, N., Kumar, M., Guzel, M., Hassoun, A., & Lorenzo, J. M. (2023). Recent advancements in natural colorants and their application as coloring in food and in intelligent food packaging. *Food Chemistry*, *404*, 134453. https://doi.org/10.1016/j.foodchem.2022.134453

Elmarzugi, N., LK, C., A, A., FD, A., & A, E. (2016). Phytochemical Properties and Health Benefits of Hylocereus undatus. *Nanomedicine & Nanotechnology Open Access*, *1*(1). https://doi.org/10.23880/NNOA-16000103

Elsabee, M. Z., & Abdou, E. S. (2013). Chitosan based edible films and coatings: A review. *Materials Science and Engineering: C*, *33*(4), 1819–1841. https://doi.org/10.1016/j.msec.2013.01.010

Esposito, G., Sciuto, S., & Acutis, P. L. (2018). Quantification of TMA in fishery products by direct sample analysis with high resolution mass spectrometry. *Food Control*, *94*, 162–166. https://doi.org/10.1016/j.foodcont.2018.07.010

Esteves, L. C., Pinheiro, A. C., Pioli, R. M., Penna, T. C., Baader, W. J., Correra, T. C., & Bastos, E. L. (2018). Revisiting the Mechanism of Hydrolysis of Betanin. *Photochemistry and Photobiology*, *94*(5), 853–864. https://doi.org/10.1111/php.12897

Etxabide, A., Maté, J. I., & Kilmartin, P. A. (2021). Effect of curcumin, betanin and anthocyanin containing colourants addition on gelatin films properties for intelligent films development. *Food Hydrocolloids*, *115*, 106593 . https://doi.org/10.1016/j.foodhyd.2021.106593

Ezati, P., Tajik, H., Moradi, M., & Molaei, R. (2019). Intelligent pH-sensitive indicator based on starch-cellulose and alizarin dye to track freshness of rainbow trout fillet. *International Journal of Biological Macromolecules*, *132*, 157–165. https://doi.org/10.1016/j.ijbiomac.2019.03.173

Fernández-López, J., Ponce-Martínez, A. J., Rodríguez-Párraga, J., Solivella-Poveda, A. M., Fernández-López, J. A., Viuda -Martos, M., & Pérez-Alvarez, J. A. (2023). Beetroot juices as colorant in plant-based minced meat analogues: Color, betalain composition and antioxidant activity as affected by juice type. *Food Bioscience*, *56*, 103156. https://doi.org/10.1016/j.fbio.2023.103156

Freshtag by Vitsab | Freshtag 4 your business. (n.d.). Retrieved March 6, 2025, from https://vitsab.com/

FRY, S. C. (1989). The Structure and Functions of Xyloglucan. *Journal of Experimental Botany*, *40*(1), 1–11. https://doi.org/10.1093/jxb/40.1.1

Fu, L., Liu, S., Li, S., Li, Y., & Ma, M. (2017). Characterization of Hemicelluloses Extracted from *Populus tomentosa* Carr. By the Hydrothermal Method with Ethanol. *Paper and Biomaterials*, *2*(3), 1–11. https://doi.org/10.26599/PBM.2017.9260015

Gandía-Herrero, F., & García-Carmona, F. (2013). Biosynthesis of betalains: Yellow and violet plant pigments. *Trends in Plant Science*, *18*(6), 334–343. https://doi.org/10.1016/j.tplants.2013.01.003

Gao, L., Liu, P., Liu, L., Li, S., Zhao, Y., Xie, J., & Xu, H. (2022). κ-carrageenan-based pH-sensing films incorporated with anthocyanins or/and betacyanins extracted from purple sweet potatoes and peels of dragon fruits. *Process Biochemistry*, *121*, 463–480. https://doi.org/10.1016/j.procbio.2022.07.019

Gengatharan, A., Dykes, G. A., & Choo, W. S. (2015). Betalains: Natural plant pigments with potential application in functional foods. *LWT - Food Science and Technology*, *64*(2), 645–649. https://doi.org/10.1016/j.lwt.2015.06.052

Ghanbarzadeh, B., Musavi, M., Oromiehie, A. R., Rezayi, K., Razmi Rad, E., & Milani, J. (2007). Effect of plasticizing sugars on water vapor permeability, surface energy and microstructure properties of zein films. *LWT - Food Science and Technology*, *40*(7), 1191–1197. https://doi.org/10.1016/j.lwt.2006.07.008

Gidley, M. J., Lillford, P. J., Rowlands, D. W., Lang, P., Dentini, M., Crescenzi, V., Edwards, M., Fanutti, C., & Grant Reid, J. S. (1991). Structure and solution properties of tamarind-seed polysaccharide. *Carbohydrate Research*, *214*(2), 299–314. https://doi.org/10.1016/0008-6215(91)80037-N

Gnanasambandam, R., & Proctor, A. (2000). Determination of pectin degree of esterification by diffuse reflectance Fourier transform infrared spectroscopy. *Food Chemistry*, *68*(3), 327–332. https://doi.org/10.1016/S0308-8146(99)00191-0

Guo, Q., Yuan, Y., He, M., Zhang, X., Li, L., Zhang, Y., & Li, B. (2023). Development of a multifunctional food packaging for meat products by incorporating carboxylated cellulose nanocrystal and beetroot extract into sodium alginate films. *Food Chemistry*, *415*, 135799. https://doi.org/10.1016/j.foodchem.2023.135799

Gurunathan, K. (2024). Time–Temperature Indicators (TTIs) for Monitoring Food Quality. In *Smart Food Packaging Systems* (pp. 281–304). John Wiley & Sons, Ltd. https://doi.org/10.1002/9781394189595.ch11

Halloub, A., Raji, M., Essabir, H., Nekhlaoui, S., Bensalah, M.-O., Bouhfid, R., & Qaiss, A. el kacem. (2023). Stable smart packaging betalain-based from red prickly pear covalently linked into cellulose/alginate blend films. *International Journal of Biological Macromolecules*, *234*, 123764. https://doi.org/10.1016/j.ijbiomac.2023.123764

Han, J., Meade, J., Devine, D., Sadeghpour, A., Rappolt, M., & Goycoolea, F. M. (2024). Chitosan-coated liposomal systems for delivery of antibacterial peptide LL17-32 to Porphyromonas gingivalis. *Heliyon*, *10*(14). https://doi.org/10.1016/j.heliyon.2024.e34554

Hansen, N. M. L., & Plackett, D. (2008). Sustainable films and coatings from hemicelluloses: A review. *Biomacromolecules*, *9*(6), 1493–1505. https://doi.org/10.1021/bm800053z

Harivaindaran, K. V., Rebecca, O. P. S., & Chandran, S. (2008). Study of optimal temperature, pH and stability of dragon fruit (Hylocereus polyrhizus) peel for use as potential natural colorant. *Pakistan Journal of Biological Sciences*, *11*(18), 2259–2263. https://doi.org/10.3923/PJBS.2008.2259.2263

Helander, I. M., Nurmiaho-Lassila, E.-L., Ahvenainen, R., Rhoades, J., & Roller, S. (2001). Chitosan disrupts the barrier properties of the outer membrane of Gram-negative bacteria. *International Journal of Food Microbiology*, *71*(2), 235–244. https://doi.org/10.1016/S0168-1605(01)00609-2

Herbach, K. M., Stintzing, F. C., & Carle, R. (2005). Identification of heat-induced degradation products from purified betanin, phyllocactin and hylocerenin by high-performance liquid chromatography/electrospray ionization mass spectrometry. *Rapid Communications in Mass Spectrometry*, *19*(18), 2603–2616. https://doi.org/10.1002/rcm.2103

Herbach, K. M., Stintzing, F. C., & Carle, R. (2006a). Betalain Stability and Degradation—Structural and Chromatic Aspects. *Journal of Food Science*, *71*(4), R41–R50. https://doi.org/10.1111/j.1750-3841.2006.00022.x

Herbach, K. M., Stintzing, F. C., & Carle, R. (2006b). Stability and Color Changes of Thermally Treated Betanin, Phyllocactin, and Hylocerenin Solutions. *Journal of Agricultural and Food Chemistry*, *54*(2), 390–398. https://doi.org/10.1021/jf051854b

Herbach, K. M., Stintzing, F., & Carle, R. (2006c). Betalain stability and degradation–structural and chromatic aspects. *Journal of Food Science*, *71*, 6. https://doi.org/10.1111/J.1750-3841.2006.00022.X

Heredia, N., Caballero, C., Cárdenas, C., Molina, K., García, R., Solís, L., Burrowes, V., Bartz, F. E., De Aceituno, A. F., Jaykus, L.-A., García, S., & Leon, J. (2016). Microbial Indicator Profiling of Fresh Produce and Environmental Samples from Farms and Packing Facilities in Northern Mexico. *Journal of Food Protection*, *79*(7), 1197–1209. https://doi.org/10.4315/0362-028X.JFP-15-499

Hu, H., Yao, X., Qin, Y., Yong, H., & Liu, J. (2020). Development of multifunctional food packaging by incorporating betalains from vegetable amaranth (Amaranthus tricolor

L.) into quaternary ammonium chitosan/fish gelatin blend films. *International Journal of Biological Macromolecules*, *159*, 675–684. https://doi.org/10.1016/j.ijbiomac.2020.05.103

Huang, A. S., & Elbe, J. H. V. (1987). Effect of pH on the Degradation and Regeneration of Betanine. *Journal of Food Science*, *52*(6), 1689–1693. https://doi.org/10.1111/j.1365-2621.1987.tb05907.x

Huang, B., Hill, R., & van de Ven, T. (2012). Nanopaper: Thin Films Prepared from Polymeric Nanotubes. *Macromolecular Materials and Engineering*, *297*(8), 821–830. https://doi.org/10.1002/mame.201100322

Islam, Md. N., Liza, A. A., Faruk, M. O., Habib, M. A., & Hiziroglu, S. (2020). Formulation and characterization of tamarind (Tamarindus indica L.) seed kernel powder (TKP) as green adhesive for lignocellulosic composite industry. *International Journal of Biological Macromolecules*, *142*, 879–888. https://doi.org/10.1016/j.ijbiomac.2019.10.027

Jackman, R. L., & Smith, J. L. (1996). Anthocyanins and betalains. In G. A. F. Hendry & J. D. Houghton (Eds.), *Natural Food Colorants* (pp. 244–309). Springer US. https://doi.org/10.1007/978-1-4615-2155-6_8

Jalgaonkar, K., Mahawar, M. K., Bibwe, B., & Kannaujia, P. (2022). Postharvest Profile, Processing and Waste Utilization of Dragon Fruit (Hylocereus Spp.): A Review. *Food Reviews International*, *38*(4), 733–759. https://doi.org/10.1080/87559129.2020.1742152

Janiszewska-Turak, E., Walczak, M., Rybak, K., Pobiega, K., Gniewosz, M., Woźniak, Ł., & Witrowa-Rajchert, D. (2022). Influence of Fermentation Beetroot Juice Process on the Physico-Chemical Properties of Spray Dried Powder. *Molecules*, *27*(3), 1008. https://doi.org/10.3390/molecules27031008

Jay, J. M., Loessner, M. J., & Golden, D. A. (2005). *Modern Food Microbiology*. Springer US. https://doi.org/10.1007/b100840

Jiang, H., Zhang, W., Li, X., Shu, C., Jiang, W., & Cao, J. (2021a). Nutrition, phytochemical profile, bioactivities and applications in food industry of pitaya (Hylocereus spp.) peels: A comprehensive review. *Trends in Food Science & Technology*, *116*, 199–217. https://doi.org/10.1016/j.tifs.2021.06.040

Jiang, H., Zhang, W., Li, X., Shu, C., Jiang, W., & Cao, J. (2021b). Nutrition, phytochemical profile, bioactivities and applications in food industry of pitaya (Hylocereus spp.) peels: A comprehensive review. *Trends in Food Science & Technology*, *116*, 199–217. https://doi.org/10.1016/j.tifs.2021.06.040

Jiang, H., Zhang, W., Pu, Y., Chen, L., Cao, J., & Jiang, W. (2023). Development and characterization of a novel active and intelligent film based on pectin and betacyanins from peel waste of pitaya (Hylocereus undatus). *Food Chemistry*, *404*, 134444. https://doi.org/10.1016/j.foodchem.2022.134444

Kanatt, S. R. (2020). Development of active/intelligent food packaging film containing Amaranthus leaf extract for shelf life extension of chicken/fish during chilled storage. *Food Packaging and Shelf Life*, *24*. https://doi.org/10.1016/j.fpsl.2020.100506

Ke, F., Liu, D., Qin, J., & Yang, M. (2024). Functional pH-Sensitive Film Containing Purple Sweet Potato Anthocyanins for Pork Freshness Monitoring and Cherry Preservation. *Foods*, *13*(5), 736. https://doi.org/10.3390/foods13050736

Khan, M. I. (2016). Plant Betalains: Safety, Antioxidant Activity, Clinical Efficacy, and Bioavailability: Nutritional biochemistry of betalains…. *Comprehensive Reviews in Food Science and Food Safety*, *15*(2), 316–330. https://doi.org/10.1111/1541-4337.12185

Khan, M. I., Liu, J., Saini, R. K., & Khurshida, S. (2024). Plant betalains-mixed active/intelligent films for meat freshness monitoring: A review of the fabrication parameters. *Journal of Food Science and Technology*, *61*(7), 1238–1251. https://doi.org/10.1007/s13197-023-05881-2

Kumar, G., Battu, G., Kotha, N., & Raju, L. (2011). Isolation and evaluation of tamarind seed polysaccharide being used as a polymer in pharmaceutical dosage forms. *Research Journal of Pharmaceutical, Biological and Chemical Sciences*. https://www.semanticscholar.org/paper/Isolation-and-evaluation-of-tamarind-seed-being-as-Kumar-Battu/01e0a076e51a5cd64a680538623125bc9051ca51

Kumar, N., Pratibha, Trajkovska Petkoska, A., Khojah, E., Sami, R., & Al-Mushhin, A. A. M. (2021). Chitosan Edible Films Enhanced with Pomegranate Peel Extract: Study on Physical, Biological, Thermal, and Barrier Properties. *Materials*, *14*(12), Article 12. https://doi.org/10.3390/ma14123305

Kumbhar, V., Pandey, A., Varghese, A., & Wanjari, S. (2022). An overview of production, properties and prospects of tamarind seed oil biodiesel as an engine fuel. *International Journal of Ambient Energy*, *43*(1), 3356–3364. https://doi.org/10.1080/01430750.2020.1824946

Kushwaha, R., Kumar, V., Vyas, G., & Kaur, J. (2018). Optimization of Different Variable for Eco-friendly Extraction of Betalains and Phytochemicals from Beetroot Pomace. *Waste and Biomass Valorization*, *9*(9), 1485–1494. https://doi.org/10.1007/s12649-017-9953-6

Lang, P., & Kajiwara, K. (1993). Investigations of the architecture of tamarind seed polysaccharide in aqueous solution by different scattering techniques. *Journal of Biomaterials Science. Polymer Edition*, *4*(5), 517–528. https://doi.org/10.1163/156856293x00177

Law, J. W.-F., Ab Mutalib, N.-S., Chan, K.-G., & Lee, L.-H. (2015). Rapid methods for the detection of foodborne bacterial pathogens: Principles, applications, advantages and limitations. *Frontiers in Microbiology*, *5*. https://doi.org/10.3389/fmicb.2014.00770

Lawrie, G., Keen, I., Drew, B., Chandler-Temple, A., Rintoul, L., Fredericks, P., & Grøndahl, L. (2007). Interactions between Alginate and Chitosan Biopolymers Characterized Using FTIR and XPS. *Biomacromolecules*, *8*(8), 2533–2541. https://doi.org/10.1021/bm070014y

Lazăr, S., Constantin, O. E., Stănciuc, N., Aprodu, I., Croitoru, C., & Râpeanu, G. (2021). Optimization of Betalain Pigments Extraction Using Beetroot by-Products as a Valuable Source. *Inventions 2021, Vol. 6, Page 50*, *6*(3), 50. https://doi.org/10.3390/INVENTIONS6030050

Le, L. T., Tien, N. N. T., Vo, H. T. D., Vu, L. T. K., & Le, N. L. (2024). Comparison of Physical and Functional Characteristics of Biodegradable Smart Films Embedded with Betacyanin-Rich Extracts from Different Sources. *Waste and Biomass Valorization*, *15*(12), 7017–7032. https://doi.org/10.1007/s12649-024-02620-2

Lee, Y. N., & Wiley, R. C. (1981). Betalaine Yield from a Continuous Solid-Liquid Extraction System as Influenced by Raw Product, Post-Harvest and Processing Variables. *Journal of Food Science*, *46*(2), 421–424. https://doi.org/10.1111/j.1365-2621.1981.tb04875.x

Li, B., Chen, H., Ma, Q., Tang, T., & Bai, Y. (2025). A Novel Polyvinyl Alcohol/Chitosan-Based Anthocyanin Electrospun Colorimetric Film for Monitoring Chicken Breast Freshness. *Food Analytical Methods*. https://doi.org/10.1007/s12161-025-02757-3

Li, X., Yang, X., Deng, H., Guo, Y., & Xue, J. (2020). Gelatin films incorporated with thymol nanoemulsions: Physical properties and antimicrobial activities. *International Journal of Biological Macromolecules*, *150*, 161–168. https://doi.org/10.1016/j.ijbiomac.2020.02.066

Li, X., Zhang, Z.-H., Qiao, J., Qu, W., Wang, M.-S., Gao, X., Zhang, C., Brennan, C. S., & Qi, X. (2022). Improvement of betalains stability extracted from red dragon fruit peel by ultrasound-assisted microencapsulation with maltodextrin. *Ultrasonics Sonochemistry*, *82*, 105897. https://doi.org/10.1016/j.ultsonch.2021.105897

Liang, T., Sun, G., Cao, L., Li, J., & Wang, L. (2019). A pH and NH3 sensing intelligent film based on *Artemisia sphaerocephala* Krasch. Gum and red cabbage anthocyanins anchored by carboxymethyl cellulose sodium added as a host complex. *Food Hydrocolloids*, *87*, 858–868. https://doi.org/10.1016/j.foodhyd.2018.08.028

Liaotrakoon, W., De Clercq, N., Van Hoed, V., Van de Walle, D., Lewille, B., & Dewettinck, K. (2013). Impact of Thermal Treatment on Physicochemical, Antioxidative and Rheological Properties of White-Flesh and Red-Flesh Dragon Fruit (Hylocereus spp.) Purees. *Food and Bioprocess Technology*, *6*(2), 416–430. https://doi.org/10.1007/s11947-011-0722-4

Liu, D., Cui, Z., Shang, M., & Zhong, Y. (2021). A colorimetric film based on polyvinyl alcohol/sodium carboxymethyl cellulose incorporated with red cabbage anthocyanin for monitoring pork freshness. *Food Packaging and Shelf Life*, *28*, 100641. https://doi.org/10.1016/j.fpsl.2021.100641

Liu, G., Shi, K., & Sun, H. (2023). Research Progress in Hemicellulose-Based Nanocomposite Film as Food Packaging. *Polymers*, *15*(4), Article 4. https://doi.org/10.3390/polym15040979

Liu, S., Lian, J., Xu, Z., Ning, Y., Shi, M., Zhao, Z., & Zhang, Z. (2022). Chitosan-coated nanoliposomes for efficient delivery of betanin with enhanced stability and bioavailability. *Food Hydrocolloids*, *132*, 107871. https://doi.org/10.1016/j.foodhyd.2022.107871

López, N., Puértolas, E., Condón, S., Raso, J., & Alvarez, I. (2009). Enhancement of the extraction of betanine from red beetroot by pulsed electric fields. *Journal of Food Engineering*, *90*(1), 60–66. https://doi.org/10.1016/j.jfoodeng.2008.06.002

Luo, K., Kim, H.-Y., Oh, M.-H., & Kim, Y.-R. (2020). Paper-based lateral flow strip assay for the detection of foodborne pathogens: Principles, applications, technological challenges and opportunities. *Critical Reviews in Food Science and Nutrition*, *60*(1), 157–170. https://doi.org/10.1080/10408398.2018.1516623

Manamoongmongkol, K., Sriprom, P., Narkrugsa, W., Phumjan, L., Permana, L., Kaewbutra, S., & Assawasaengrat, P. (2024). Study on chemical structure stability and properties of chitosan-incorporated tamarind seed kernel xyloglucan hydrogels. *Colloids and Surfaces A: Physicochemical and Engineering Aspects*, *702*, 135114. https://doi.org/10.1016/j.colsurfa.2024.135114

Mansingh, B. B., Binoj, J. S., Sai, N. P., Hassan, S. A., Siengchin, S., Sanjay, M. R., & Liu, Y. C. (2021). Sustainable development in utilization of Tamarindus indica L. and its by-products in industries: A review. *Current Research in Green and Sustainable Chemistry*, *4*, 100207. https://doi.org/10.1016/j.crgsc.2021.100207

Maran, J. P., & Priya, B. (2016). Multivariate statistical analysis and optimization of ultrasound-assisted extraction of natural pigments from waste red beet stalks. *Journal of Food Science and Technology*, *53*(1), 792–799. https://doi.org/10.1007/s13197-015-1988-8

Mercy, L. K., Wariara, K., Fredah, K. R., & Remmy, K. W. (2019). Evaluation of morphological diversity of tamarind (Tamarindus indica) accessions from Eastern parts of Kenya. *Journal of Horticulture and Forestry*, *11*(1), 1–7. https://doi.org/10.5897/JHF2018.0552

Mishra, A., & Malhotra, A. V. (2009). Tamarind xyloglucan: A polysaccharide with versatile application potential. *Journal of Materials Chemistry*, *19*(45), 8528–8536. https://doi.org/10.1039/B911150F

Mohammadian, E., Alizadeh-Sani, M., & Jafari, S. M. (2020). Smart monitoring of gas/temperature changes within food packaging based on natural colorants. *Comprehensive Reviews in Food Science and Food Safety*, *19*(6), 2885–2931. https://doi.org/10.1111/1541-4337.12635

Moreno-Ley, C. M., Osorio-Revilla, G., Hernández-Martínez, D. M., Ramos-Monroy, O. A., & Gallardo-Velázquez, T. (2021). Anti-inflammatory activity of betalains: A comprehensive review. *Human Nutrition & Metabolism*, *25*, 200126. https://doi.org/10.1016/j.hnm.2021.200126

Moßhammer, M. R., Stintzing, F. C., & Carle, R. (2005). Colour studies on fruit juice blends from Opuntia and Hylocereus cacti and betalain-containing model solutions derived therefrom. *Food Research International*, *38*(8), 975–981. https://doi.org/10.1016/j.foodres.2005.01.015

Moustafa, H., Hemida, M. H., Shemis, M. A., Dufresne, A., & Morsy, M. (2023). Functionalized GO nanoplatelets with folic acid as a novel material for boosting humidity sensing of chitosan/PVA nanocomposites for active food packaging. *Surfaces and Interfaces*, *41*, 103229. https://doi.org/10.1016/j.surfin.2023.103229

Muller, F., Manet, S., Jean, B., Chambat, G., Boué, F., Heux, L., & Cousin, F. (2011). SANS Measurements of Semiflexible Xyloglucan Polysaccharide Chains in Water Reveal Their Self-Avoiding Statistics. *Biomacromolecules*, *12*(9), 3330–3336. https://doi.org/10.1021/bm200881x

Mutwakil. (2011). Meat Spoilage Mechanisms and Preservation Techniques: A Critical Review. *American Journal of Agricultural and Biological Sciences*, *6*(4), 486–510. https://doi.org/10.3844/ajabssp.2011.486.510

Naghdi, S., Rezaei, M., & Abdollahi, M. (2021). A starch-based pH-sensing and ammonia detector film containing betacyanin of paperflower for application in intelligent packaging of fish. *International Journal of Biological Macromolecules*, *191*, 161–170. https://doi.org/10.1016/j.ijbiomac.2021.09.045

Narayanan, G. P., Radhakrishnan, P., Baiju, P., & S, A. M. (2023). Fabrication Of Butterfly Pea Flower Anthocyanin-Incorporated Colorimetric Indicator Film Based On Gelatin/Pectin For Monitoring Fish Freshness. *Food Hydrocolloids for Health*, *4*, 100159. https://doi.org/10.1016/j.fhfh.2023.100159

Narkrugsa, W., Palaya, P., Jaipakdeea, T., & Yodudom, S. (2019). Effect of jellose and sweet tamarind pulp of thailand on some physical properties and sensory characteristics of tamarind gelato ice cream. *VRU Research and Development Journal Science and Technology*, *14*(1), Article 1.

Nowacka, M., Dadan, M., Janowicz, M., Wiktor, A., Witrowa-Rajchert, D., Mandal, R., Pratap-Singh, A., & Janiszewska-Turak, E. (2021). Effect of nonthermal treatments on selected natural food pigments and color changes in plant material. *Comprehensive Reviews in Food Science and Food Safety*, *20*(5), 5097–5144. https://doi.org/10.1111/1541-4337.12824

Ortiz Hernández, Y. D., & Carrillo Salazar, J. A. (2012). Pitahaya (Hylocereus spp.): A short review. *Comunicata Scientiae*, *3*(4), 220–237.

Ortiz-Hernández, Y. D., & Carrillo-Salazar, J. A. (2012). Pitahaya (Hylocereus spp.): A short review. *Comunicata Scientiae*, *3*(4), 220–237. https://doi.org/10.14295/cs.v3i4.334

Pandian, A. T., Chaturvedi, S., & Chakraborty, S. (2021). Applications of enzymatic time–temperature indicator (TTI) devices in quality monitoring and shelf-life estimation of food products during storage. *Journal of Food Measurement and Characterization*, *15*(2), 1523–1540. https://doi.org/10.1007/s11694-020-00730-8

Parlapani, F. F., Boziaris, I. S., & Drosinos, E. H. (2024). Detection of Fish Spoilage. In *Handbook of Seafood and Seafood Products Analysis* (2nd ed.). CRC Press.

Pechová, V., Gajdziok, J., Muselík, J., & Vetchý, D. (2018). Development of Orodispersible Films Containing Benzydamine Hydrochloride Using a Modified Solvent Casting Method. *AAPS PharmSciTech*, *19*(6), 2509–2518. https://doi.org/10.1208/s12249-018-1088-y

Pennanen, K., Focas, C., Kumpusalo-Sanna, V., Keskitalo-Vuokko, K., Matullat, I., Ellouze, M., Pentikäinen, S., Smolander, M., Korhonen, V., & Ollila, M. (2015). European Consumers' Perceptions of Time–Temperature Indicators in Food Packaging. *Packaging Technology and Science*, *28*(4), 303–323. https://doi.org/10.1002/pts.2105

Pereira, P. F. M., Picciani, P. H. S., Calado, V. M. A., & Tonon, R. V. (2020). Gelatin-Based Nanobiocomposite Films as Sensitive Layers for Monitoring Relative Humidity in Food Packaging. *Food and Bioprocess Technology*, *13*(6), 1063–1073. https://doi.org/10.1007/s11947-020-02462-5

Permana, L., Sriprom, P., Manamoongmongkol, K., Phumjan, L., & Assawasaengrat, P. (2024). Optimization of betalain extraction from dragon fruit (Hylocereus undatus) peel and effect of pH on its properties. *Biomass Conversion and Biorefinery*. https://doi.org/10.1007/s13399-023-05260-z

Pichayajittipong, P., & Thaiudom, S. (2014). Optimum Condition of Beta-Cyanin Colorant Production from Red Dragon Fruit (Hylocercus polyrhizus) Peels using Response

Surface Methodology. *Chiang Mai University Journal of Natural Sciences*, *13*(1). https://doi.org/10.12982/CMUJNS.2014.0051

Picout, D. R., Ross-Murphy, S. B., Errington, N., & Harding, S. E. (2003). Pressure Cell Assisted Solubilization of Xyloglucans: Tamarind Seed Polysaccharide and Detarium Gum. *Biomacromolecules*, *4*(3), 799–807. https://doi.org/10.1021/bm0257659

Prajapati, R. A., & Jadeja, G. C. (2024). Optimization of ultrasound-assisted deep eutectic solvent extraction of betanin and its application in chitosan-based biofilm. *Biomass Conversion and Biorefinery*, *14*(14), 15405–15417. https://doi.org/10.1007/s13399-023-03808-7

Prieto-Santiago, V., Cavia, M. M., Alonso-Torre, S. R., & Carrillo, C. (2020). Relationship between color and betalain content in different thermally treated beetroot products. *Journal of Food Science and Technology*, *57*(9), 3305–3313. https://doi.org/10.1007/s13197-020-04363-z

Priyadarshi, R., Ezati, P., & Rhim, J.-W. (2021). Recent Advances in Intelligent Food Packaging Applications Using Natural Food Colorants. *ACS Food Science & Technology*, *1*(2), 124–138. https://doi.org/10.1021/acsfoodscitech.0c00039

Qin, Y., Liu, Y., Zhang, X., & Liu, J. (2020a). Development of active and intelligent packaging by incorporating betalains from red pitaya (Hylocereus polyrhizus) peel into starch/polyvinyl alcohol films. *Food Hydrocolloids*, *100*. https://doi.org/10.1016/j.foodhyd.2019.105410

Qin, Y., Liu, Y., Zhang, X., & Liu, J. (2020b). Development of active and intelligent packaging by incorporating betalains from red pitaya (Hylocereus polyrhizus) peel into starch/polyvinyl alcohol films. *Food Hydrocolloids*, *100*, 105410. https://doi.org/10.1016/j.foodhyd.2019.105410

Qin, Y., Liu, Y., Zhang, X., & Liu, J. (2020c). Development of active and intelligent packaging by incorporating betalains from red pitaya (Hylocereus polyrhizus) peel into starch/polyvinyl alcohol films. *Food Hydrocolloids*, *100*, 105410. https://doi.org/10.1016/j.foodhyd.2019.105410

Qin, Y., Wang, Y., Tang, Z., Chen, K., Wang, Z., Cheng, G., Chi, H., & Soteyome, T. (2024). A pH-sensitive film based on chitosan/gelatin and anthocyanin from *Zingiber striolatum* Diels for monitoring fish freshness. *Food Chemistry: X*, *23*, 101639. https://doi.org/10.1016/j.fochx.2024.101639

Ramos, A. C., Gales, A. C., Monteiro, J., Silbert, S., Chagas-Neto, T., Machado, A. M. O., & Carvalhaes, C. G. (2017). Evaluation of a rapid immunochromatographic test for detection of distinct variants of Klebsiella pneumoniae carbapenemase (KPC) in Enterobacteriaceae. *Journal of Microbiological Methods*, *142*, 1–3. https://doi.org/10.1016/j.mimet.2017.08.016

Ravachol, J., de Philip, P., Borne, R., Mansuelle, P., Maté, M. J., Perret, S., & Fierobe, H.-P. (2016). Mechanisms involved in xyloglucan catabolism by the cellulosome-producing bacterium Ruminiclostridium cellulolyticum. *Scientific Reports*, *6*(1), Article 1. https://doi.org/10.1038/srep22770

Rawdkuen, S., Faseha, A., Benjakul, S., & Kaewprachu, P. (2020). Application of anthocyanin as a color indicator in gelatin films. *Food Bioscience*, *36*, 100603. https://doi.org/10.1016/j.fbio.2020.100603

Robertson, G. L. (2013). *Food packaging: Principles and practice* (3rd ed). CRC Press.

Romainor, A. N., Chin, S. F., & Lihan, S. (2022). Antimicrobial Starch-Based Film for Food Packaging Application. *Starch - Stärke*, *74*(3–4), 2100207. https://doi.org/10.1002/star.202100207

Sadowska-Bartosz, I., & Bartosz, G. (2021a). Biological properties and applications of betalains. *Molecules*, *26*(9). Scopus. https://doi.org/10.3390/molecules26092520

Sadowska-Bartosz, I., & Bartosz, G. (2021b). Biological Properties and Applications of Betalains. *Molecules*, *26*(9), 2520. https://doi.org/10.3390/molecules26092520

Sahoo, D., Sahoo, S., Mohanty, P., Sasmal, S., & Nayak, P. L. (2009). Chitosan: A New Versatile Bio-polymer for Various Applications. *Designed Monomers and Polymers*, *12*(5), 377–404. https://doi.org/10.1163/138577209X12486896623418

Said, N. S., & Sarbon, N. M. (2023). Monitoring the freshness of fish fillets by colorimetric gelatin composite film incorporated with curcumin extract. *Biocatalysis and Agricultural Biotechnology*, *50*, 102722. https://doi.org/10.1016/j.bcab.2023.102722

Schwartz, S. J., & von Elbe, J. H. (1983). Identification of betanin degradation products. *Zeitschrift Für Lebensmittel-Untersuchung Und Forschung*, *176*(6), 448–453. https://doi.org/10.1007/BF01042560

Sen, R., & Baruah, A. M. (2023). Phenolic profile and pigment stability of Hylocereus species grown in North-East India. *Journal of Food Composition and Analysis*, *116*, 105078. https://doi.org/10.1016/j.jfca.2022.105078

Sipilä, E., Virkki, J., Sydänheimo, L., & Ukkonen, L. (2016). Experimental Study on Brush-Painted Passive RFID-Based Humidity Sensors Embedded into Plywood Structures. *International Journal of Antennas and Propagation*, *2016*, 1–8. https://doi.org/10.1155/2016/1203673

Sohany, M., Tawakkal, I. S. M. A., Ariffin, S. H., Shah, N. N. A. K., & Yusof, Y. A. (2021). Characterization of Anthocyanin Associated Purple Sweet Potato Starch and Peel-Based pH Indicator Films. *Foods*, *10*(9), Article 9. https://doi.org/10.3390/foods10092005

Souza, M. P., Vaz, A. F. M., Silva, H. D., Cerqueira, M. A., Vicente, A. A., & Carneiro-da-Cunha, M. G. (2015). Development and Characterization of an Active Chitosan-Based Film Containing Quercetin. *Food and Bioprocess Technology*, *8*(11), 2183–2191. https://doi.org/10.1007/s11947-015-1580-2

Sriprom, P., Neramittagapong, S., Lin, C., Neramittagapong, A., & Assawasaengrat, P. (2023). Lignin removal from synthetic wastewater via Fenton-like reaction over Cu supported on MCM-41 derived from bagasse: Optimization and reaction intermediates. *Heliyon*, *9*(2), e13157. https://doi.org/10.1016/j.heliyon.2023.e13157

Sriprom, P., Neramittagapong, S., Lin, C., Wantala, K., Neramittagapong, A., & Grisdanurak, N. (2015). Optimizing chemical oxygen demand removal from synthesized wastewater containing lignin by catalytic wet-air oxidation over CuO/Al2O3 catalysts. *Journal of the Air & Waste Management Association*, *65*(7), 828–836. https://doi.org/10.1080/10962247.2015.1023908

Stintzing, F. C., & Carle, R. (2007). Betalains – emerging prospects for food scientists. *Trends in Food Science & Technology*, *18*(10), 514–525. https://doi.org/10.1016/j.tifs.2007.04.012

Stintzing, F. C., Herbach, K. M., Mosshammer, M. R., Carle, R., Yi, W., Sellappan, S., Akoh, C. C., Bunch, R., & Felker, P. (2005). Color, Betalain Pattern, and Antioxidant Properties of Cactus Pear (*Opuntia* spp.) Clones. *Journal of Agricultural and Food Chemistry*, *53*(2), 442–451. https://doi.org/10.1021/jf048751y

Strack, D., Vogt, T., & Schliemann, W. (2003). Recent advances in betalain research. *Phytochemistry*, *62*(3), 247–269. https://doi.org/10.1016/S0031-9422(02)00564-2

Tan, E. L., Ng, W. N., Shao, R., Pereles, B. D., & Ong, K. G. (2007). A Wireless, Passive Sensor for Quantifying Packaged Food Quality. *Sensors*, *7*(9), 1747–1756. https://doi.org/10.3390/s7091747

Tanpichai, S., Srimarut, Y., Woraprayote, W., & Malila, Y. (2022). Chitosan coating for the preparation of multilayer coated paper for food-contact packaging: Wettability, mechanical properties, and overall migration. *International Journal of Biological Macromolecules*, *213*, 534–545. https://doi.org/10.1016/j.ijbiomac.2022.05.193

Tao, Y., Qian, L.-H., & Xie, J. (2011). Effect of chitosan on membrane permeability and cell morphology of *Pseudomonas aeruginosa* and *Staphyloccocus aureus*. *Carbohydrate Polymers*, *86*(2), 969–974. https://doi.org/10.1016/j.carbpol.2011.05.054

Tarjan, L., Šenk, I., Tegeltija, S., Stankovski, S., & Ostojic, G. (2014). A readability analysis for QR code application in a traceability system. *Computers and Electronics in Agriculture*, *109*, 1–11. https://doi.org/10.1016/j.compag.2014.08.015

Tavassoli, M., Alizadeh Sani, M., Khezerlou, A., Ehsani, A., Jahed-Khaniki, G., & McClements, D. J. (2022). Smart Biopolymer-Based Nanocomposite Materials Containing pH-Sensing Colorimetric Indicators for Food Freshness Monitoring. *Molecules*, *27*(10), 3168. https://doi.org/10.3390/molecules27103168

Tekin, İ., Özcan, K., & Ersus, S. (2023). Optimization of ionic gelling encapsulation of red beet (Beta vulgaris L.) juice concentrate and stability of betalains. *Biocatalysis and Agricultural Biotechnology*, *51*, 102774. https://doi.org/10.1016/j.bcab.2023.102774

Thippeswamy, B., Joshi, A., Sethi, S., Dahuja, A., Kaur, C., Tomar, B. S., & Varghese, E. (2022). Chemical Additives for Preserving the Betalain Pigment and Antioxidant Activity of Red Beetroot. *Sugar Tech*, *24*(3), 890–899. https://doi.org/10.1007/s12355-021-01104-0

Tominaga, T. (2018). Rapid detection of Klebsiella pneumoniae, Klebsiella oxytoca, Raoultella ornithinolytica and other related bacteria in food by lateral-flow test strip immunoassays. *Journal of Microbiological Methods*, *147*, 43–49. https://doi.org/10.1016/j.mimet.2018.02.015

Urakawa, H., Mimura, M., & Kajiwara, K. (2002). Diversity and Versatility of Plant Seed Xyloglucan. *Trends in Glycoscience and Glycotechnology*, *14*(80), 355–376. https://doi.org/10.4052/tigg.14.355

von Elbe, J. H., & Attoe, E. L. (1985). Oxygen involvement in betanine degradation—Measurement of active oxygen species and oxidation reduction potentials. *Food Chemistry*, *16*(1), 49–67. https://doi.org/10.1016/0308-8146(85)90019-6

Wattanadumrong, B., & Liampreecha, W. (2023). THE BENEFIT-COST ANALYSIS OF THE GIANT SOUR TAMARIND PRODUCT: CASE STUDY OF PHITSANULOK AND PHETCHABUN, THAILAND. *Economic and Social Development: Book of Proceedings*, 262–269.

Wazir, H., Chay, S. Y., Zarei, M., Hussin, F. S., Mustapha, N. A., Wan Ibadullah, W. Z., & Saari, N. (2019). Effects of Storage Time and Temperature on Lipid Oxidation and Protein Co-Oxidation of Low-Moisture Shredded Meat Products. *Antioxidants*, *8*(10), 486. https://doi.org/10.3390/antiox8100486

Wiggers, H. J., Chevallier, P., Copes, F., Simch, F. H., Da Silva Veloso, F., Genevro, G. M., & Mantovani, D. (2022). Quercetin-Crosslinked Chitosan Films for Controlled Release of Antimicrobial Drugs. *Frontiers in Bioengineering and Biotechnology*, *10*, 814162. https://doi.org/10.3389/fbioe.2022.814162

Wiley, R. C., & Lee, Y.-N. (1978). Recovery of Betalaines from Red Beets by a Diffusion-Extraction Procedure. *Journal of Food Science*, *43*(4), 1056–1058. https://doi.org/10.1111/j.1365-2621.1978.tb15231.x

Wisudawaty, P., Djatna, T., & Sugiarto. (2024). Analysis and design of smart food packaging monitoring model based on chipless RFID sensor. *IOP Conference Series: Earth and Environmental Science*, *1358*(1), 012038. https://doi.org/10.1088/1755-1315/1358/1/012038

Wu, C., Li, Y., Du, Y., Wang, L., Tong, C., Hu, Y., Pang, J., & Yan, Z. (2019). Preparation and characterization of konjac glucomannan-based bionanocomposite film for active food packaging. *Food Hydrocolloids*, *89*, 682–690. https://doi.org/10.1016/j.foodhyd.2018.11.001

Wybraniec, S., Platzner, I., Geresh, S., Gottlieb, H. E., Haimberg, M., Mogilnitzki, M., & Mizrahi, Y. (2001). Betacyanins from vine cactus Hylocereus polyrhizus. *Phytochemistry*, *58*(8), 1209–1212. https://doi.org/10.1016/S0031-9422(01)00336-3

Yam, K. L., Takhistov, P. T., & Miltz, J. (2005). Intelligent Packaging: Concepts and Applications. *Journal of Food Science*, *70*(1), R1–R10. https://doi.org/10.1111/j.1365-2621.2005.tb09052.x

Yang, J., & Xu, Y. (2021). Prediction of fruit quality based on the RGB values of time–temperature indicator. *Journal of Food Science*, *86*(3), 932–941. https://doi.org/10.1111/1750-3841.15518

Yang, L., Yuan, Q., Li, T.-T., Lou, C.-W., Hung, C., & Lin, J.-H. (2025). Exploration and application prospect of the advanced technology of time–temperature indicators. *Textile Research Journal*, *95*(3–4), 404–428. https://doi.org/10.1177/00405175241266999

Yao, X., Hu, H., Qin, Y., & Liu, J. (2020). Development of antioxidant, antimicrobial and ammonia-sensitive films based on quaternary ammonium chitosan, polyvinyl alcohol and betalains-rich cactus pears (Opuntia ficus-indica) extract. *Food Hydrocolloids*, *106*, 105896. https://doi.org/10.1016/j.foodhyd.2020.105896

Yao, X., Liu, J., Hu, H., Yun, D., & Liu, J. (2022). Development and comparison of different polysaccharide/PVA-based active/intelligent packaging films containing red pitaya betacyanins. *Food Hydrocolloids*, *124*. https://doi.org/10.1016/j.foodhyd.2021.107305

Yao, X., Qin, Y., Zhang, M., Zhang, J., Qian, C., & Liu, J. (2021). Development of active and smart packaging films based on starch, polyvinyl alcohol and betacyanins from

different plant sources. *International Journal of Biological Macromolecules*, *183*, 358–368. https://doi.org/10.1016/j.ijbiomac.2021.04.152

Yong, Y. Y., Dykes, G., Lee, S. M., & Choo, W. S. (2018). Effect of refrigerated storage on betacyanin composition, antibacterial activity of red pitahaya (Hylocereus polyrhizus) and cytotoxicity evaluation of betacyanin rich extract on normal human cell lines. *LWT*, *91*, 491–497. https://doi.org/10.1016/j.lwt.2018.01.078

You, S., Zhang, X., Wang, Y., Jin, Y., Wei, M., & Wang, X. (2022). Development of highly stable color indicator films based on κ-carrageenan, silver nanoparticle and red grape skin anthocyanin for marine fish freshness assessment. *International Journal of Biological Macromolecules*, *216*, 655–669. https://doi.org/10.1016/j.ijbiomac.2022.06.206

Zhang, X., Zhao, Y., Li, Y., Zhu, L., Fang, Z., & Shi, Q. (2020). Physicochemical, mechanical and structural properties of composite edible films based on whey protein isolate/psyllium seed gum. *International Journal of Biological Macromolecules*, *153*, 892–901. https://doi.org/10.1016/j.ijbiomac.2020.03.018

Zou, Y., Chen, S., Dou, H., Zhu, W., Zhao, D., Wang, Y., Wang, H., & Xia, X. (2024). Development of a colorimetric nanofibrous film sensor based on polycaprolactone (PCL) incorporated with alizarin for tracking shrimp freshness. *Food Packaging and Shelf Life*, *42*, 101249. https://doi.org/10.1016/j.fpsl.2024.101249

APPENDIX

1. Betalain extract in different pH

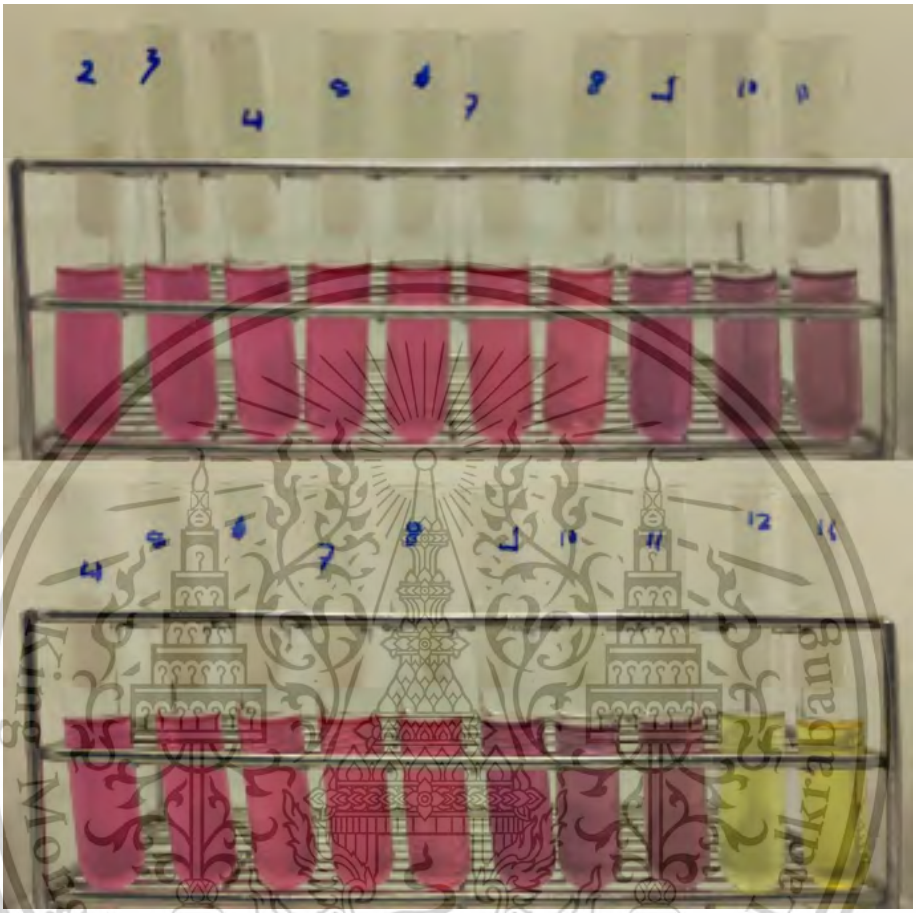

Appendix Figure 1 Photograph of betalain extract under different pH from pH 2 to pH 13

2. Intelligent film of xyloglucan-chitosan film

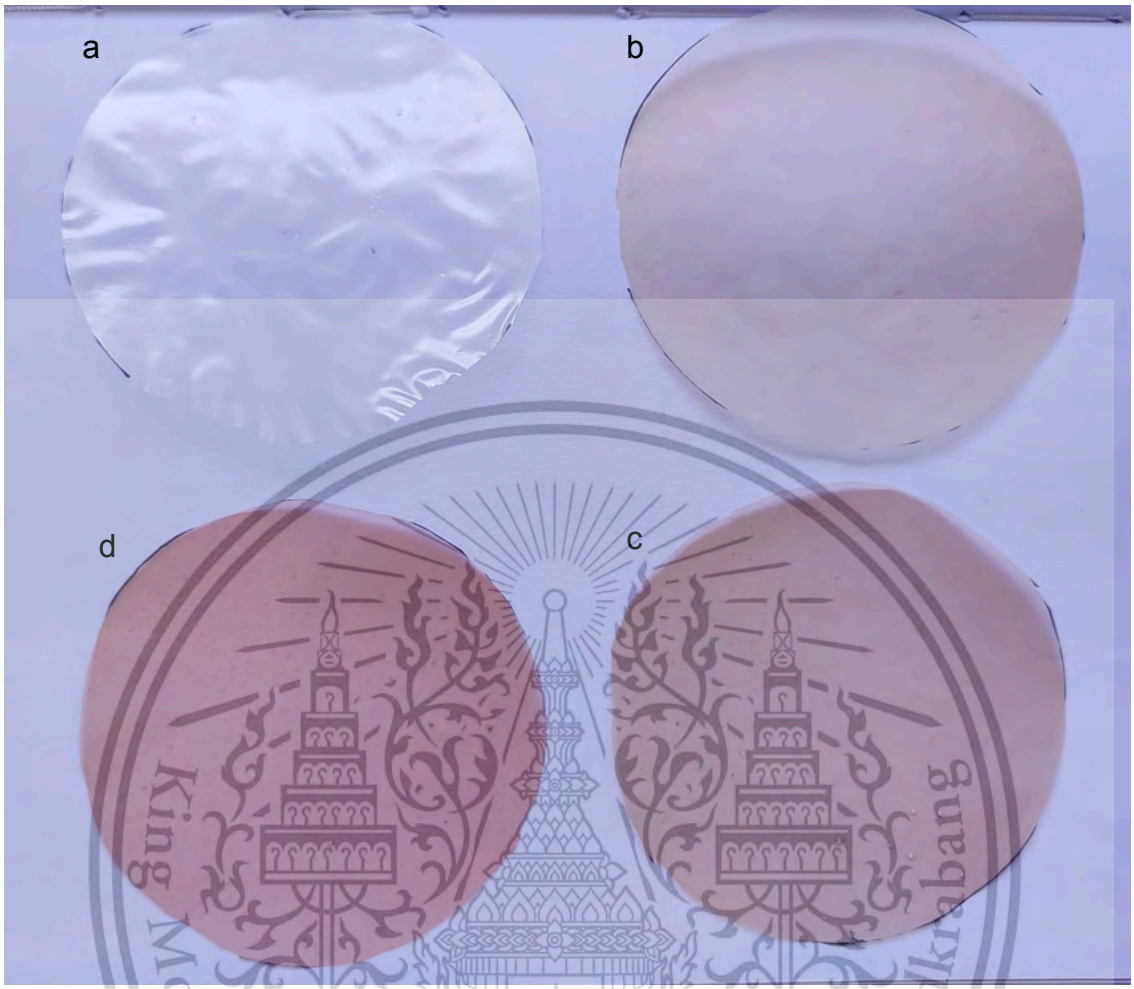

Appendix Figure 2 Photograph of film (a). XC Film, (b) XC-EB3, (c) XC-EB5, and (d) XC-EB7

3. Application of films to shrimp spoilage detection

Appendix Table 1 Photograph of shrimp with intelligent packaging film during storage

	XC Film	XC-EB3	XC-EB5	XC-EB7
Day 0				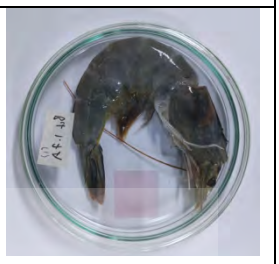
Day 2	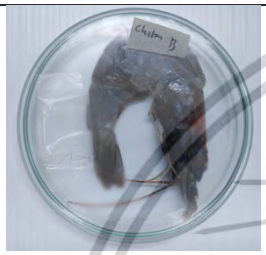	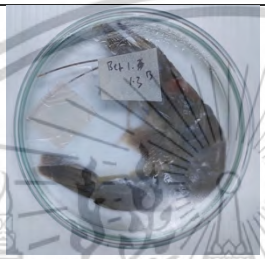		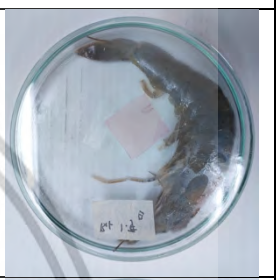
Day 4	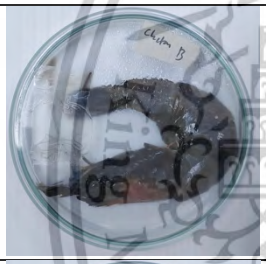			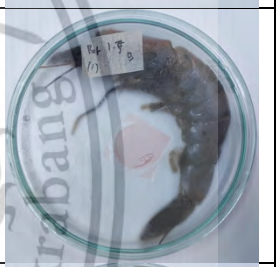
Day 6				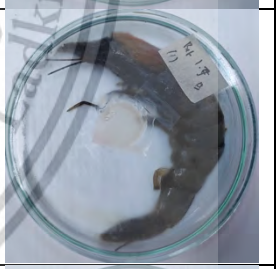
Day 8				

4. Statistical Analysis

4.1. Optimization of extraction: Evaluate the effects of pH, temperature, extraction time, and solvent ratio on betalain yield from dragon fruit peels

Coded Coefficients

Term	Coef	SE Coef	T-Value	P-Value	VIF
Constant	136.0	24.4	5.57	0.000	
PH	4.80	3.90	1.23	0.242	84.40
Temperature	-0.313	0.606	-0.52	0.614	14.40
Time	-0.278	0.289	-0.96	0.354	72.16
Ratio	-5.150	0.643	-8.01	0.000	89.44
PH*PH	-0.897	0.319	-2.82	0.016	37.25
Temperature*Temperature	0.00188	0.00566	0.33	0.745	82.25
Time*Time	0.00314	0.00204	1.54	0.150	18.89
Ratio*Ratio	0.04008	0.00816	4.91	0.000	44.81
PH*Temperature	-0.0221	0.0490	-0.45	0.661	40.00
PH*Time	-0.0604	0.0294	-2.05	0.063	18.88
PH*Ratio	0.1963	0.0589	3.34	0.006	27.52
Temperature*Time	-0.00301	0.00392	-0.77	0.457	33.88
Temperature*Ratio	0.00519	0.00785	0.66	0.521	42.52
Time*Ratio	0.01172	0.00471	2.49	0.028	21.40

Model Summary

S	R-sq	R-sq(adj)	R-sq(pred)
2.94276	98.01%	95.69%	90.37%

Analysis of Variance

Source	DF	Adj SS	Adj MS	F-Value	P-Value
Model	14	5124.65	366.046	42.27	0.000
Linear	4	713.24	178.310	20.59	0.000
PH	1	13.10	13.101	1.51	0.242
Temperature	1	2.32	2.318	0.27	0.614
Time	1	8.06	8.057	0.93	0.354

Ratio	1	555.94	555.937	64.20	0.000
Square	4	414.88	103.721	11.98	0.000
PH*PH	1	68.70	68.705	7.93	0.016
Temperature*Temperature	1	0.96	0.956	0.11	0.745
Time*Time	1	20.53	20.532	2.37	0.150
Ratio*Ratio	1	209.14	209.140	24.15	0.000
2-Way Interaction	6	197.12	32.853	3.79	0.024
PH*Temperature	1	1.76	1.756	0.20	0.661
PH*Time	1	36.48	36.482	4.21	0.063
PH*Ratio	1	96.33	96.334	11.12	0.006
Temperature*Time	1	5.11	5.108	0.59	0.457
Temperature*Ratio	1	3.78	3.783	0.44	0.521
Time*Ratio	1	53.66	53.656	6.20	0.028
Error	12	103.92	8.660		
Lack-of-Fit	10	76.86	7.686	0.57	0.779
Pure Error	2	27.06	13.529		
Total	26	5228.57			

Regression Equation in Uncoded Units

Betalain Yield = 36.0 + 4.80 PH - 0.313 Temperature - 0.278 Time - 5.150 Ratio - 0.897 PH*PH + 0.00188 Temperature*Temperature + 0.00314 Time*Time + 0.04008 Ratio*Ratio - 0.0221 PH*Temperature - 0.0604 PH*Time + 0.1963 PH*Ratio - 0.00301 Temperature*Time + 0.00519 Temperature*Ratio + 0.01172 Time*Ratio

Fits and Diagnostics for Unusual Observations

Betalain

Obs	Yield 2	Fit	Resid	Std Resid	
10	48.17	52.00	-3.83	-2.02	R

R Large residual

Parameters

Response	Goal	Lower	Target	Upper	Weight	Importance
Betalain Yield 2	Maximum	16.81	72.37		1	1

Solution

Solution	PH	Temperature	Time	Ratio	Betalain Yield 2 Fit	Composite Desirability
1	3.61616	30	10	15	72.4710	1

Multiple Response Prediction

Variable	Setting
PH	3.61616
Temperature	30
Time	10
Ratio	15

Response	Fit	SE Fit	95% CI	95% PI
Betalain Yield 2	72.47	3.36	(65.15, 79.79)	(62.74, 82.20)

4.2. Intelligent-film packaging formation: Develop and characterize Intelligent-film packaging based on the xyloglucan-chitosan-betalain complex

Descriptives

		N	Mean	Std. Deviation	Std. Error	95% Confidence Interval for Mean		Minimum	Maximum
						Lower Bound	Upper Bound		
Swelling	XC	3	442.463733	33.8649289	19.5519258	358.338586	526.588880	406.7568	474.1228
	XC-EB3	3	687.319733	14.9358334	8.6232074	650.217066	724.422400	670.2857	698.1735
	XC-EB5	3	726.883667	25.5030746	14.7242070	663.530517	790.236816	700.7547	751.7110
	XC-EB7	3	747.445200	21.7124513	12.5356896	693.508481	801.381919	730.4348	771.9008
	Total	12	651.028083	129.5386939	37.3945999	568.723124	733.333043	406.7568	771.9008
L	XC	5	90.1660	.13126	.05870	90.0030	90.3290	90.02	90.29
	XC-EB3	5	83.9860	.65813	.29432	83.1688	84.8032	83.05	84.70
	XC-EB5	5	78.8420	.62528	.27963	78.0656	79.6184	78.01	79.53
	XC-EB7	5	76.4880	1.58059	.70686	74.5254	78.4506	73.85	77.86
	Total	20	82.3705	5.45569	1.21993	79.8172	84.9238	73.85	90.29
a	XC	5	.1180	.05357	.02396	.0515	.1845	.03	.16
	XC-EB3	5	9.5860	.81941	.36645	8.5686	10.6034	8.75	10.64
	XC-EB5	5	17.1520	.91437	.40892	16.0167	18.2873	16.07	18.40
	XC-EB7	5	21.6800	2.14621	.95981	19.0151	24.3449	19.85	25.25
	Total	20	12.1340	8.46162	1.89208	8.1738	16.0942	.03	25.25

b	XC	5	.4660	.41519	.18568	-.0495	.9815	.12	1.06
	XC-EB3	5	-.4600	.20964	.09375	-.7203	-.1997	-.78	-.24
	XC-EB5	5	-1.9180	.40345	.18043	-2.4189	-1.4171	-2.51	-1.50
	XC-EB7	5	-4.4360	.28130	.12580	-4.7853	-4.0867	-4.92	-4.20
	Total	20	-1.5870	1.92476	.43039	-2.4878	-.6862	-4.92	1.06
EaB	XC	5	144.67380	3.531943	1.579533	140.28831	149.05929	139.783	148.670
	XC-EB3	5	172.38220	2.225776	.995397	169.61853	175.14587	170.370	175.817
	XC-EB5	5	185.07060	4.415721	1.974770	179.58776	190.55344	178.390	189.753
	XC-EB7	5	190.33020	3.912525	1.749734	185.47216	195.18824	185.243	195.567
	Total	20	173.11420	18.428571	4.120754	164.48936	181.73904	139.783	195.567
Tensile	XC	5	32.47400	1.457508	.651817	30.66426	34.28374	30.250	33.910
	XC-EB3	5	29.06600	1.825015	.816172	26.79994	31.33206	27.830	32.280
	XC-EB5	5	22.34800	2.248737	1.005666	19.55582	25.14018	19.570	24.660
	XC-EB7	5	16.72600	.717969	.321086	15.83452	17.61748	15.910	17.550
	Total	20	25.15350	6.419805	1.435512	22.14894	28.15806	15.910	33.910
Width	XC	5	.03700	.002449	.001095	.03396	.04004	.034	.040
	XC-EB3	5	.03480	.001924	.000860	.03241	.03719	.033	.038
	XC-EB5	5	.03800	.006745	.003017	.02962	.04638	.027	.044
	XC-EB7	5	.03500	.002121	.000949	.03237	.03763	.032	.037
	Total	20	.03620	.003806	.000851	.03442	.03798	.027	.044
Water	XC	5	15.44660	.217700	.097358	15.17629	15.71691	15.229	15.800
	XC-EB3	5	15.41620	.464307	.207644	14.83969	15.99271	14.719	15.845

	XC-EB5	5	15.29260	.189581	.084783	15.05720	15.52800	15.005	15.469
	XC-EB7	5	15.27140	.431465	.192957	14.73567	15.80713	14.591	15.749
	Total	20	15.35670	.328901	.073545	15.20277	15.51063	14.591	15.845
DE	XC	5	4.00480	.367527	.164363	3.54845	4.46114	3.553	4.464
	XC-EB3	5	12.07525	1.013852	.453408	10.81639	13.33411	11.026	13.480
	XC-EB5	5	20.93004	1.082172	.483962	19.58634	22.27373	19.673	22.411
	XC-EB7	5	25.96145	2.675158	1.196367	22.63980	29.28310	23.670	30.420
	Total	20	15.74288	8.738185	1.953917	11.65329	19.83248	3.553	30.420
Water Contact Angle	XC	6	92.4833	1.21230	.49492	91.2111	93.7556	90.90	94.10
	XC-EB3	8	92.0625	.66319	.23447	91.5081	92.6169	91.30	93.00
	XC-EB5	8	70.1250	2.29767	.81235	68.2041	72.0459	66.70	73.10
	XC-EB7	8	73.6750	1.62195	.57345	72.3190	75.0310	70.20	75.20
	Total	30	81.3933	10.51560	1.91988	77.4667	85.3199	66.70	94.10
WVTR	XC	3	1.4818	.05902	.03408	1.3352	1.6284	1.42	1.53
	XC-EB3	3	1.5509	.01883	.01087	1.5041	1.5976	1.54	1.57
	XC-EB5	3	1.6365	.07700	.04445	1.4452	1.8278	1.57	1.72
	XC-EB7	3	1.8138	.04650	.02685	1.6983	1.9293	1.76	1.84
	Total	12	1.6207	.13783	.03979	1.5332	1.7083	1.42	1.84
WVP	XC	3	3.4733	.14224	.08212	3.1200	3.8267	3.31	3.57
	XC-EB3	3	4.4103	.15094	.08715	4.0353	4.7852	4.27	4.57
	XC-EB5	3	4.9533	.10693	.06173	4.6877	5.2190	4.83	5.02
	XC-EB7	3	5.9233	.14978	.08647	5.5513	6.2954	5.80	6.09

Total	12	4.6901	.93423	.26969	4.0965	5.2837	3.31	6.09

ANOVA

		Sum of Squares	df	Mean Square	F	Sig.
Swelling	Between Groups	179599.506	3	59866.502	96.104	<.001
	Within Groups	4983.500	8	622.937		
	Total	184583.005	11			
L	Between Groups	552.169	3	184.056	220.453	<.001
	Within Groups	13.358	16	.835		
	Total	565.527	19			
a	Between Groups	1335.915	3	445.305	291.212	<.001
	Within Groups	24.466	16	1.529		
	Total	1360.381	19			
b	Between Groups	68.556	3	22.852	199.482	<.001
	Within Groups	1.833	16	.115		
	Total	70.389	19			
EaB	Between Groups	6243.692	3	2081.231	159.374	<.001
	Within Groups	208.941	16	13.059		
	Total	6452.632	19			
Tensile	Between Groups	738.955	3	246.318	89.348	<.001
	Within Groups	44.109	16	2.757		
	Total	783.064	19			
Width	Between Groups	.000	3	.000	.813	.505
	Within Groups	.000	16	.000		
	Total	.000	19			
Water Contact Angle	Between Groups	.115	3	.038	.316	.813
	Within Groups	1.940	16	.121		
	Total	2.055	19			
DE	Between Groups	1412.799	3	470.933	198.485	<.001
	Within Groups	37.962	16	2.373		
	Total	1450.762	19			
WCA	Between Groups	3140.962	3	1046.987	413.721	<.001
	Within Groups	65.797	26	2.531		
	Total	3206.759	29			
WVTR	Between Groups	.185	3	.062	20.689	<.001

	Within Groups	.024	8	.003		
	Total	.209	11			
WVP	Between Groups	9.447	3	3.149	163.832	<.001
	Within Groups	.154	8	.019		
	Total	9.601	11			

Swelling Index

Duncan[a]

		Subset for alpha = 0.05		
Sampel	N	1	2	3
XC	3	442.463733		
XC-EB3	3		687.319733	
XC-EB5	3		726.883667	726.883667
XC-EB7	3			747.445200
Sig.		1.000	.088	.343

Means for groups in homogeneous subsets are displayed.

a. Uses Harmonic Mean Sample Size = 3.000.

L

Duncan[a]

		Subset for alpha = 0.05			
ampel	J				
C-EB7		6.4880			
C-EB5			8.8420		
C-EB3				3.9860	
C					0.1660
ig.		.000	.000	.000	.000

Means for groups in homogeneous subsets are displayed.

a. Uses Harmonic Mean Sample Size = 5.000.

a

Duncan[a]

		Subset for alpha = 0.05			
Sampel	N	1	2	3	4

XC	5	.1180			
XC-EB3	5		9.5860		
XC-EB5	5			17.1520	
XC-EB7	5				21.6800
Sig.		1.000	1.000	1.000	1.000

Means for groups in homogeneous subsets are displayed.

a. Uses Harmonic Mean Sample Size = 5.000.

b

Duncan[a]

		Subset for alpha = 0.05			
Sampel	N	1	2	3	4
XC-EB7	5	-4.4360			
XC-EB5	5		-1.9180		
XC-EB3	5			-.4600	
XC	5				.4660
Sig.		1.000	1.000	1.000	1.000

Means for groups in homogeneous subsets are displayed.

a. Uses Harmonic Mean Sample Size = 5.000.

EaB

Duncana

		Subset for alpha = 0.05			
Sampel	N	1	2	3	4
XC	5	144.67380			
XC-EB3	5		172.38220		
XC-EB5	5			185.07060	
XC-EB7	5				190.33020
Sig.		1.000	1.000	1.000	1.000

Means for groups in homogeneous subsets are displayed.

a. Uses Harmonic Mean Sample Size = 5.000.

Tensile Strength

Duncan[a]

		Subset for alpha = 0.05			
Sampel	N	1	2	3	4
XC-EB7	5	16.72600			
XC-EB5	5		22.34800		
XC-EB3	5			29.06600	
XC	5				32.47400
Sig.		1.000	1.000	1.000	1.000

Means for groups in homogeneous subsets are displayed.

a. Uses Harmonic Mean Sample Size = 5.000.

Width of film

Duncan[a]

		Subset for alpha = 0.05
Sampel	N	1
XC-EB3	5	.03480
XC-EB7	5	.03500
XC	5	.03700
XC-EB5	5	.03800
Sig.		.245

Means for groups in homogeneous subsets are displayed.

a. Uses Harmonic Mean Sample Size = 5.000.

Moisture Content

Duncana

		Subset for alpha = 0.05
Sampel	N	1
XC-EB7	5	15.27140

XC-EB5	5	15.29260
XC-EB3	5	15.41620
XC	5	15.44660
Sig.		.475

Means for groups in homogeneous subsets are displayed.

a. Uses Harmonic Mean Sample Size = 5.000.

DE

Duncan[a]

		Subset for alpha = 0.05			
Sampel	N	1	2	3	4
XC	5	4.00480			
XC-EB3	5		12.07525		
XC-EB5	5			20.93004	
XC-EB7	5				25.96145
Sig.		1.000	1.000	1.000	1.000

Means for groups in homogeneous subsets are displayed.

a. Uses Harmonic Mean Sample Size = 5.000.

Water Contact Angle

Duncana,b

		Subset for alpha = 0.05		
Sampel	N	1	2	3
XC-EB5	8	70.1250		
XC-EB7	8		73.6750	
XC-EB3	8			92.0625
XC	6			92.4833
Sig.		1.000	1.000	.616

Means for groups in homogeneous subsets are displayed.

a. Uses Harmonic Mean Sample Size = 7.385.

b. The group sizes are unequal. The harmonic mean of the group sizes is used. Type I error levels are not guaranteed.

Water Vapour Transmision Rate

Duncan[a]

		Subset for alpha = 0.05		
Sampel	N	1	2	3
XC	3	1.4818		
XC-EB3	3	1.5509	1.5509	
XC-EB5	3		1.6365	
XC-EB7	3			1.8138
Sig.		.160	.091	1.000

Means for groups in homogeneous subsets are displayed.

a. Uses Harmonic Mean Sample Size = 3.000.

Water Vapour Permeability

Duncan[a]

		Subset for alpha = 0.05			
Sampel	N	1	2	3	4
XC	3	3.4733			
XC-EB3	3		4.4103		
XC-EB5	3			4.9533	
XC-EB7	3				5.9233
Sig.		1.000	1.000	1.000	1.000

Means for groups in homogeneous subsets are displayed.

a. Uses Harmonic Mean Sample Size = 3.000.

4.3. Application of films to shrimp spoilage detection

Descriptives

Total Volatile Base Nitrogen (TVB-N)

	N	Mean	Std. Deviation	Std. Error	95% Confidence Interval for Mean		Minimum	Maximum
					Lower Bound	Upper Bound		
Day 0	3	14.87743	.318329	.183787	14.08666	15.66821	14.510	15.070
Day 2	3	20.10998	.087162	.050323	19.89345	20.32650	20.010	20.170
Day 4	3	25.87244	.286268	.165277	25.16131	26.58357	25.670	26.200
Day 6	3	43.41329	.328110	.189434	42.59822	44.22836	43.055	43.700
Day 8	3	70.82771	.450494	.260093	69.70862	71.94679	70.314	71.156
Total	15	35.02017	21.034069	5.430973	23.37189	46.66845	14.510	71.156

ANOVA

TVB-N

	Sum of Squares	df	Mean Square	F	Sig.
Between Groups	6193.046	4	1548.262	15436.902	<.001
Within Groups	1.003	10	.100		
Total	6194.049	14			

TVB-N

Duncan[a]

		Subset for alpha = 0.05				
Day	N	1	2	3	4	5
Day 0	3	14.87743				
Day 2	3		20.10998			
Day 4	3			25.87244		
Day 6	3				43.41329	
Day 8	3					70.82771
Sig.		1.000	1.000	1.000	1.000	1.000

Means for groups in homogeneous subsets are displayed.

a. Uses Harmonic Mean Sample Size = 3.000.

Curriculum Vitae

Full Name: : Lasuardi Permana

Birthdate : 16 October 1986

Address : Perum Murai Indah Permai, A3, Jl. P. Senopati, Jatimulyo Jatiagung, Lampung Selatan, Lampung, Indonesia, 35365

Educational:

2013 – 2016	Study Program in Food Science and Technology, Faculty of Agricultural Technology, Universitas Gadjah Mada, Yogyakarta (GPA: 3.73/4.00)
2006 – 2011	Department of Food Technology and Agricultural Products, Faculty of Agricultural Technology, Universitas Gadjah Mada, Yogyakarta

Work Experience:

2017 – present	Lecture - Institute Technology of Sumatera, Lampung, Indonesia
2011 – 2013	Technical Sales Representative- PT Sriboga Flour Mill, Semarang Indonesia

Publication:

Chokelarb, W., Sriprom, P., **Permana, L.**, & Assawasaengrat, P. (2024). Assessment of overall remaining useful life of lubricants by integrating oil quality and performance. *Heliyon*, *10*(18).

Manamoongmongkol, K., Sriprom, P., Narkrugsa, W., Phumjan, L., **Permana, L.**, Kaewbutra, S., & Assawasaengrat, P. (2024). Study on chemical structure stability and properties of chitosan-incorporated tamarind seed kernel xyloglucan hydrogels. *Colloids and Surfaces A: Physicochemical and Engineering Aspects*, *702*, 135114.

Janjamroon, W., Sriprom, P., Kaewlaoyoong, A., Cheruiyot, N. K., **Permana, L.**, Manamoongmongkol, K., & Phumjan, L. (2024). Organochlorine pesticide residues persist throughout the sugar production process. *Journal of Food Composition and Analysis*, *125*, 105720.

Permana, L., Sriprom, P., Manamoongmongkol, K., Phumjan, L., & Assawasaengrat, P. (2024). Optimization of betalain extraction from dragon fruit (Hylocereus undatus) peel and effect of pH on its properties. *Biomass Conversion and Biorefinery*, 1-12.

Manamoongmongkol, K., Sriprom, P., Phumjan, L., **Permana, L**., & Assawasaengrat, P. (2023). Production of antimicrobial film-reinforced purified cellulose derived from bamboo shoot shell. *Bioresource Technology Reports*, 22, 101429.

Adair, P., Sriprom, P., Narkrugsa, W., Phumjan, L., Manamoongmongkol, K., **Permana, L.**, & Assawasaengrat, P. (2023). Preparation, characterization, and antimicrobial activity of xyloglucan-chitosan film from tamarind (tamarind indica L.) seed kernel. *Progress in Organic Coatings*, 179, 107486.

Saputri, N., Aminy, A., Rahmadi, I., Nasution, S., Mareta, D. T., **Permana, L.**, & Nurdin, S. U. (2022). Comparison of Proximate Analysis Value of Fresh Fruits and Vacuum Fried Fruit Chips. In *E3S Web of Conferences* (Vol. 344, p. 04001). EDP Sciences.

Fithriyani, D., Pangastuti, H. A., Wahyuningtyas, A., & **Permana, L.** (2022). Evaluasi Pemenuhan Elemen Cara Produksi Pangan yang Baik untuk Industri Rumah Tangga (CPPB-IRT) pada UKM Pempek. *CARADDE: Jurnal Pengabdian Kepada Masyarakat*, 4(3), 385-392.

Permana, L., Pangastuti, H. A., Fitriani, V., Mareta, D. T., & Wahyuningtyas, A. (2021). Product Development of Andaliman (Zanthoxylum acanthopodium DC) Chili Sauce With Retort Pouch Packaging: Physical, Chemical, and Sensory Characteristic Studies. *Jurnal Aplikasi Teknologi Pangan*, 10(2).

Rahmadi, I., Nasution, S., Mareta, D. T., **Permana, L**., Talitha, Z. A., Saputri, A., & Nurdin, S. U. (2021). NILAI MUTU KERIPIK BUAH HASIL PENGGORENGAN VAKUM. *Jurnal Standardisasi*, 23(3), 303-312.

Pangastuti, H. A., & **Permana, L.** (2021). Pengukuran Pati Resisten Tipe 5 Secara In Vitro pada Nasi Uduk. *Jurnal Pengolahan Pangan*, 6(2), 42-48.

Mareta, D. T., Pangastuti, H. A., **Permana, L.**, Fitriani, V., & Wahyuningtyas, A. (2021). Hedonic Test Of Lado Mudo Chili Sauce By Addition Of Various Concentrations Of Citric Acid. *AGRITEPA: Jurnal Ilmu Dan Teknologi Pertanian*, 8(1), 41-50.

Fitriani, V., Ayuningtyas, H., Mareta, D. T., **Permana, L**., & Wahyuningtyas, A. (2021). Karakterisasi Fisik, Kimia, dan Sensoris Saus Sambal Mangga Kweni (Mangifera odorata Griff) dengan Variasi Konsentrasi Asam Sitrat dan Durasi Sterilisasi. *Journal of Science and Applicative Technology*, 5(1), 158-162.

Permana, L., Pangastuti, H. A., & Wahyuningtyas, A. (2021). Young Adult Perception of Fermented Durian (Tempoyak) in Lampung Province, Indonesia. *Journal of Science and Applicative Technology*, 5(1), 38-42.

Pangastuti, H. A., **Permana, L**., Mareta, D. T., Fitriani, V., & Wahyuningtyas, A. (2021). Kajian sifat fisik, kimia, dan sensoris sambal tempoyak (durian

terfermentasi) berkemasan retort pouch. *Jurnal Teknologi Pertanian Andalas*, 24(2), 157-165.

Pangastuti, H. A., & **Permana, L.** (2020). The effect of citric acid on chemical and physical characteristics of andaliman (Zanthoxylum acanthopodium) chili paste in retort packaging.

Research Project

Simlitabmas Research Grant: "Peningkatan Produk Turunan Kelapa Sawit: Penggunaan Red Palm Oil pada Produk Pangan Confectionary" (2020)

Simlitabmas Research Grant: "Potensi Kompleks Amilolipid dari Nasi Uduk sebagai Pati Resisten Tipe 5 untuk Mendukung Pangan Lokal" (2019)

Simlitabmas Research Grant: "Improvisasi Pengemasan Durian Terfermentasi (Tempoyak) Sebagai Upaya Komersialisasi Produk Pangan Lokal Indonesia" (2019)

Institut Teknologi Sumatera Research Grant "Pengembangan Sambal Otentik Sumatera Sebagai Sambal Instan Dalam Upaya Mendukung Pelestarian Makanan Tradisional Indonesia" (2019)

Book

Editor and author Kuliner Khas Sumatera: Tradisi hingga Nilai Gizi. ITERA Press. Lampung Selatan.

Hesti A. Pangastuti, **Lasuardi Permana**. 2022. Dasar Teknologi Pengemasan Pangan. ITERA Press. Lampung Selatan.

Hesti A. Pangastuti, dkk. 2021. Panganpedia: Penjelasan Sains dari Fenomena Pangan Sehari-Hari. ITERA Press. Lampung Selatan.